
Universidad Politécnica de Madrid

ESCUELA TÉCNICA SUPERIOR DE INGENIERÍA AGRONÓMICA, ALIMENTARIA Y DE BIOSISTEMAS


# Quantum Computation in Industry 4.0 Cyber-Physical Systems

Tesis doctoral
presentada por


Ing. Javier Villalba-Díez


2022

Complex Systems Group

ESCUELA TÉCNICA SUPERIOR DE INGENIERÍA AGRONÓMICA, ALIMENTARIA Y DE BIOSISTEMAS

# Quantum Computation in Industry 4.0 Cyber-Physical Systems

Ing. Javier Villalba-Díez

Advisor: Dr. Juan Carlos Losada

2022

This page was intentionally left blank

However, since the page contains this writing, it is not blank.

The rest of the work hereinafter is true.

# Acknowledgments

First of all, I would like to thank the Universidad Politécnica de Madrid in general, the Escuela de Doctorado, and the Escuela Técnica Superior de Ingenieros Agrónomos in particular, for giving me the opportunity to pursue my doctoral studies in Complex Systems at its headquarters.

I would also like to thank the members of the Complex Systems Group for their professionalism and rigor in ensuring an academic process that guarantees the high quality standards required by the Universidad Politécnica de Madrid. In particular, my thanks go to Prof. Rosa María Benito for her always both warm and firm scientific advice. She is the heart and soul of the Complex Systems Group at Universidad Politecnica de Madrid and the very reason why I decided to enroll in the program in the first place. Thanks to Prof. Fabio Revuelta and Prof. Florentino Borodo for their clever advice on structuring the doctoral thesis and its presentation. I also want to thank Prof. Ana González–Marcos and Prof. Joaquín Ordieres–Meré for their tireless support and help in crafting and honing the quantum multi–layered network method presented in this work.

I have purposely left my tutor and thesis director, Prof. Juan Carlos Losada, for the end. I can say little about his scientific rigor and professionalism, since his trajectory speaks for itself. Of course, I have learned, thanks to his wise advice and indications, to structure my mind properly to analyze problems from a complex systems perspective in general and in quantum computing in particular. Undoubtedly, without his careful advice, the presented results would never have come to happen. But this is not the most important thing, in my opinion. The key lesson I take away from Juan Carlos is that he has taught me that character and competence must be balanced as a preparation for growth. Juan Carlos has forged my character in this sense with patience and firmness. An excellent tutor that I recommend to future doctoral students.

To all the members of the UPM team, thank you very much for everything I have learned!

# Quantum Computation in Industry 4.0 Cyber-Physical Systems

## Resumen – Abstract


### Resumen

El diseño estratégico de las organizaciones en un entorno donde la complejidad aumenta constantemente, como en los sistemas ciberfísicos típicos de la Industria 4.0, es un proceso lleno de incertidumbres. Los líderes se ven obligados a tomar decisiones que afectan a otras unidades organizativas sin tener la certeza de que sus decisiones sean las correctas. Hasta la fecha, los algoritmos genéticos y redes bayesianas eran capaces de calcular el estado de alineación de los procesos industriales medido a través de ciertos indicadores clave de rendimiento (KPI) para asegurar que los líderes de la Industria 4.0 toman decisiones alineadas con los objetivos estratégicos de la organización. Sin embargo, el coste computacional de estos algoritmos aumenta exponencialmente con el número de KPIs.

El objetivo principal de esta tesis es desarrollar algoritmos cuánticos que permitan realizar diseños estratégicos de organizaciones industriales complejas en tiempo real y su implementación práctica. Para ello hemos demostrado que los circuitos cuánticos pueden mejorar los resultados de los algoritmos genéticos y redes bayesianas a la hora de optimizar ciertos procesos industriales complejos. Hemos desarrollado algoritmos que permiten resolver casos prácticos sencillos de cadenas de mando y dependencia en procesos industriales. Como objetivo último hemos implementado el desarrollo teórico basado en principios cuánticos en un dispositivo que permite discernir en tiempo real la necesidad de modificar un proceso industrial por la presencia de errores de producción y conseguir una interface intuitiva para las personas que lo utilicen.

La metodología que hemos utilizado a lo largo de la investigación parte del desarrollo de circuitos cuánticos espejo de los procesos industriales que se pretenden diseñar de una manera óptima. Los datos que van a permitir validar los algoritmos cuánticos se han obtenido de una serie de sensores instalados en varios equipos industriales con los que ha sido posible diseñar diferentes casos de estudio. Para la integración de las simulaciones cuánticas en los equipos industriales hemos utilizado sensores Radio Frequency Identification basados en computación de bajo coste en un Raspberry Pi y para conseguir interfaces que puedan ser fácilmente interpretables.

Abstract

The strategic design of organizations in an environment where complexity is constantly increasing, as in the cyber-physical systems typical of Industry 4.0, is a process full of uncertainties. Leaders are forced to make decisions that affect other organizational units without being certain that their decisions are the right ones. To date, genetic algorithms and Bayesian networks were able to calculate the alignment status of industrial processes measured through certain key performance indicators (KPIs) to ensure that Industry 4.0 leaders make decisions aligned with the organization's strategic objectives. However, the computational cost of these algorithms increases exponentially with the number of KPIs.

The main objective of this thesis is to develop quantum algorithms that enable real-time strategic designs of complex industrial organizations and their practical implementation. To this end, we have demonstrated that quantum circuits can improve the results of genetic algorithms and Bayesian networks when optimizing certain complex industrial processes. We have developed algorithms that allow solving simple practical cases of chains of command and dependence in industrial processes. As a final objective we have implemented the theoretical development based on quantum principles in a device that allows to discern in real time the need to modify an industrial process due to the presence of production errors and to achieve an intuitive interface for the people who use it.

The methodology we have used throughout the research is based on the development of quantum mirror circuits of the industrial processes to be designed in an optimal way. The data that will allow validation of the quantum algorithms have been obtained from a series of sensors installed in various industrial equipment with which it has been possible to design different case studies. For the integration of quantum simulations in industrial equipment we have used Radio Frequency Identification sensors based on low cost computing on a Raspberry Pi and to achieve interfaces that can be easily interpreted.

# Contents

# Listing of figures

# List of Tables

# 1 Introduction

## 1.1 Motivation

The most significant aspect of strategic planning in an organization is, according to Grant [3], the strategic process: "a dialog through which knowledge is shared and consensus is achieved and commitment towards action and results is built". As shown in [4], consensus in organizations as legitimation of action towards certain strategic goals have attracted increasing levels of attention for legitimation facilitates the access to necessary resources to achieve such goals. These consensus can and should occur in different organizational settings. To unify common efforts and hence support the strategic organizational goals, it is during this dialogue that a sometimes delicate balance of forces is sought between the interests of different organizational agents.

We start by defining some preliminary concepts fundamental to the precise terminology use of the content presented in the following chapters of this work:

- Industry 4.0. Industry 4.0 has gained a lot of attention since it was first released [5], claiming for the necessity of a new paradigm shift in favour of a less centralized manufacture structure. It is regarded as the fourth industrial revolution, the first three being mechanization through the use of vapor energy, mass production through electricity generation, and, ultimately, the digital revolution through the integration of electronics and information technology. The industry 4.0 ought to allow a larger independence of the manufacturing process, since technology is more interrelated and the machines can interact with each other creating a cyber–physical system [6–11].

- Cyber–physical systems. Cyber–physical systems in the context of Industry 4.0 relates to the close bonding and alignment between computing and material resources. A new paradigm of technological systems based on embedded collaborative software is impacting the development of such systems [12–14]. Kagermann [15] places cyber–physical systems as the key driver to trigger the Industry 4.0 paradigm, paralleling its role with the one played, respectively, by steam machines, mass production lines, and integrated circuits in the previous three industrial revolutions. Cyber–physical systems can be defined as "Systems of collaborating computational entities which are in intensive connection with the surrounding physical world and its on-going processes, providing and using, at the same time, data-accessing and data-processing services available on the Internet" [16]. As stated by Lee, Bagheri, and Kao [17] "Cyber–physical system consists of two main functional components: (1) the advanced connectivity that ensures real-time data acquisition from the physical world and information feedback from the cyber space; and (2) intelligent data management, analytic and computational capability that constructs the cyber space". Thus, Cyber–physical system lead to a decentralized control system characteristic of the Industry 4.0, in which machines show great autonomy, share information with other machines, and handle large amounts of data. The term cyber–physical systems refers to a new generation of systems with integrated computational and physical capabilities that can interact with humans through many new modalities. The ability to interact with and expand the capabilities of the physical world through computation, communication, and control is a key enabler for future technology development. When cyber–physical systems are understood within the industrial practice fueled by additional technologies such as Internet of Things, people refer to the Industry 4.0 paradigm. In industrial practice, many engineering systems have been designed by decoupling the control system design from the hardware/software implementation details. After the control system is designed and verified by extensive simulation, ad–hoc tuning methods have been used to address the modeling uncertainty and random disturbances. However, the integration of various subsystems, while keeping the system functional and operational, has been time–

consuming [18].

- Lean Management. Lean management systems in a cyber–physical environment of Industry 4.0 are described as socio-technical structures designed to consistently reduce the variability of value creating processes and therefore increase their effectiveness and profitability [19–22, 22–29].

  Variability in this context is understood as any deviation from the desired process state. In quantifiable terms, this work assumes the variability of a process as measured by the systematic reduction of the standard deviation associated with the indicators measuring its performance [20, 30].

- Complex Networked Organizational Design. According to the network organizational paradigm, modern cyber–physical systems oriented to the lean management of Industry 4.0 can be seen as a socio-technical symbiotic ecosystem of human networks [31] interacting with distributed physical sensors interconnected in an increasingly complex network interconnected sensors [32], which readings are modeled as time-dependent signals at the vertices, human or cyber–physical respectively. That means that in the structure of the network nodes you can find characteristics that represent them in the form of a certain time series that describes the key performance indicators (KPIs). These networks can be understood as complex since the interaction between their elements gives rise to emergent phenomena that could not take place without the interaction of their multiple agents.

- Complex cyber–physical networks. For any given time $t$, complex cyber–physical networks, $\Gamma(t)$ can be described as time-dependent *graphs* given by

$$\Omega(t) = [\Gamma(t); E(t)], \tag{1.1}$$

  which can be understood as lists of $\Gamma(t)$ human and cyber–physical nodes and its standard communication $E(t) \subset (\Gamma(t)x\Gamma(t))$ edges [20]. The very emergence of complex networked organizational design configurations in the form of lean structural networks is only possible through a continuous improvement-oriented standardization of the organizational network edges, the business communication protocols, between the network elements [20]. These boundary conditions allow to represent the systems of Industry 4.0 as cyber–physical complex networks, allowing a systematic and quantitative analysis of the systems by means of lean management algorithms strategically oriented to the systematic reduction of the variability of the value creation processes. For this reason, this thesis is focuses solely on lean management systems in an Industry 4.0 cyber–physical context.

On the basis of the previous concepts, the lean management of complex cyber–physical systems networked within an Industry 4.0 context, may be defined as business systems that seek systematically to decrease the inherent variability of industrial value creation processes, considering them as complex networks of interdependent computational and physical elements. Effective and efficient calculation of the information that flows through these elements is the key factor for achieving lasting and sustained business success.

With the advent of the Industry 4.0 paradigm, the possibilities of controlling manufacturing processes through the information provided by a network of sensors connected to work centers have expanded. Real-time monitoring of each parameter makes it possible to determine whether the values yielded by the corresponding sensor are in their normal operating range. In the interplay of the multitude of parameters, deterministic analysis quickly becomes intractable and one enters the realm of "uncertain knowledge". Bayesian decision networks are a recognized tool to control the effects of conditional probabilities in such systems. However, determining whether a manufacturing process is out of range requires significant computation time for a decision network, thus delaying the triggering of a malfunction alarm. From its origins, JIDOKA was conceived as a means to provide mechanisms to facilitate real-time identification of malfunctions in any step of the process, so that the production line could be stopped, the cause of the disruption identified for resolution, and ultimately the number of defective parts minimized. Our hypothesis is that we can model the internal sensor network of a computer numerical control machine with quantum simulations that show better performance than classical models based on decision networks. We show a successful test of our hypothesis by implementing a quantum digital twin that allows for the integration of quantum computing and Industry 4.0. This quantum digital twin simulates the intricate sensor network within a machine and permits, due to its high computational performance, to apply JIDOKA in real time within manufacturing processes.

Driven by an unprecedented level of transparency based on the global availability of information, companies are facing extremely competitive global markets in which customers' expectations have risen to demand very high quality standards at a low price and ever-increasing speeds [33]. Adding to this, requests for customized products are growing as to become the pattern in certain industries [34]. Manufacturing industry is relying on technology to face this challenging environment, with Industry 4.0 emerging as a paradigm that can provide solutions to keep track of the markets [35, 36].

For Industry 4.0 to be effective, interdisciplinary knowledge from engineering, computer science, business, and various other academic disciplines is crucial [37]. Lean Management

stands out as a consolidated managerial paradigm that tries to tackle the previously mentioned challenges, with a large history since it was grounded in the 1940s by Toyota production managers [20, 38–40]. The main goal of both Industry 4.0 and lean management is to find ways to deal with an ever increasing complexity in the manufacturing industry that nowadays partially stems from digitization, as well as mass customization. Although Industry 4.0 puts the focus on the technological elements, lean methods seek to find ways to reduce the complexity by designing clear and controllable processes that minimise non value-adding activities throughout the value chain [41]. To achieve this goal, a wide range of tools, initially conceived under the umbrella of the Toyota just-in-time system, such as synchronized production, Kanban, single minute exchange of die, cross-functional work force [42], and others, that evolved to gain its own field of development as total productive maintenance or total quality management [43], have been developed and put into practice in manufacturing environments. These techniques have shown significant positive effects in different industries and even synergistic benefits through their combined implementation [19, 44]. Combining the methodologies from Industry 4.0 and lean manufacturing has been an increasingly popular research topic, resulting in the so-called Lean 4.0 [45]. There are mixed opinions regarding whether lean management is needed to enable Industry 4.0 or Industry 4.0 advance lean management [46]. Yet, one of the key ideas about Industry 4.0 is the integration of varied technologies due to the limited effect of focusing on a single technology [47]. In fact, several of the many lean tools have been examined in the context of Industry 4.0 [48–50], leading to the conclusion that a leaner production is easier to integrate into an Industry 4.0 context and, in many cases, it is possible to combine the ideas and techniques from both frameworks [51, 52]. Moreover, it seems to be a necessary evolutionary step for further raising the level of operational excellence (i.e., to coordinate actions, to optimize resource efficiency, to improve work safety, to decrease in cost) [45].

Within organizations relevant process information is typically described by a series of KPIs. Such KPIs are interdependent and describe certain time–dependent trajectories in a $N$–dimensional space, in which $N$ is the number of nodes [53]. A node is to be in alignment at any given moment in time if the key performance indicator's trajectory presents asymptotic stability at this point in time [54]. In other words, the condition for alignment at any given time interval $t+\Delta t$ is given by

$$D_{t,t+\Delta t} < D_{t-\Delta t,t}, \forall \Delta t > 0 \tag{1.2}$$

where $D_{i,j}$ represents the euclidean distance between two points $i$ and $j$ in the key performance indicators's

trajectory. Consequently, the probability that the node is not in alignment is given by

$$D_{t,t+\Delta t} \geq D_{t-\Delta t,t}, \forall \Delta t > 0. \tag{1.3}$$

Alignment is thus a binary property of each cyber–physical node. Furthermore, since the trajectories are known for all times, we can calculate the conditional probability that the nodes within the complex networked strategic organizational design are simultaneously in alignment or not, by the simple application of the well known Bayes Theorem [55]. In fact, within this time interval $\Delta t$, the graph $\Omega$ described by Equation 1.1 converts into a decision network $\Omega' = [\Gamma', E']$ formed by a set of $\Gamma'$ nodes and $E'$ edges, where $\Gamma' = [\gamma_1, \gamma_2, ..., \gamma_N]$ represents the set of all the nodes being part of the network in $\Delta t$, and the edges are determined by the known probabilistic dependence of alignment occurrence in a node $\gamma_j$ depending on the alignment occurrence on another $\gamma_i$. The node $\gamma_i$ is thus called *parent* and node $\gamma_j$ the child. The root nodes are those that do not depend on any other. Subsequently, as described by [56], the joint probability on the nodes can be decomposed into the product of the marginal probabilities given by

$$P(\gamma_1, \gamma_2, ..., \gamma_N) = \prod_{i=1}^{N} P\left(\gamma_i | \prod \gamma_i\right), \tag{1.4}$$

where $\prod \gamma_i$ represents the set of parent nodes associated with $\gamma_i$. For the root nodes, $P(\gamma_i | \prod \gamma_i)$ becomes the marginal distribution $P(\gamma_i)$.

The interaction of these interdependent organizational agents shapes hierarchically nested complex networks [57]. These support managerial decision making towards an ideally coordinated effort to attain organizational strategic goal achievement called *organizational alignment*. These alignment efforts can occur in different organizational settings, although in this thesis we focus on complex networked cyber–physical systems within an Industry 4.0 context.

Leading Industry 4.0 processes to the coordinated achievement of objectives is a probabilistic process. Uncertainty in thus the name of the game for managers. As a consequence, value–creating networks can be considered as decision networks or probabilistic directed acyclic graphical models [55, 58] with known conditional probabilities, and such network per process, when considered as an ensemble, is nothing else than a multiple complex systems. Multiple complex systems can be found as well in many other fields such as the human nervous system [59], forests [60], city transportation systems [61], social networks [62] or insect colonies [63], which present a multilayered hierarchical network structure. The emergence of this type of configuration confers on the system a series of evolutionary fitness advantages [64] such as the development

of distributed swarm intelligence [65], systemic learning through information aggregation [66], effective goal achievement and complex problem solving [67], or greater resilience to changes [68]. Indeed, the strategic design of organizations takes such complexity into account[69] for cyber–physical systems of Industry 4.0 [70], where they start to be understood as socio–technical complex networked configurations at various levels of complexity [71–74].

The simulation of individual systems in Industry 4.0 is frequently addressed by means of digital twins. Although the digital twin concept is well established, it is usually crafted in different ways depending on the application and discipline, and they have the vision for representing physical assets, allowing different component models [75]. Most of the effort in creating digital twins are spent in gathering data and training models. However, little efforts have been done to exploit the hierarchical relationship between systems in an integrated way. Therefore, a significant gap regarding digital twins is the lack of integration, not only at the same level, losing the capability of promoting their interactions fostering the information value chain, but even vertically, where the upper hierarchical levels are not aware of the status of subsystems or components, relevant for their processing status. The main reason is because of the high complexity involved, which makes it hard to consider all components at all hierarchical levels.

Scientific literature proposes approaches to qualitatively model organizational alignment [76–81]. Approaches that allow for a quantification of organizational alignment are less common, which shows the alignment state of each node is known at each discrete time interval. The Nemawashi approach [53], based on genetic algorithms, is however computationally very costly and therefore difficult to implement in practice. While calculating the alignment state of the entire network is theoretically possible with this method, in practice, it is a challenge that leads to an exponential increase of calculation time with augmenting network size. For this reason, there is an urgent need to provide organizational leaders with a fast algorithm that allows for a calculation of the alignment status of the organization.

Quantum computing is a novel computation paradigm that might prove useful to this end [82]. Quantum computing examines the flow and processing of information as physical phenomena that follow the laws of quantum mechanics. This is possible because quantum computing makes use of "superposition", which is the ability of quantum computers to be simultaneously in multiple different states [83]. By doing so, quantum computing has shown promising performance increases in solving certain unassailable problems for classic computing such as Shor's algorithm [84] and Grover's algorithm [85]. It has opened new ways of solving some problems, e.g., in machine learning [86], finance [87], or human interaction [88]. Industry 4.0 problems using machine learning are likely to benefit from quantum models of computation [89]. A quantum simulation

may also be used to optimize the configuration of the cyber–physical resources that conform to these systems. It has already been shown how quantum simulations can be used to describe networks of interdependent resources [90, 91].

## 1.2 Quantum Industry 4.0 Cyber–Physical System Framework

To provide the reader with an adequate framework in which to contextualize the thesis, the below a graphical abstract of Figure 1.1 combines the system theory as well as its digital translation, and the use of quantum decision networks to propose a quantum framework for Industry 4.0 cyber–physical systems, able to deal with its hierarchical interdependent nature. This figure shows a two–dimensional socio–technical multilayered network framework in which the resources that make up the cyber–physical system are modeled as a network of qubits (elementary units of information exchange in quantum computing) [92]. Each of these elements present a certain probability of alignment that is bounded by upper– and lower– specification limits (USL, LSL) respectively that represent the process capability measures.

In Figure 1.1 the horizontal axis represents the social dimension with different networks of qubits describing social systems of increasing complexity:

- network of wearables within a person,
- network of people within a team,
- network of teams within an organization,
- network of organizations within a supra–organization.

In Figure 1.1 the vertical axis represents the hierarchical dimension describing technical systems of increasing complexity:

- network of sensors within a machine,
- networks of machine within a process,
- network of processes within a factory,
- network of factories within a supply–chain.

This framework provides a hierarchically nested configuration in which the lower level is integrated in the upper level, i.e. the network of sensors measuring the state of a machine are within the machine

and hence within the the network of machines. Each system component is independent and connected with others as defined by the users, facilitating the assembly of a multilayered network structure. This allows users to assess different strategies according to various situations or configurations. Furthermore, this thesis develops methods to evaluate the effects of resource or system failure at a specific level as well as its propagation and impact.

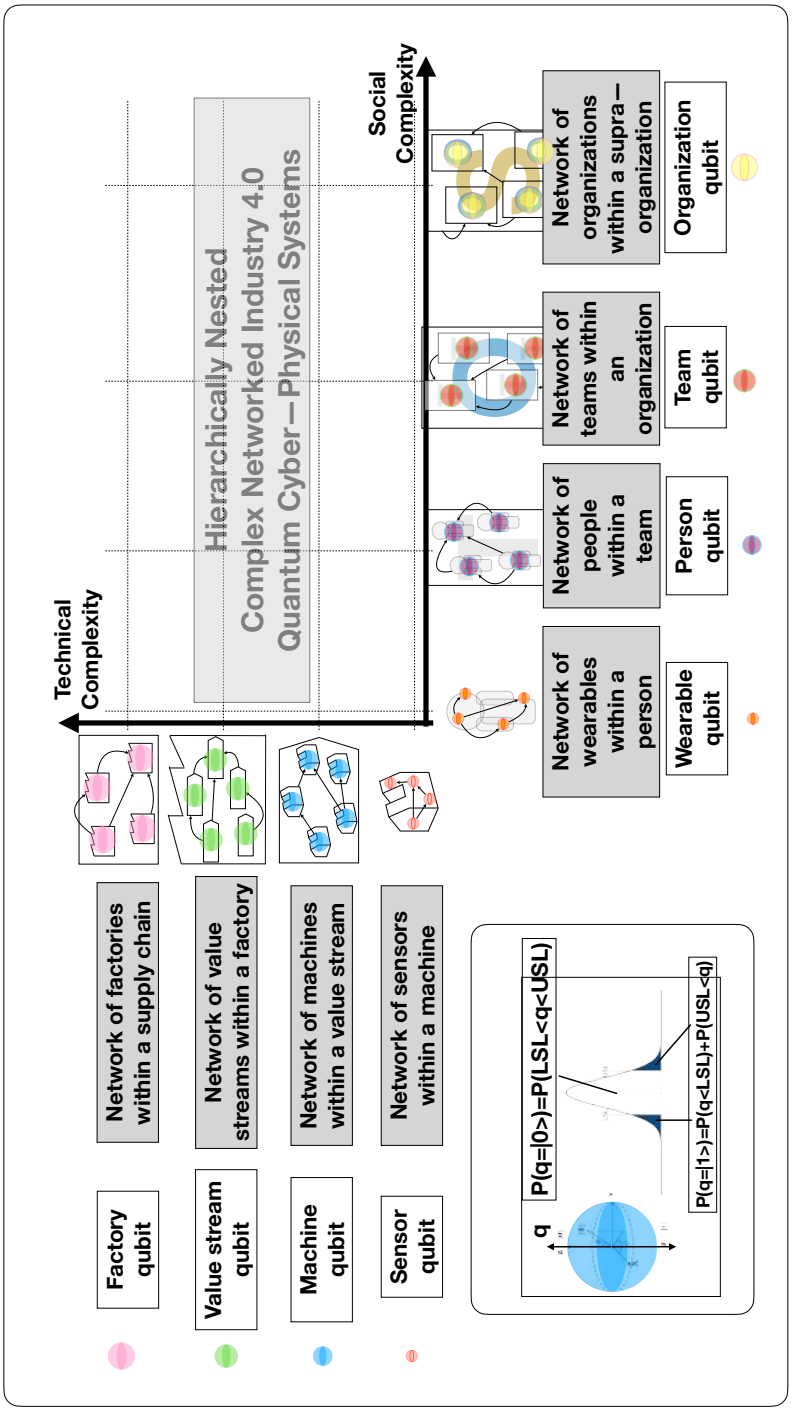


**Figure 1.1:** Framework for Quantum Industry 4.0 Cyber–Physical Systems

## 1.3 Objectives

The main goal of this thesis is to propose efficient quantum computation algorithms for real–time strategic design of lean complex cyber–physical industrial networked organizations and their practical implementation and, therefore, support the leaders of organizations in their decision–making process.

With this goal in mind, this thesis aims to:

1. **O1**. Propose a novel quantum strategic organizational design (QSOD) configuration of distributed quantum circuits in multi–layered complex networks that enable the evaluation of Industry 4.0 lean complex networks.

2. **O2**. Propose two different mechanisms for the integration of information between circuits operating at different layers, and analyze and compare their behavior with the classical conditional probability tables linked to the Bayesian networks.

3. **O3**. Demonstrate that quantum circuits can improve the performance of classic algorithms in optimizing certain complex industrial processes by solving simple practical cases of chains of command and dependency in industrial processes.

4. **O4**. Implement the theoretical development based on quantum principles in a device that allows to discern in real time the need to modify an industrial process due to the presence of production errors and to achieve an intuitive interface for the people who use it.

## 1.4 Structure of the thesis

The rest of the thesis hereinafter continues as follows: first, Chapter 2 begins by defining some essential preliminary concepts for the precise use of terminology in the following chapters of the thesis and then presents an original work describing a model and design principles for enabling organizational leaders to perform QSOD. Second, Chapter 3 proposes a novel QSOD configuration of distributed circuits in multi–layered complex networks that enable the evaluation in Industry 4.0 lean complex networks and proposes two different mechanisms for the integration of information between circuits operating at different layers, analyze and compare their behavior with the classical conditional probability tables linked to the Bayesian networks. Third, Chapter 4 presents several implementation cases of the theoretical developments in different Industry 4.0 organizational contexts. Fourth, in Chapter 5, we implement the theoretical development based on quantum principles in a

device that allows to discern in real time the need to modify an industrial process due to the presence of production errors and to achieve an intuitive interface for the people who use it. Fifth, in Chapter 6, we present an improvement of a node sorting algorithm in an industrial value creation chain by means of a novel quantum circuit that improves the state of the art performance. Finally, Chapter 7 outlines the conclusions and some final remarks.

# 2

# Fundamentals of Quantum Strategic Organizational Design

In this Chapter we present the fundamentals of QSOD. First, we start by outlining in Section 2.1 the basic concepts of quantum computation. Second, in Section 2.2 we present a systematic approach to design decision networks as quantum circuits. Finally, in order to make these concepts clear for the interested reader, in Section 2.3 we present a numerical example that applies these concepts in a four node organizational configuration.

## 2.1 Quantum Computing Fundamentals

This section briefly present several quantum computing fundamentals for the general reader:

- **Qubits**

  Information may be represented in many different ways. Quantum computing uses quantum discrete units of information, called the qubit (quantum bit) [93]. Qubits represent elementary units of information exchange in quantum computing, similar to the "bits" of classical computing. A *bit* is always in two basic states, 0 or 1, while a qubit can be in "both" of these states simultaneously. The characteristic is also known as *superposition*. Quantum computing normally uses the Dirac notation that represents the two bases of computing of these states as $|0\rangle$ and $|1\rangle$. The *superposition* of a $|\Psi\rangle$ qubit is merely a linear combination of the two basic states $|0\rangle$ and $|1\rangle$, expressed as

$$|\Psi\rangle = c_0 |0\rangle + c_1 |1\rangle , \tag{2.1}$$

  where $c_0, c_1 \in \mathbb{C}$ such that they satisfy the equation:

$$|c_0|^2 + |c_1|^2 = 1, \tag{2.2}$$

  where $|c_0|^2$ and $|c_1|^2$ are, respectively, the probabilities of finding the qubit in $|0\rangle$ and $|1\rangle$ after a measurement.

- **Bloch's sphere**

  Bloch's sphere, sketched in Figure 2.1A, is commonly used to geometrically represent a qubit [94]. This is a useful and common geometric image of the quantum evolution of a single- or two-level system.

  On the Bloch sphere, of unitary radius, the $Z$-axis is the computational axis and its positive direction coincides with the state $|0\rangle$, and the negative one with the state $|1\rangle$. A qubit can be represented as a point on the Bloch sphere with the help of two parameters $(\theta, \varphi)$, as expressed by:

$$|\Psi\rangle = \cos\left(\frac{\theta}{2}\right) |0\rangle + e^{i\varphi} \sin\left(\frac{\theta}{2}\right) |1\rangle . \tag{2.3}$$

  When several qubit are utilized, their aggregated state can be determined utilizing the tensorial product of the individual qubits. If the multiple qubit state can be expressed as a linear combination of the $|0\rangle$ and $|1\rangle$ states, then the aggregated state can be represented as in equation:

$$|\Psi_1\rangle \otimes |\Psi_2\rangle = c_{11}c_{21} |00\rangle + c_{11}c_{22} |01\rangle + c_{12}c_{21} |10\rangle + c_{12}c_{22} |11\rangle , \tag{2.4}$$

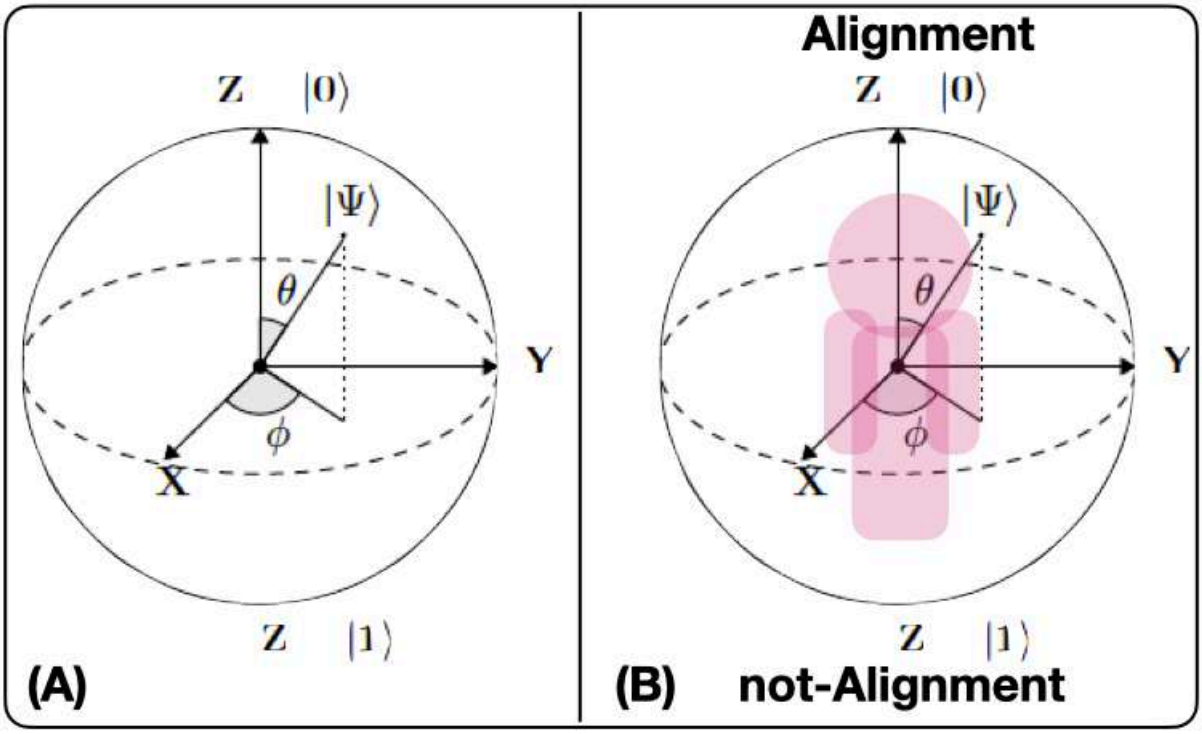


**Figure 2.1:** (A) Bloch sphere standard representation. (B) Quantum Strategic Organizational Design Bloch sphere as a node of a decision complex–networked cyber–physical lean management system.

where $|\Upsilon_1\rangle = c_{11}|0\rangle + c_{12}|1\rangle$ and $|\Upsilon_2\rangle = c_{21}|0\rangle + c_{22}|1\rangle$. Certainly, if the aggregate state cannot be expressed as the product of the individual states, in other words, if no qubit states $|a\rangle$ and $|b\rangle$ can be found such that $|\Upsilon\rangle = |a\rangle|b\rangle$, this state is called *entangled state*, which is a purely quantum correlation much stronger than any other classical one [95].

The reduced purity $\kappa_j$ of a qubit $q_j$ in an $N-$ *qubit* state $|\Upsilon\rangle$, given by Equation 2.5, is a coefficient $\kappa_j \in [0.5, 1]$ that indicates the level of a qubit entanglement in the state [92]. A value of $\kappa_j = 1$ indicates that the qubit is not entangled with the other $N-1$ qubits, while a value of $\kappa_j = 0.5$ indicates that the qubit is maximally entangled with the other qubits in the state.

$$\kappa_j = Tr[Tr_{i\in[0,N-1],i\neq j}\ |\psi\rangle\langle\psi|]^2. \tag{2.5}$$

- **Quantum Circuit**

A quantum circuit is a computational sequence that consists of performing a series of coherent quantum (unitary) operations on qubits. By organizing the qubits into an orderly sequence of quantum gates, measurements, and resets, all of which can be conditioned and use data from the classical calculation in real-time, quantum computing can be simulated. These sequences typically follow a standardized

pattern:

1. Initialization and reset. First, we begin our quantum calculation with a specified quantum state for each qubit. This is achieved using the initialization operations, typically on the $Z$-computation axis, and reset. The resets can be done using a *single-qubit* gate combination that tracks whether we have succeeded in creating the desired state through measurements. qubit initialization in a desired state $|\Psi\rangle$ can then continue to apply *single-qubit* gates.
2. Quantum gates. Second, we implement a sequence of quantum gates that manipulate the qubits as needed by the targeted algorithm following certain quantum circuit design principles.
3. Measurement. Third, we measure the qubits. Classical computers translate the measurements of each qubit as classical results (0 and 1) and store them in either one of the two classical bits. Measurement is understood to be projected into the $Z$-computational basis unless otherwise stated.

- **Quantum gate**

A quantum gate consists of several mathematical operations applied to the qubits that change the amplitude of their probabilities and thus perform the intended computations [92]. The quantum computing basic elements are described in detail:

– The $U_3(\theta, \varphi, \lambda)$ gate is a single qubit gate that has three parameters $\theta$, $\varphi$ and $\lambda$ which represent a sequence of rotations around the Bloch sphere's axes such as $[\lambda]$ around the $Z$ axis, $[\pi/2]$ around the $X$ axis, $[\theta]$ around the $Z$ axis, $[-\pi/2]$ around the $X$ axis, and $[\varphi]$ around the $Z$ axis. It can be used to obtain any single qubit gate. Equation 2.6 provides its mathematical representation.

$$U_3 |\Psi\rangle = \begin{bmatrix} cos(\frac{\theta}{2}) & -e^{i\lambda} sin(\frac{\theta}{2}) \\ e^{i\varphi} sin(\frac{\theta}{2}) & e^{i(\varphi+\lambda)} cos(\frac{\theta}{2}) \end{bmatrix} |\Psi\rangle \,. \tag{2.6}$$

Equation 2.7 represents its quantum circuit equivalent:

$$|\Psi\rangle \quad \boxed{U_3(\theta, \varphi, \lambda)} \quad . \tag{2.7}$$

– The *CNOT* or conditional NOT gate is a two qubit computation gate with one *qubit* acting as *control* $|\Psi_1\rangle$ and the other as *target* $|\Psi_2\rangle$. The *CNOT* gate performs a selective negation of the

target qubit. If the control qubit is in *superposition*, then *CNOT* creates *entanglement*. Equation 2.8 provides its mathematical representation.

$$CNOT\left|\Psi_1\right\rangle\left|\Psi_2\right\rangle = \left|\Psi_1\right\rangle\left|\Psi_1 \oplus \Psi 2\right\rangle. \tag{2.8}$$

Equation 2.9 represents its quantum circuit equivalent:

$$\begin{matrix}\left|\Psi_1\right\rangle \\ \left|\Psi_2\right\rangle\end{matrix} \quad \begin{matrix}\bullet \\ \oplus\end{matrix} \quad = \begin{bmatrix} 1 & 0 & 0 & 0 \\ 0 & 1 & 0 & 0 \\ 0 & 0 & 0 & 1 \\ 0 & 0 & 1 & 0 \end{bmatrix}. \tag{2.9}$$

– The *ccX* or Toffoli gate is a three qubit computation gate with two qubits $\left|\Psi_1\right\rangle$ and $\left|\Psi_2\right\rangle$ acting as controls and one qubit $\left|\Psi_3\right\rangle$ acting as target. The *ccX* gate applies an $X$ to the target qubit $\left|\Psi_3\right\rangle$ only when both controls $\left|\Psi_1\right\rangle$ and $\left|\Psi_2\right\rangle$ qubits are in state $\left|1\right\rangle$. Equation 2.10 provides its mathematical representation.

$$ccX\left|\Psi_1\right\rangle\left|\Psi_2\right\rangle\left|\Psi_3\right\rangle = \left|\Psi_1\right\rangle\left|\Psi_1 \oplus \Psi 2\right\rangle\left|\Psi_1\right\rangle\left|\Psi_1 \oplus \Psi 3\right\rangle. \tag{2.10}$$

Equation 2.11 represents its quantum circuit equivalent [92]:

$$\begin{matrix}\left|\Psi_1\right\rangle \\ \left|\Psi_2\right\rangle \\ \left|\Psi_3\right\rangle\end{matrix} \quad \begin{matrix}\bullet \\ \bullet \\ \oplus\end{matrix} \quad = \quad \begin{matrix}\left|\Psi_1\right\rangle \\ \left|\Psi_2\right\rangle \\ \left|\Psi_3\right\rangle\end{matrix} \quad \begin{matrix}\bullet & \\ \oplus & \bullet \\ & \oplus\end{matrix} \quad = \begin{bmatrix} 1 & 0 & 0 & 0 & 0 & 0 & 0 & 0 \\ 0 & 1 & 0 & 0 & 0 & 0 & 0 & 0 \\ 0 & 0 & 1 & 0 & 0 & 0 & 0 & 0 \\ 0 & 0 & 0 & 1 & 0 & 0 & 0 & 0 \\ 0 & 0 & 0 & 0 & 1 & 0 & 0 & 0 \\ 0 & 0 & 0 & 0 & 0 & 1 & 0 & 0 \\ 0 & 0 & 0 & 0 & 0 & 0 & 0 & 1 \\ 0 & 0 & 0 & 0 & 0 & 0 & 1 & 0 \end{bmatrix}. \tag{2.11}$$

– The $Z$ − *measurement* of a quantum state – a self-adjoint operator on the Hilbert space – results in the measured object being in an eigenstate of the $Z$ operator or computational basis, with the corresponding eigenvalue being the value measured. The measurement, also called observation, of a quantum state, is a stochastic non-reversible operation and therefore cannot be considered

as a quantum gate, as it allocates a unique value to the variable observed. In mathematical terms, the probability $p$ of a measurement result $m$ occurring when the state $|\Psi\rangle$ is measured is given by Equation 2.12.

$$p(m) = \langle\Psi|M_m^\dagger M_m|\Psi\rangle\,, \tag{2.12}$$

where $[M_m]$ represents a set of operators acting on the state space such that $I = \sum_m p(m)$ and the state of the system after the measurement $|\Psi'\rangle$ is given by:

$$|\Psi'\rangle = \frac{M_m\,|\Psi\rangle}{\sqrt{p(m)}}. \tag{2.13}$$

Equation 2.14 shows its quantum circuit equivalent as a symbolic box:

$|\Psi\rangle$  . (2.14)

- **Density Matrix**

An alternative representation of the quantum state as applied to an entry $x$, $\langle\Psi(x)|$ is given by an Hermitian operator $\rho(x) = |\Psi(x)\rangle\langle\Psi(x)|$ called density matrix which contains all the observable information of the quantum state. Quantum circuits map therefore the input into a high–dimensional feature space in which statistical properties of the measurement $\mathscr{M}$ are interpreted as output of the quantum circuit. These measurements, which correspond to a Hermitian operator $\mathscr{M}$ acting on vectors in the Hilbert space of the quantum circuit $\mathscr{H}$ and live in a subspace of the data–encoding feature space $\mathscr{F}$ are in general not linear in the Hilbert space $\mathscr{H}$ of the quantum circuit [96]. However, according to the celebrated *representer theorem* [97], an optimal quantum kernel can be found that allows describing the quantum circuits as linear models in the space of the Hermitian operator $\rho(x)$ with the form $\mathrm{tr}\left[\left(\sum_{m=1}^{M}\alpha_m\rho(x^m)\right)\rho(x)\right]$ where $x^m$, $m = 1,\ldots,M$, is the input data and $\alpha_m \in \mathbb{R}$. In other words, if we find a linear transformation of our quantum state vector $|\Psi(x)\rangle$, we are guaranteed that the best measurements for our quantum circuit only has $M << 2^{2n}$ degrees of freedom, rather than the $\mathcal{O}(2^{2n})$ degrees of freedom of a quantum circuit with n qubits.

## 2.2 Quantum Circuit Design

This section outlines several design principles for enabling organizational leaders to perform QSOD. This model consists of three steps: first, it introduces in Section 2.2.1 the definition of the QSOD qubit as a fractal unit of the decision Industry 4.0 complex–networked cyber–physical lean management systems. Second, it outlines in Section 2.2.2 the design principles that are to be applied to represent such systems as a quantum circuit. Finally, it provides in Section 2.3 guidelines for the interpretation of the results by means of a case of study.

### 2.2.1 Quantum Strategic Organizational Design Qubit.

We define the QSOD qubit, as depicted in Figure 2.1B, as the node of a decision complex–networked cyber–physical lean management system: a human or cyber–physical asset that is in the center of an imaginary Bloch sphere (2.1B), in which the state of alignment and not-alignment references respectively with the QSOD qubit $|0\rangle$ and $|1\rangle$ computational states.

### 2.2.2 Quantum Strategic Organizational Design principles.

- **Calculation of conditional probabilities**

  The conditional probabilities that will give rise to the quantum circuit are derived from a preliminary analysis of the KPIs associated with each node of the complex network in question. This analysis, as indicated above, is based on the method based on genetic algorithms presented in [53]. Specifically, for each node, there are typically three KPIs related. The selected chromosome has subsequently 12 real numbers between 0 and 1, and we have used real value crossover and mutation with probabilities of 60% and 7% respectively. The population was built over 8000 individuals and it ran over 1000 generations. Once the trajectories associated with each node have been calculated, by applying the Bayes theorem, it is trivial to calculate the relative probability of alignment or non-alignment at each node concerning those to which it is connected.

- **Initialization and reset**

  The initialization and reset of the qubits is typically standardized to the state $|0\rangle$ on the computational $Z$-axis.

- **Rotation angle computation**

The conditional probabilities translate into qubit rotation angles depending on its decision network dependencies:

- For a root node with no parents, the possible states are two $|0\rangle$ and $|1\rangle$. A trivial application of Equation 2.3 states that a qubit intialized to state $|0\rangle$ and rotated by a gate $U_3(\theta, 0, 0)$, being $\varphi = 0$, transforms it into $|\Psi\rangle = \cos\left(\frac{\theta}{2}\right)|0\rangle + \sin\left(\frac{\theta}{2}\right)|1\rangle$. Therefore, taking Equation 2.1 into account and the definition of the Bloch sphere's angles, the rotation angle $\theta$ required to calculate the probabilities of being in state $|0\rangle$ and $|1\rangle$ can be expressed by:

$$\theta = 2\arctan\left[\tan\left(\frac{\theta}{2}\right)\right] = 2\arctan\sqrt{\frac{sin^2\left(\frac{\theta}{2}\right)}{\cos^2\left(\frac{\theta}{2}\right)}} \overset{Eq.2.1}{=} 2\arctan\sqrt{\frac{p(|1\rangle)}{p(|0\rangle)}}. \tag{2.15}$$

- In general, for a child node $\gamma_i$ with m parents there are $2^m$ possible states $\prod \gamma_i^*$ with $i = [1, , ..., m]$. Subsequently, taking Equation 1.4, Equation 2.1 and Equation 2.3 into account, as well as the definition of the Bloch sphere's angles, the rotation angle is given by:

$$\theta_{\gamma_i, \prod \gamma_i^*} \overset{Eq.1.4-Eq.2.1}{=} 2\arctan\sqrt{\frac{p(|1\rangle \,|\, \prod \gamma_i = \prod \gamma_i^*)}{p(|0\rangle \,|\, \prod \gamma_i = \prod \gamma_i^*)}}. \tag{2.16}$$

- **Controlled rotations**

Controlled rotations are not elementary quantum gates and need to be deconstructed into elementary operations. As described by Nielsen and Chuang [92], being $m$ the maximum number of parent nodes a child has, the controlled rotation expressing the conditional probabilities needs of the addition of $a_i$ "dummy" or "ancilla" qubits $i = [1, ..., m-1]$ in order to decompose the controlled rotation into $2(m-1)$ *CNOT* gates and one $U_3(\theta, 0, 0)$. This is exemplified in Equation 2.17 for $m = 5$ qubits, $a_i$ "dummy" qubits $i = 1, ..., (m-1=4)$ and a total of $2(m-1) = 8$ *CNOT* gates.

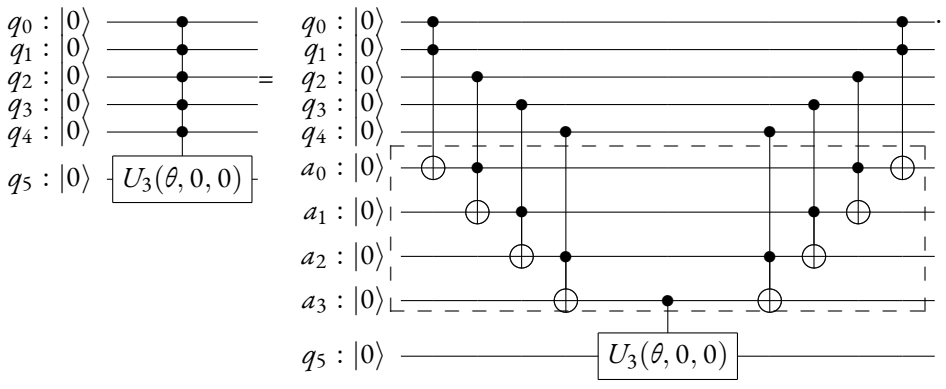


(2.17)

As first shown in [98] it is important to highlight that $U_3(\theta, 0, 0)$ is best decomposed as

$$U_3(\theta,0,0)\,|\Psi_1\rangle\,|\Psi_2\rangle = U_3\left(\frac{\theta}{2},0,0\right)|\Psi_2\rangle\,CNOT|\Psi_1\rangle\,|\Psi_2\rangle\,U_3\left(\frac{-\theta}{2},0,0\right)|\Psi_2\rangle\,CNOT|\Psi_1\rangle\,|\Psi_2\rangle\,. \tag{2.18}$$

And as a direct application of Equation 2.9, this equation converts into:

$$U_3(\theta,0,0)\,|\Psi_1\rangle\,|\Psi_2\rangle \overset{Eq.2.9}{=} U_3\left(\frac{\theta}{2},0,0\right)|\Psi_2\rangle\,|\Psi_1\rangle\,|\Psi_1\oplus\Psi 2\rangle\,U_3\left(\frac{-\theta}{2},0,0\right)|\Psi_2\rangle\,|\Psi_1\rangle\,|\Psi_1\oplus\Psi 2\rangle\,. \tag{2.19}$$

or in its quantum circuit equivalent shown by:

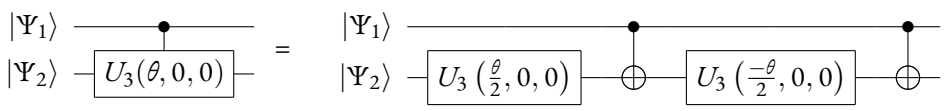


. (2.20)

This method works because if the control qubit $|\Psi_1\rangle$ is in state $|0\rangle$, all we have is $U_3\left(\frac{\theta}{2},0,0\right)$ followed by a $U_3\left(\frac{-\theta}{2},0,0\right)$ and the effect is trivial. If the control qubit $|\Psi_1\rangle$ is in state $|1\rangle$, the net effect is a controlled rotation $U_3(\theta,0,0)$ on the $|\Psi_2\rangle$ qubit.

- **Measurement**

  The measurements used in the end to extract computational results from the quantum states. This will allow us to explore the quantum states of the qubits and to make an interpretation that allows improving the management system related to the industrial process.

## 2.3 Example of Quantum Strategic Organizational Design Circuit

To illustrate the implementation of the outlined principles for QSOD method within a cyber–physical complex networked lean management system in an Industry 4.0 context, this section shows an example of a quantum circuit that allows calculating the alignment states of the system. Following the recommendations of [99], we follow a clear case study roadmap to ensure the replicability and soundness of the results obtained. This roadmap has several phases:

- Section 2.3.1. Scope establishment.
- Section 2.3.2. Specification of population and sampling.
- Section 2.3.3. QSOD circuit design.

### 2.3.1 Scope establishment

We aim to study the organizational alignment state of an Industry 4.0 factory that resembles a cyber–physical complex networked lean management system by modeling the strategic organizational design throughout a quantum circuit. Specifically, our goal is to calculate the absolute alignment probabilities of each node within the network with aid of the QSOD pronciples described in the previous section.

### 2.3.2 Specification of population and sampling

As described in Figure 2.2, the system consists on four managers forming a reporting network. Data on these four team members in a factory at three relevant hierarchical levels are taken over twelve weeks daily. At level 1 the factory leader, at level 2 a logistics leader, and a production leader both reporting to level 1 and at level 3 a production line leader reporting to the level 2 production leader. Each leaders' performance is measured through three KPIs, so there is a total of 12 KPIs being measured with the same frequency.

The case study starts by representing a decision network from this data as indicated in Section 2.2.2. In this figure we observe four nodes $q_A$, $q_B$, $q_C$, $q_D$, corresponding to each process owner. The respective alignment conditional probabilities are shown in Figure 2.2, for instance the probability of alignment of node $q_A$, given by $P_A(|0\rangle)$, is 0.75 and the probability of alignment of node $q_B$ conditioned to the alignment of node $q_A$, given by $P_{B|A}(|0\rangle \,|\, |0\rangle)$, is 0.65.

### 2.3.3 Quantum strategic organizational design circuit design

We now proceed to implement each of the indicated steps in Section 2.2.2 in a systematic way to generate a QSOD circuit that represents the alignment probabilities of the whole system. To allow for a better understanding of the elements of the quantum circuit and to facilitate the visualization of the effect of each step on the whole system, each one of the 37 steps of the circuit has been denoted with a number.

- **Calculation of conditional probabilities**

  As shown in [53], for each node, there are typically three KPIs related. The selected chromosome has subsequently 12 real numbers between 0 and 1, and we have used real value crossover and mutation with

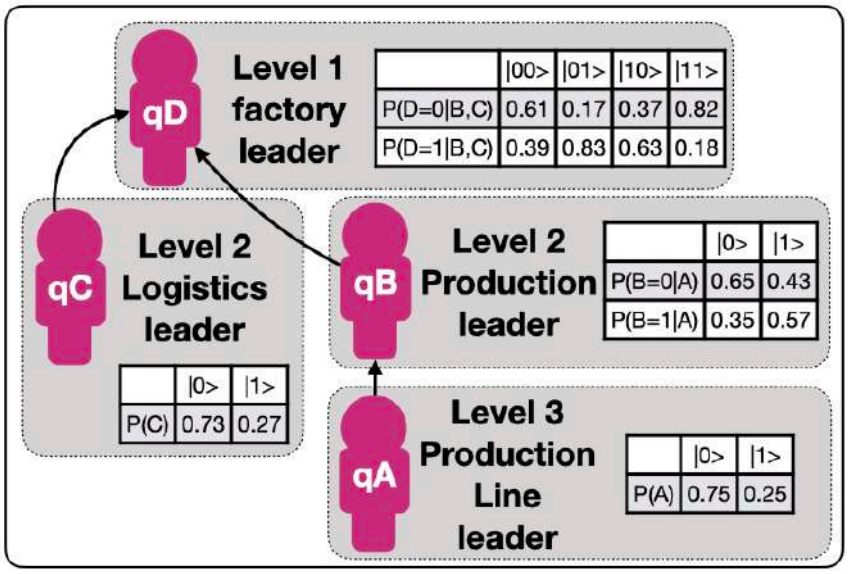


**Figure 2.2:** Example. Strategic Organizational Design Decision Network with Conditional Alignment Probabilities.

probabilities of 60% and 7% respectively. The population was built over 8000 individuals and it ran over 1000 generations. Once the trajectories associated with each node have been calculated, it is trivial to calculate the relative probability of alignment or non-alignment at each node concerning those to which it is connected. These probabilities are shown in Figure 2.2. This process is executed for each node in parallel without loss of performance.

- **Initialization and reset**

  In Step 0, each one of the nodes is assigned to a qubit, $q_A$, $q_B$, $q_C$, $q_D$, and a "dummy" node $q^*$ is created. The qubits are initialized and reset to $|0\rangle$ state. This allows for a controlled comparison of the probabilities through qubit rotations.

- **Rotation angle computation**

  Equation 2.15 applied to each root qubit, we obtain following results given by:

$$\theta_A \overset{Eq.2.15}{=} 2\arctan\sqrt{\frac{0.25327658}{0.74672341}} = 1.16479 \text{ rad}, \quad \theta_C \overset{Eq.2.15}{=} 2\arctan\sqrt{\frac{0.27}{0.73}} = 1.0928 \text{ rad}. \tag{2.21}$$

Equation 2.16 applied to each child qubit, we obtain following results given by:

$$\begin{aligned}
\theta_{B,|0\rangle} &\overset{Eq.2.16}{=} 2\arctan\sqrt{\tfrac{0.35}{0.65}} = 1.2661 \text{ rad}, & \theta_{B,|1\rangle} &\overset{Eq.2.16}{=} 2\arctan\sqrt{\tfrac{0.57}{0.43}} = 1.7113 \text{ rad} \\
\theta_{D,|00\rangle} &\overset{Eq.2.16}{=} 2\arctan\sqrt{\tfrac{0.39}{0.61}} = 1.3489 \text{ rad}, & \theta_{D,|01\rangle} &\overset{Eq.2.16}{=} 2\arctan\sqrt{\tfrac{0.83}{0.17}} = 2.29161 \text{ rad} \\
\theta_{D,|10\rangle} &\overset{Eq.2.16}{=} 2\arctan\sqrt{\tfrac{0.63}{0.37}} = 1.83382 \text{ rad}, & \theta_{D,|11\rangle} &\overset{Eq.2.16}{=} 2\arctan\sqrt{\tfrac{0.18}{0.82}} = 0.87629 \text{ rad}.
\end{aligned} \tag{2.22}$$

- **Controlled rotations**

  As shown in Equations 2.21 and 2.22, which systematically apply Equation 2.17 to each qubit, we obtain the QSOD circuit shown in Figure 2.3.

  The quantum state of each step of the final state has been visualized in Figure 2.4A. The Bloch sphere provides a global view of a multi–qubit quantum state in the computational basis. Node size is proportional to state probabilities, and color reflects the phase of each basis state as shown in Figure 2.4B.

  To improve the clarity of the explanation, the 37 steps that make up the QSOD have been divided into six distinct phases. We now comment on the logic behind each of them:

  – **Phase** 0**. Step** 0. Phase 0 performs the initialization and reset as previously explained in Section 2.3.3.

  – **Phase** 1**. Steps** 1 – 11. This phase is subdivided in three conceptual parts: first. This phase starts in Step 1 by rotating $q_A$ and $q_C$ by $\theta_A = 1.16479$ rad and $\theta_C = 1.0928$ rad respectively as calculated in Equation 2.21. This is because both $q_A$ and $q_C$ are root qubits and Equation 2.15 applies. Second, two controlled rotations on qubit $q_B$ in Steps 1-3 are performed as calculated in Equation 2.22. As described in Equation 2.20, since qubit $q_B$ has a parent qubit $q_A$, we need to perform two controlled rotations properly aligned by CNOT gates. Depending on the state of qubit $q_A$: $\frac{\theta_{B,|1\rangle}}{2} = 0.85592$ rad in Step 1 and $\frac{-\theta_{B,|1\rangle}}{2} = -0.85592$ rad in Step 3, in the case that $q_A$ is in state $|1\rangle$, and $\frac{\theta_{B,|0\rangle}}{2} = 0.63305$ rad in Step 5 and $\frac{-\theta_{B,|0\rangle}}{2} = -0.63305$ rad in the case that $q_A$ is in state $|0\rangle$. In this case a $U_3(\pi, -\frac{\pi}{2}, \frac{\pi}{2})$ is performed so as to generate proper alignment. Third, on qubit $q_D$ we need to perform a total of four controlled rotations throughout the circuit. This is because each of its parent qubits $q_B$ and $q_C$ can have two states, and we need to represent the rotations

corresponding to the states $|00\rangle$, $|10\rangle$, $|01\rangle$, and $|11\rangle$. A controlled rotation $\theta_{D,|11\rangle}$ is performed on qubit $q_D$ conditioned by the state $|11\rangle$ of its parent qubits $q_B$ and $q_C$ as calculated in Equation 2.22. This is done with a controlled rotation $\frac{\theta_{D,|11\rangle}}{2} = 0.43814$ rad in Step 1 and a controlled rotation $\frac{-\theta_{D,|11\rangle}}{2} = -0.43814$ rad in Step 11, properly aligned through CNOT and ccX gates as described in Equation 2.17 in Steps 9–10 and Steps 31–33.

– **Phase** 2. **Steps** 12 – 17. In phase 2, we perform the second controlled rotation on qubit $q_D$ as related to the states $|00\rangle$ of qubit $q_B$ and $q_C$. A controlled rotation $\theta_{D,|00\rangle}$ is performed on qubit $q_D$ conditioned by the state $|00\rangle$ of its parent qubits $q_B$ and $q_C$ as calculated in Equation 2.22. This is done with a controlled rotation $\frac{\theta_{D,|00\rangle}}{2} = 0.67449$ rad in Step 13 and a controlled rotation $\frac{-\theta_{D,|00\rangle}}{2} = -0.67449$ rad in Step 17, properly aligned through CNOT and ccX gates as described in Equation 2.17 in Steps 12 and Steps 14–16.

– **Phase** 3. **Steps** 18 – 24. In phase 3, we perform the second controlled rotation on qubit $q_D$ as related to the states $|10\rangle$ of qubit $q_B$ and $q_C$. A controlled rotation $\theta_{D,|10\rangle}$ is performed on qubit $q_D$ conditioned by the state $|10\rangle$ of its parent qubits $q_B$ and $q_C$ as calculated in Equation 2.22. This is done with a controlled rotation $\frac{\theta_{D,|10\rangle}}{2} = 0.91690$ rad in Step 19 and a controlled rotation $\frac{-\theta_{D,|10\rangle}}{2} = -0.91690$ rad in Step 24, properly aligned through CNOT and ccX gates as described in Equation 2.17 in Steps 18 and Steps 20–23.

– **Phase** 4. **Steps** 25 – 30. In phase 4, we perform the second controlled rotation on qubit $q_D$ as related to the states $|01\rangle$ of qubit $q_B$ and $q_C$. A controlled rotation $\theta_{D,|10\rangle}$ is performed on qubit $q_D$ conditioned by the state $|01\rangle$ of its parent qubits $q_B$ and $q_C$ as calculated in Equation 2.22. This is done with a controlled rotation $\frac{\theta_{D,|01\rangle}}{2} = 1.1458$ rad in Step 26 and a controlled rotation $\frac{-\theta_{D,|01\rangle}}{2} = -1.1458$ rad in Step 30, properly aligned through CNOT and ccX gates as described in Equation 2.17 in Steps 25 and Steps 27–29.

– **Phase** 5. **Steps** 31 – 33. As mentioned earlier, in phase 5 the controlled rotation of qubit $q_D$ as related to the states $|00\rangle$ of qubit $q_B$ and $q_C$ started in Phase 1, qubits 1 and 9–11, is completed.

– **Phase** 6. **Steps** 34 – 37. Finally, in phase 6 each one of the qubits is measured as expressed by

Equation 2.13.

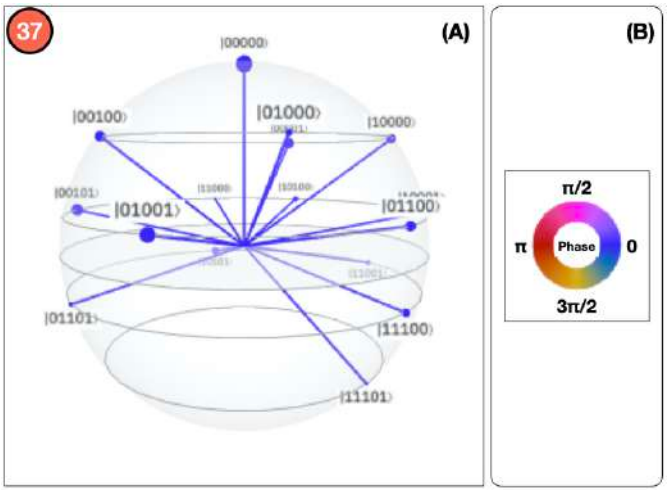


**Figure 2.4:** (A) Quantum Strategic Organizational Design Bloch sphere measurements of final state. (B) Phase state color code.

The circuit is simulated on qiskit tool, a Python–based quantum computing platform developed by IBM [100]. A total number of 8192 runs were carried out on the simulation with a total runtime of 3.8 seconds. In contrast, a genetic algorithm that would solve a similar problem with 12 KPIs (three per process owner) would take hundreds of hours to determine 48 real numbers between 0 and 1 in the chromosome with a value crossover and mutation with probabilities of 60% and 7% respectively with a population built over 8000 individuals and would run over 1000 generations. Compared with that, the performance increase of QSOD is remarkable. This has very powerful practical applications for industry leaders since with this new approach they can potentially allow a better understanding of the complex processes underlying the strategic design of organizations and above all make decisions in real-time.

Although we will describe the results of other implementation cases in more detail later, suffice it to say now that the obtained results are summarized as follows: the total probability of each process owner $P_j(|0\rangle)$ to be in alignment and the reduced purity $\kappa_j$ of each qubit in the final state. We observe how the probability of alignment of the process owner D $P_D(|0\rangle) = 49\%$, which indicates that the management system, as configured does not give a probability of achieving the alignment better than chance. That is why the probability of alignment of the root node representing process owner C $P_C(|0\rangle) = 73\%$, the same as that presented in the decision network. The alignment probabilities representing process owners B $P_B(|0\rangle) = 58.335\%$ and A $P_A(|0\rangle) = 69.745\%$ are mixed probabilities. The nodes have a purity coefficient of over 90%, which indicates that there is almost no entanglement between them.

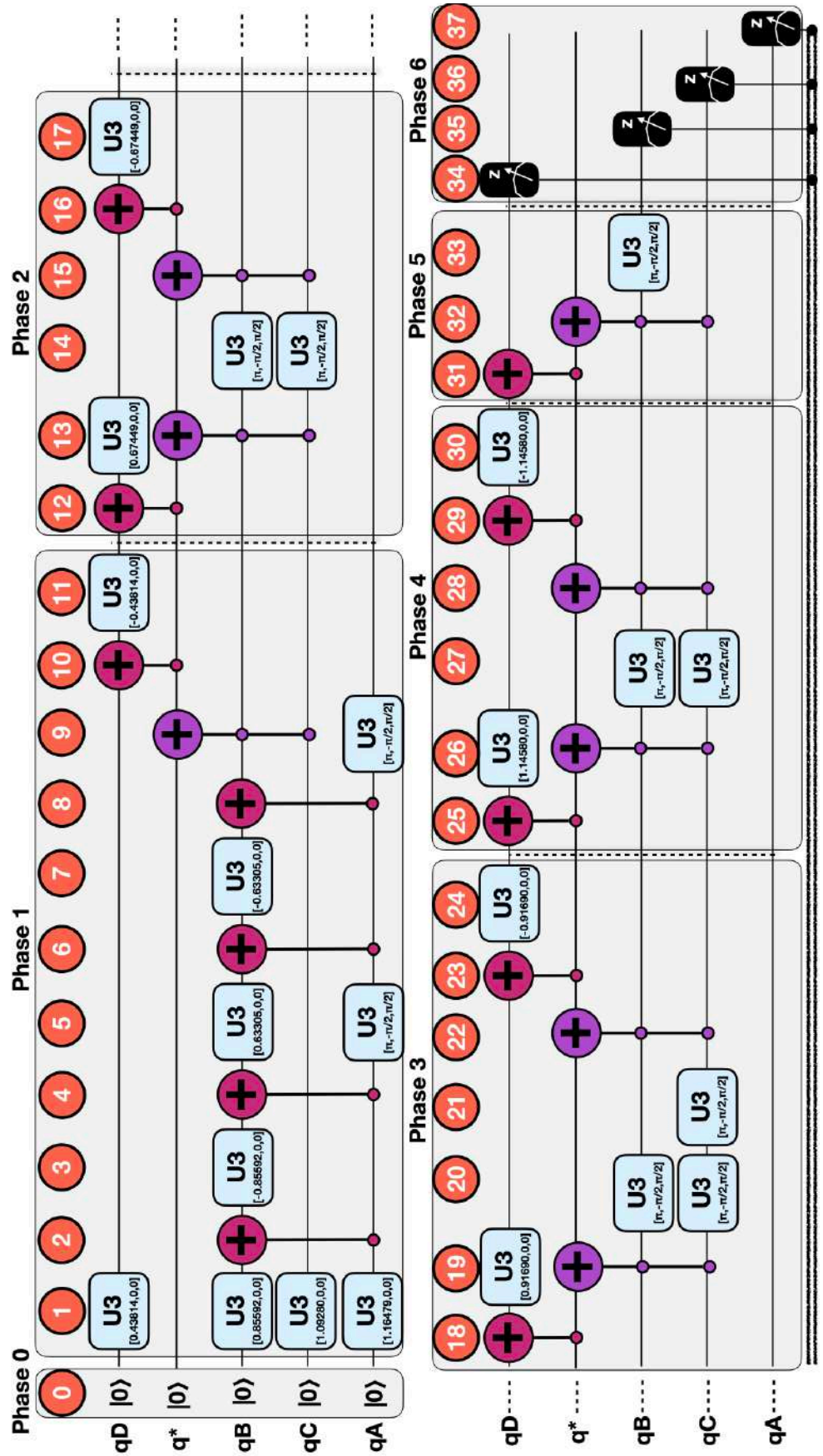


**Figure 2.3:** Equivalent Quantum Strategic Organizational Design Circuit to Decision Network from Figure 2.2

# 3

# Quantum Multilayered Networks

In general, we can state that Industry 4.0 systems can be designed as a network of processes [101] and the failure of one of these processes leads to a performance loss of the system [102]. We aim to inspect the behavior of the system when some of its elements are not operating within the standard operating procedure tolerances [20]. Industrial processes are designed following strict standard operating procedures that constrain them within certain limits, to ensure the competitiveness and quality of the products [103, 104].

Our proposal assigns one qubit $q$ to each of the cyber–physical resources of the multilayered socio–technical network. Specifically, the probability that the cyber–physical resource is within the specifications defined in the standard operating procedure will be assigned as the probability of $P(q = |0\rangle)$ and $P(q = |1\rangle)$ otherwise (see Figure 1.1) These resources will be linked to others to build a system, depending on the aspect under consideration in such a way that *multilayer network* becomes a natural architecture. Indeed, the state space of a composite physical system is the tensor product of the state spaces of the component physical systems, and this principle can be easily translated to the quantum environment.

Bloch's sphere, as stated previously, is commonly used to geometrically represent a qubit [94]. A qubit can be represented as a point on the Bloch sphere with the help of two parameters $\theta$, $\varphi$), as expressed by Equation 2.3. When several qubits are utilized in a circuit describing a layer of $M$ elements, their aggregated state can be determined utilizing the tensorial product given by $|\Psi\rangle = |\Psi_1\rangle \otimes |\Psi_2\rangle \otimes ... \otimes |\Psi_M\rangle$. This tensorial product maps the entry $x \in \mathbb{C}^n$ in a complex Hilbert space $\mathscr{H}$, which for $n$ qubits is the $\mathbb{C}^{2^n}$.

A multilayer network $\mathcal{M}$ is given by the quadruplet $\mathcal{M} = (\Gamma_M, \mathcal{E}_M, V, \mathcal{L})$, in which $\Gamma_M$ indicates the set of node–layer tuplets related to a set of nodes $V$, and $\mathcal{L}$ representing the set of perspectives built upon a set of elementary layers being relevant to the set of aspects $\mathcal{A}$. Therefore, a multilayer network can have $N_A$ number of aspects, being $N_A$ the cardinality of $\mathcal{A}$. Based on those aspects a sequence of sets of layers is defined as $\mathcal{L} = \{ \mathrm{L}_\alpha \}, \alpha \in (1, 2, \ldots, N_A)$ , where $\mathrm{L}_\alpha$ represents the set of layers related to the $\alpha$ aspect. The whole group of layers are built based on the cartesian product of the sets as per aspect, $L_1 \times L_2 \times \cdots \times L_{N_A}$, and then $\Gamma_M \subseteq V \times L_1 \times L_2 \times \cdots \times L_{N_A}$. The nodes can be connected pairwise by means of edges, $\mathcal{E}_M \subseteq \Gamma_M \times \Gamma_M$ where according to the definition, connections can happen inside layers or inter–layers. The multilayer network can still be represented as graph $\mathcal{G}_M = (\Gamma_M, \mathcal{E}_M)$.

We now extend the preliminary concepts presented in Chapter 1, and state that for any given time $t$ complex cyber–physical networks are described as time–dependent *graphs* given by:

$$\mathcal{G}_M(t) = (\Gamma_M(t), \mathcal{E}_M(t)), \tag{3.1}$$

which can be understood as lists of $\Gamma_M(t)$ human and cyber–physical nodes and its standard communication $\mathcal{E}_M(t) \subset (\Gamma_M(t) x \Gamma_M(t))$ edges. The emergence of complex networked organizational design configurations in the form of lean structural networks is only possible through a continuous improvement–oriented standardization of the organizational network edges (business communication protocols between the network elements.) [20]

## 3.1 Implementation of the Hierarchical Relationship

This section proposes a quantum multilayered network that presents several computational advantages: on the one hand, the state of each qubit can be fully computed as a wave function of the quantum circuit that conforms it at a lower level. This allows for an effective computation of the interactions between different layers and greatly reduces the computational resources needed to elaborate virtual representations of the system as compared with other approaches such as twin factories [105]. On the other hand, it allows

for a distributed ledger computation of organizational states and can therefore flexibly and securely evaluate different decision network configurations and aggregate them into greater settings, hence enabling researchers and organizational designers to use advanced quantum simulations to accelerate managerial decision making. We present two approaches for the aggregation of the hierarchical relationship:

- Hierarchical relationship by adding additional qubits. In this approach the information of alignment conditional probabilities from lower levels is aggregated by adding an additional qubit to those qubits with a parent node in the upper level.
- Hierarchical relationship by using the state of the last node of the lower level. In this approach we add the information of alignment from lower levels directly to the initialization of the qubits in the upper level.

### 3.1.1 Hierarchical relationship by adding additional qubits

Without loss of generality, in the modeling of Industry 4.0 processes, we can always add a qubit at the end of the quantum circuit that measures a characteristic of the circuit that we are interested in measuring (i.e., quality, cost, lead time, return on invest, mean time between failures,...) and that condenses the conditional probabilities of the rest of the circuit.

As a consequence, the aggregation of the wave function $|\Psi^{l}_{\alpha_j,t}\rangle$ to the next level $l+1$ in the position $j$ is performed by two nodes: one that describes the initial rotation that represents the $|0\rangle$ probability of the last node of the circuit $P(|\Psi^{l}_{\alpha_j,N_j}\rangle = |0\rangle)$ which absorbs the initial rotation of the level $l$, and a new qubit that contains the conditional probabilities of the node in the level $l+1$. Since the root nodes at level $l+1$ do not have conditional probabilities, they only present the initial rotation. This is exemplarity shown in Figure 3.1A.

Therefore, the number of additional qubits required to represent the inter–layer connections is equal to the number of child nodes in the level $l+1$. For illustration, the quantum circuit at level $l+1$ represented in Figure 3.1A uses two additional qubits ($|\Psi^{l+1}_{\alpha^*_j,2}\rangle$ and $|\Psi^{l+1}_{\alpha^*_j,3}\rangle$). The initial state of all the qubits in the quantum circuit is $|0\rangle$ (state of no failure). Then, an initial rotation with $\theta$ angles that are conditioned on the states of the last node of the circuits at level $l$ is applied to the root nodes at level $l+1$ and the new qubits that represent the inter–layer connections:

- $P(|\Psi^{l+1}_{\alpha_j,1}\rangle = |0\rangle) = P(|\Psi^{l}_{\alpha_1,2}\rangle = |0\rangle)$.
- $P(|\Psi^{l+1}_{\alpha^*_j,2}\rangle = |0\rangle) = P(|\Psi^{l}_{\alpha_2,2}\rangle = |0\rangle)$.

- $P(|\Psi^{l+1}_{\alpha^*_j,3}\rangle = |0\rangle) = P(|\Psi^{l}_{\alpha_3,2}\rangle = |0\rangle)$.

The calculation of the initial rotation angles is given by Equation 2.15.

In the case of child nodes $|\Psi^{l+1}_{\alpha_j,2}\rangle$ and $|\Psi^{l+1}_{\alpha_j,3}\rangle$, it is necessary to define a set of probabilities conditioned on the values of the corresponding parent nodes (e.g., $|\Psi^{l+1}_{\alpha^*_j,2}\rangle$ and $|\Psi^{l+1}_{\alpha_j,1}\rangle$ for node $|\Psi^{l+1}_{\alpha_j,2}\rangle$, and $|\Psi^{l+1}_{\alpha^*_j,3}\rangle$ and $|\Psi^{l+1}_{\alpha_j,2}\rangle$ for node $|\Psi^{l+1}_{\alpha_j,3}\rangle$). Thus, $P(|\Psi^{l+1}_{\alpha_j,i}\rangle = |1\rangle \,|\, |\Psi^{l+1}_{\alpha^*_j,i}, \Psi^{l+1}_{\alpha_j,i-1}\rangle = |ab\rangle)$, where $i \in \{2,3\}$ and $|ab\rangle \in \{|11\rangle, |10\rangle, |01\rangle, |00\rangle\}$, represents the probability of failure of node $|\Psi^{l+1}_{\alpha_j,i}\rangle$ conditioned to the state of failure and/or no–failure of nodes $|\Psi^{l+1}_{\alpha^*_j,i}\rangle$ and $|\Psi^{l+1}_{\alpha_j,i-1}\rangle$.

The quantum circuit designed with this first approach can be represented by a Bayesian network. Rotation gates in the quantum circuit represent the marginal probabilities associated with root nodes, and controlled rotation gates represent the conditional probability tables associated with child nodes [58]. Thus, the results of the application of this strategy can be compared with the results of the equivalent Bayesian network. As shown in Figure 3.2 and Figure 3.3, the results obtained with both implementations, i.e, the quantum circuit and the classical Bayesian network, are the same. Failure probability propagation from the root nodes –which represent the state of the systems at level $l$– towards the final node –which represents the state of the system at level $l+1$– depends on:

- The set of conditional probabilities that quantifies the effect of the parent nodes on a child. As Figure 3.2 illustrates, higher probabilities of failure conditioned to the state of failure of both parent nodes (from 0.7 to 0.95 in our example) lead to a greater performance loss of the system meassured by some relevant KPIs.
- The distance between the root node in a state of failure and the final child node. In our example, the root node $|\Psi^{l+1}_{\alpha^*_j,3}\rangle$ has the greatest impact on the performance loss of the system (see Figure 3.2c, Figure 3.2e or Figure 3.2f).
- The number of root nodes, i.e., systems at level $l$, in a state of failure.

### 3.1.2 Hierarchical relationship by using the state of the last node of the lower level

A different proposed approach to connect different layers in the network is to use the state of the last node of the circuit in the level $l$ as initial state of nodes in the level $l+1$ instead of being initialized to $|0\rangle$. In this case,

the rotation angle can be expressed by:

$$\theta = \arccos(P(|\Psi^{l}_{\alpha_j,N_j}\rangle = |0\rangle)). \tag{3.2}$$

Thus, $\theta = 0$ if the last node of the circuit in the level $l$ has a no–failure state, $(P(|\Psi^{l}_{\alpha_j,N_j}\rangle = |0\rangle) = 1)$, and the initial state of the qubits in the level $l+1$ is set to $|0\rangle$, i.e, state of no–failure. On the other hand, as long as the system in the level $l$ is not operating properly $(P(|\Psi^{l}_{\alpha_j,N_j}\rangle = |0\rangle) \in [0,1))$, the value of $\theta$ increases from 0 to $\pi/2$ rad, which leads the initial state of the qubits in the level $l+1$ towards a state of failure.

This second approach, which is exemplarity represented in Figure 3.1B, eliminates the use of additional qubits as in the first approach. After the computation of the initial state of nodes in level $l+1$ by applying internal rotation with angles based on Equation 3.2, the wave function of the quantum circuit is calculated. To describe the case showed in Figure 3.1B, the following probabilities associated with each node need to be defined:

- $P(|\Psi^{l+1}_{\alpha_j,1}\rangle = |1\rangle)$. Probability of failure of node $|\Psi^{l+1}_{\alpha_j,1}\rangle$.
- $P(|\Psi^{l+1}_{\alpha_j,i}\rangle = |1\rangle \,|\, |\Psi^{l+1}_{\alpha_j,i-1}\rangle = |a\rangle)$, where $i \in \{2,3\}$ and $|a\rangle \in \{|1\rangle, |0\rangle\}$. Probability of failure of node $|\Psi^{l+1}_{\alpha_j,i}\rangle$ conditioned to the state of failure or no–failure of node $|\Psi^{l+1}_{\alpha_j,i-1}\rangle$.

The results of the application of this second strategy (Figure 3.4) show a non–linear behavior of the system when some of its elements are in a state of failure. In this case, the initialization performed by applying internal rotations modifies the initial probability amplitude of quantum states and changes how information propagates through the quantum circuit. Figure 3.4 shows how the dominating factors for performance loss of the system are both the increasing number of nodes (i.e., systems at level $l$) in a state of failure and their decreasing distance to the final node. Furthermore, as almost parallel lines in Figure 3.4c, 3.4e, 3.4f, and 3.4g illustrate, the impact of conditional probabilities on the state of the final node decreases with both increasing numbers of nodes in a state of failure and decreasing distance between failure nodes and the final one, which results in a saturation point where the performance loss of the system becomes flat.

## 3.2 Results and Discussion Multilayered Network

An alternative representation of the quantum state is applied to an entry $x$, $\langle\Psi(x)|$ is given by an Hermitian operator $\rho(x) = |\Psi(x)\rangle\langle\Psi(x)|$ called density matrix which contains all the observable information of the quantum state. Quantum circuits map therefore the input into a high–dimensional feature space in which

statistical properties of the measurement $\mathscr{M}$ are interpreted as output of the quantum circuit. These measurements, which correspond to a Hermitian operator $\mathscr{M}$ acting on vectors in the Hilbert space of the quantum circuit $\mathscr{H}$ and live in a subspace of the data–encoding feature space $\mathscr{F}$ are in general not linear in the Hilbert space $\mathscr{H}$ of the quantum circuit [96]. However, according to the celebrated *representer theorem* [97], an optimal quantum kernel can be found that allows describing the quantum circuits as linear models in the space of the Hermitian operator $\rho(x)$ with the form $\mathrm{tr}\left[\left(\sum_{m=1}^{M}\alpha_m\rho(x^m)\right)\rho(x)\right]$ where $x^m$, $m = 1, \ldots, M$, is the input data and $\alpha_m \in \mathbb{R}$. In other words, if we find a linear transformation of our quantum state vector $|\Psi(x)\rangle$, we are guaranteed that the best measurements for our quantum circuit only has $M << 2^{2n}$ degrees of freedom, rather than the $\mathcal{O}(2^{2n})$ degrees of freedom of a quantum circuit with n qubits.

As shown in Figure 3.1a, and the related results in Figure 3.2, the first quantum model presented in this work does exactly this: by understanding the data–encoding density matrices $\rho(x)$ as feature vectors, it describes a novel quantum kernel that allows the aggregation of hierarchical networks of qubits in such a way that the quantum models behave linearly in the space of the resulting operator when describing the observable information of the quantum state $|\Psi(x)\rangle$. In contrast, the non–linearity of the second model, shown in Figure 3.1b, and the related results depicted in Figure 3.4, shows dissipating effects in the translation of the failure probabilities from one level $l$ to the next level $l+1$ derived from the internal rotation imposed on the qubits in the hierarchical aggregation [106]. This means that while the circuit has a high–dimensional state space, the quantum model with additional qubits can be operated in a low–dimensional subspace without dissipation, while the model with internal rotations cannot. This representation can be very useful for several applications, but perhaps the most important one is that it allows us to study the temporal evolution of multilayered networked qubit systems from an optimization point of view: minimizing the cost functions represented in the space of quantum circuits would be equivalent to minimizing the same cost functions of the resulting system after the proposed transformation.

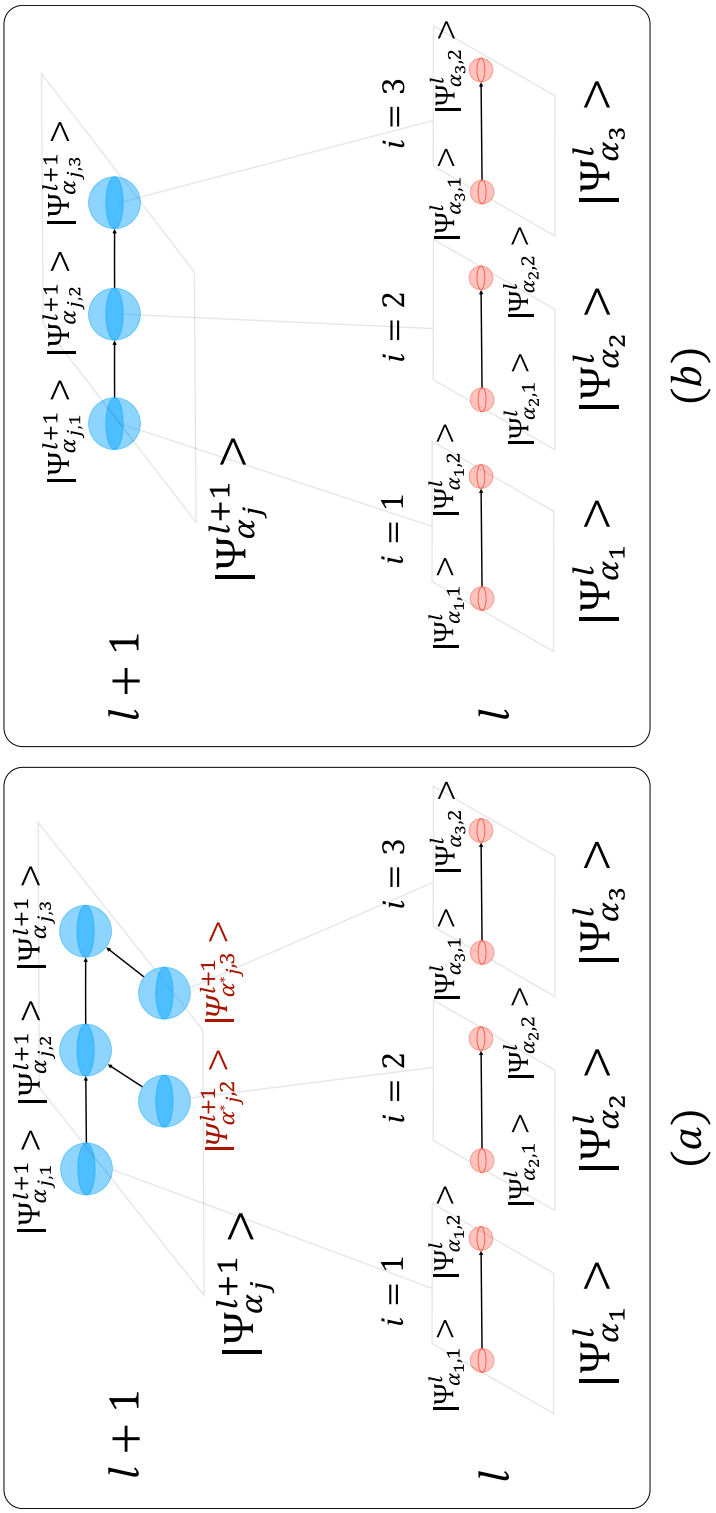


**Figure 3.1:** Aggregation of two layers network. Three qubits case. (**a**) First approach. Hierarchical relationship by adding additional qubits. (**b**) Second approach. Hierarchical relationship by using the state of the last node of the lower level.

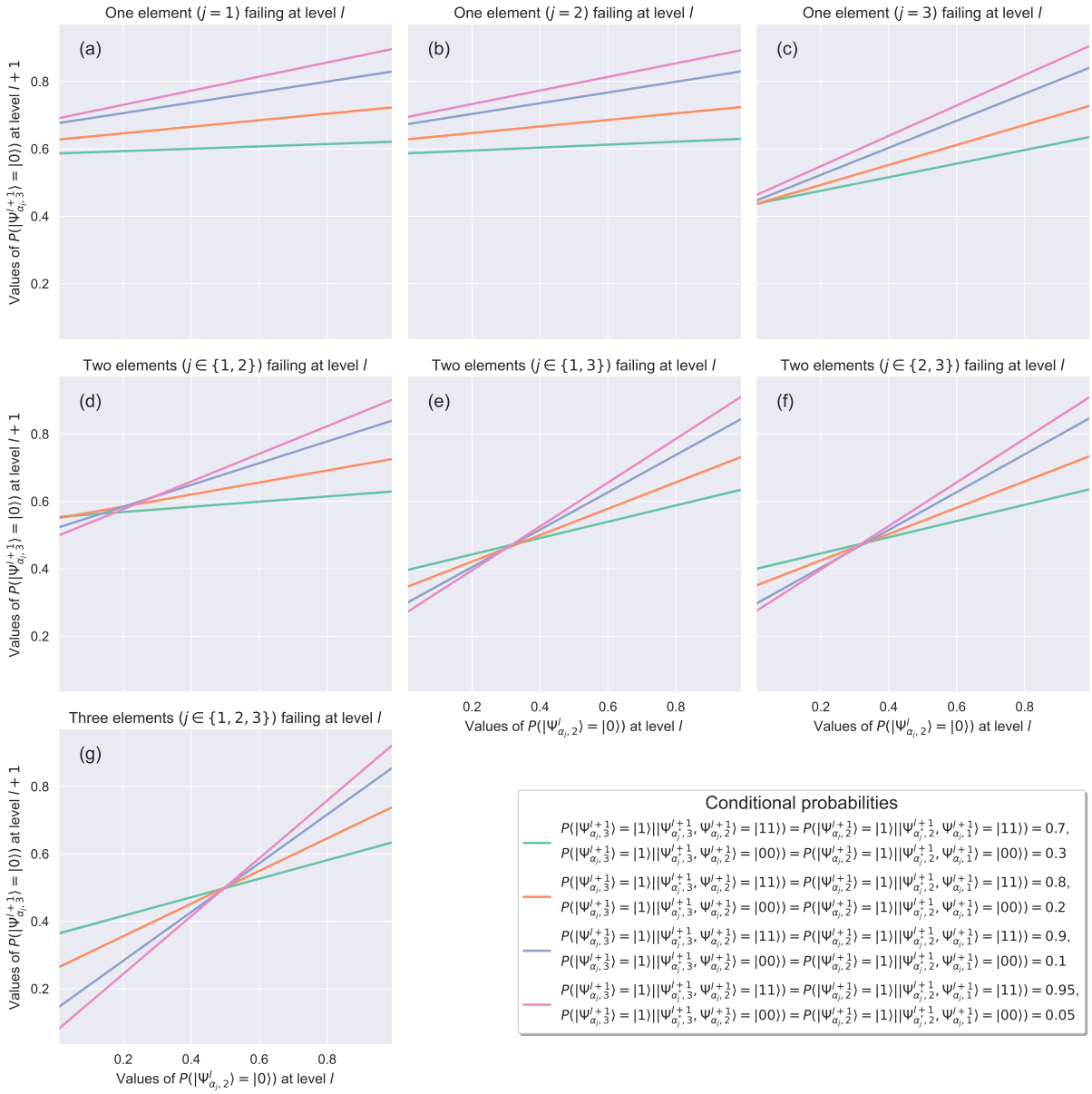


**Figure 3.2:** Performance loss of the system at level $l+1$ for different failure behaviors at level $l$, different combinations of $P(|\Psi^{l+1}_{\alpha_j,i}\rangle = |1\rangle\,||\Psi^{l+1}_{\alpha^*_j,i}, \Psi^{l+1}_{\alpha_j,i-1}\rangle = |ab\rangle)$, where $|ab\rangle \in \{|11\rangle, |00\rangle\}$, and $P(|\Psi^{l+1}_{\alpha_j,i}\rangle = |1\rangle\,||\Psi^{l+1}_{\alpha^*_j,i}, \Psi^{l+1}_{\alpha_j,i-1}\rangle = |10\rangle) = P(|\Psi^{l+1}_{\alpha_j,i}\rangle = |1\rangle\,||\Psi^{l+1}_{\alpha^*_j,i}, \Psi^{l+1}_{\alpha_j,i-1}\rangle = |01\rangle) = 0.5$. First approach. Three qubits case.

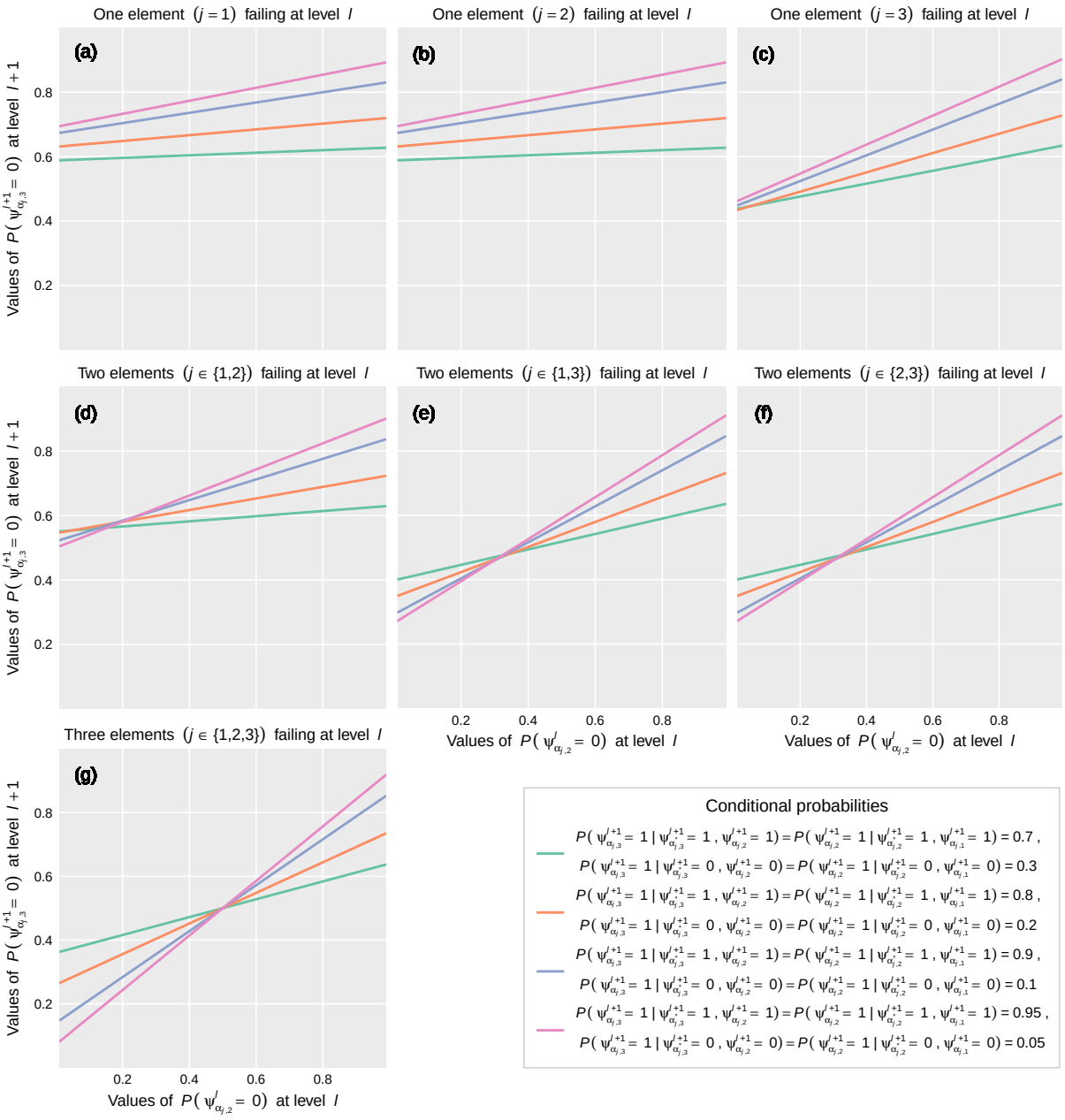


**Figure 3.3:** Performance loss of the system at level $l+1$ for different failure behaviors at level $l$, different combinations of $P(\Upsilon^{l+1}_{\alpha_j,i} = 1 | (\Upsilon^{l+1}_{\alpha^*_j,i}, \Upsilon^{l+1}_{\alpha_j,i-1}) = (a,b))$, where $(a,b) \in \{(1,1),(0,0)\}$, and $P(\Upsilon^{l+1}_{\alpha_j,i} = 1 | (\Upsilon^{l+1}_{\alpha^*_j,i}, \Upsilon^{l+1}_{\alpha_j,i-1}) = (1,0)) = P(\Upsilon^{l+1}_{\alpha_j,i} = 1 | (\Upsilon^{l+1}_{\alpha^*_j,i}, \Upsilon^{l+1}_{\alpha_j,i-1}) = (0,1)) = 0.5$. First approach. Equivalent Bayesian network.

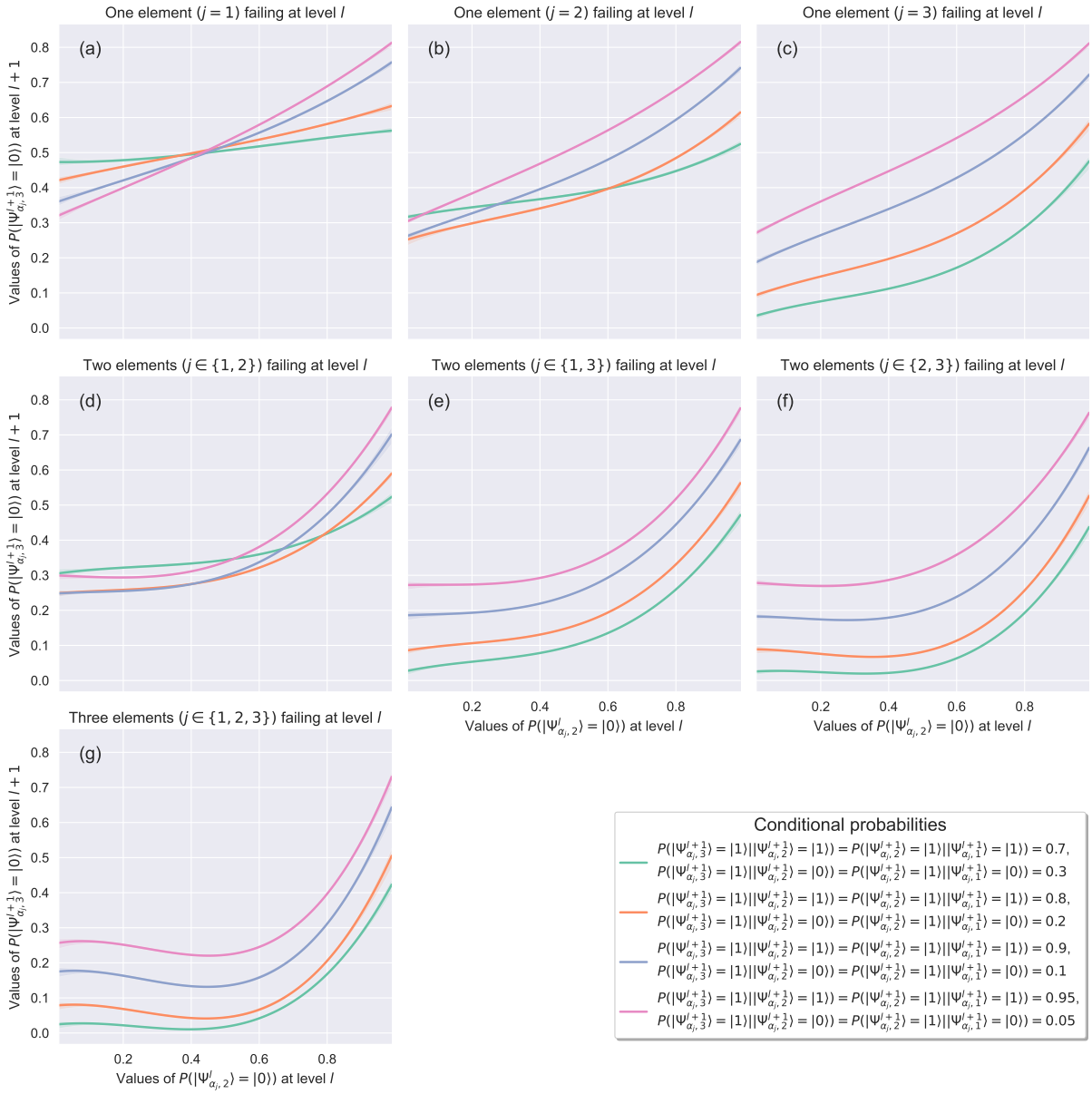


**Figure 3.4:** Performance loss of the system at level $l+1$ for different failure behaviors at level $l$ and different combinations of $P(|\Psi^{l+1}_{\alpha_j,i}\rangle = |1\rangle \,|\, |\Psi^{l+1}_{\alpha_j,i-1}\rangle = |a\rangle)$, where $i \in \{2, 3\}$ and $|a\rangle \in \{|1\rangle, |0\rangle\}$. Second approach. Three qubits case.

# 4

# Quantum Strategic Organizational Design Implementation Cases.

In this Chapter we present several implementations of the QSOD principles in an Industry 4.0 cyber–physical context. In the first three sections we implement the previously presented QSOD principles to investigate the alignment state of simple practical cases of chains of command and dependency in industrial organizational configurations. We do this through the implementation of quantum circuits that represent decision networks. In fact, through hundreds of simulations in each case, we derive insightful conclusions relevant for the organizational leader and decision maker. The cases under study are the following:

- Section 4.1. The case of two qubits: one reports to one.
- Section 4.2. The case of three qubits: two report to one.
- Section 4.3. The case of three qubits: one reports to two.

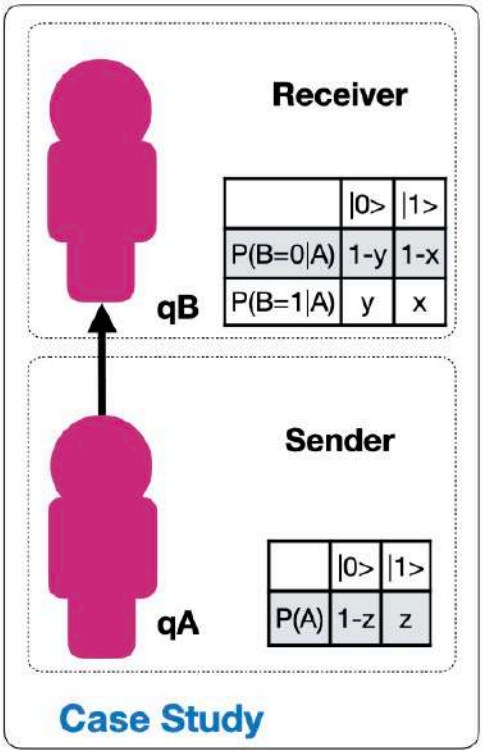


**Figure 4.1:** Case study framework two qubits: one reports to one in which the respective node alignment probabilities are parametrized.

We choose these configurations because they represent the essential motifs which adequately combined through the concepts presented in Chapter 3 yield any strategic organizational design configuration.

## 4.1 The case of two qubits: one reports to one

In this section we investigate how the relationship with a subordinate who reports to an Industry 4.0 leader and influences her alignment. We intend to expand the previously presented concepts by studying the simplest case of two organizational agents, a subordinate $A$ reporting to another agent $B$ represented in Figure 4.1, that will be simulated by means of a two-qubit quantum circuit. We do this through the implementation of quantum circuits that represent decision networks. In fact, through the quantum simulation of strategic organizational design configurations through five hundred simulations of quantum circuits, we conclude that there is an influence of the subordinate on the leader that resembles that of a harmonic under–damped oscillator around the value of 50% probability of alignment for the leader. Likewise, we have observed a self similar behavior in this type of relationships, which seems to conjecture that there is an exchange of energy between the two agents that oscillates with greater or lesser amplitude depending on certain parameters of interdependence. Self similarity in this QSOD context allows for a quantification of these complex dynamics and its pervasive effect offers robustness and resilience to the 2 qubit interaction.

Our goal is to determine the probability of alignment of agent $B$, $P(B = |0\rangle)$, as a function of the alignment probability of agent $A$, given by $P(A = |0\rangle) = z$, and the conditional alignment probabilities between agents $A$ and $B$, given by $x = P(B = |1\rangle \,|A = |0\rangle) \in [0,1]$ and $y = P(B = |1\rangle \,|A = |1\rangle) \in [0,1]$. This is achieved through the simulation of more than 500 different quantum circuit configurations in which the relative alignment probabilities $x, y, z \in [0,1]$ vary and $P(B = |0\rangle) = f(x,y,z)$ is measured. In this section we present relevant conclusions about the alignment probabilities of the higher hierarchy agent depending on the alignment state of the leadership relationship.

The rest of the section hereinafter continues as follows: first Section 4.1.1 begins with a description of the configuration of the quantum circuit computations necessary to simulate the outlined 2-qubit organizational design configuration. Second, Section 4.1.2 presents the case study that will simulate numerous quantum circuits, varying the mentioned parameters in order to obtain an optimal configuration of them. Third, in Section 4.1.3 we discuss the results obtained and propose an interpretation in perspective of previous studies and of the working hypotheses.

### 4.1.1 Quantum strategic organizational design Circuit – Two Qubits organizational design configuration

In this case, two qubits are utilized, and therefore their aggregated state can be determined utilizing the tensorial product of the individual qubits. The multiple qubit state can be expressed as a linear combination of the $|0\rangle$ and $|1\rangle$ states, then the aggregated state can be represented as in Equation 2.4.

Our initial hypothesis is that there is much intrinsic value for any organizational leader in Industry 4.0, to know their alignment status with the company's strategic objectives. Moreover, not only it is important for them to know, but the company has a great interest in having its leaders aligned with its strategic objectives, since this is expected to increase its overall organizational efficiency and effectiveness. We focus on finding answers to the question of how to maximize the probability of alignment of agent $B$, $P(B = |0\rangle)$, depending on agent $A$'s individual no–alignment probability, $z = P(A = |1\rangle) \in [0,1]$, and the relative probability of alignment between the two agents, $x = P(B = |1\rangle \,|A = |0\rangle) \in [0,1]$ and $y = P(B = |1\rangle \,|A = |1\rangle) \in [0,1]$. Mathematically speaking, we intend to find the values of $(x,y,z)$ that maximize the function $P(B = |0\rangle) = f(x,y,z)$. In other words, our challenge reduces to finding the values of $x, y, z \in [0,1]$ that maximize following equation:

$$P(B = |0\rangle) = (c_{11}c_{21})^2 + (c_{11}c_{22})^2. \tag{4.1}$$

Table 4.1: Case one reports to one: Qubit angles of rotation

| Qubit | Interpretation | Equation |
|---|---|---|
| $\|\Psi_A\rangle$ | The probability $z = P(A = \|1\rangle)$ of qubit $\|\Psi_A\rangle$ to be in no–alignment translates into the rotation angle $\theta_z$. | $\theta_z = 2 \arctan \sqrt{\frac{z}{1-z}}$ |
| $\|\Psi_B\rangle$ | The conditional probability $x = P(B = \|1\rangle \, \|A = \|0\rangle)$ of qubit $\|\Psi_B\rangle$ to be in no–alignment depending on qubit $\|\Psi_A\rangle$ translates into rotation angle $\theta_x$. | $\theta_x = 2 \arctan \sqrt{\frac{x}{1-x}}$ |
| | The conditional probability $y = P(B = \|1\rangle \, \|A = \|1\rangle)$ of qubit $\|\Psi_B\rangle$ to be in no–alignment depending on qubit $\|\Psi_A\rangle$ translates into rotation angle $\theta_y$. | $\theta_y = 2 \arctan \sqrt{\frac{y}{1-y}}$ |

Based on the principles of quantum circuit design that model decision networks presented in Chapter 2, the quantum circuit that models the interactions presented by Figure 4.1 translates into the quantum circuit given by:

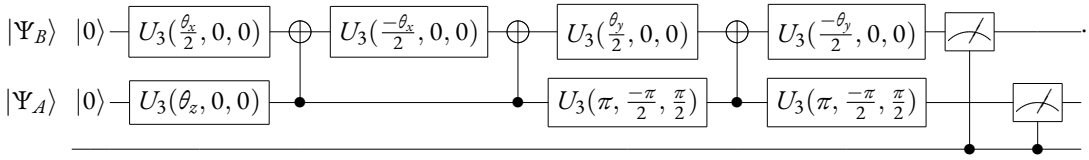

(4.2)

This circuit presents two *qubits* $|\Psi_A\rangle$, with rotation angle $\theta_z$ and initial state $|0\rangle$, and $|\Psi_B\rangle$ with rotation angles $\theta_x$, $\theta_y$ and initial state $|0\rangle$. The respective interpretation of these rotations and the equations to calculate them are described in Table 4.1.

### 4.1.2 Case study – Two Qubits organizational design configuration

In the case study we proceed, as announced, to simulate a total of 500 configurations of the circuit shown in Equation 4.2. We intend to find the values of parameters $x, y, z \in [0, 1]$ that maximize the probability of alignment of the agent $B$, $P(B = |0\rangle)$. To do this, the parameters $x, y \in [0, 1]$ are varied in 10% incremental intervals in order to make a uniform mapping and create a proper display of the results. However, not all $z \in [0, 1]$ values are relevant. We are interested in values of $z \geq 0.5$, since they indicate that the alignment probability of the agent $A$, $P(A = |1\rangle)$, is greater than or equal to 50%. In other words it is equal to or better than a random process. We map the values $z \subset \{0.5, , 0.75, 0.9, 0.99, 0.9999\}$, thus generating 500 simulations, each with a run of 3.5 seconds, giving a total computation time of 1750 seconds. The circuits were simulated on *qiskit* tool and the code and results can be accessed in this https://osf.io/9tc7u/?view_only=89c7c2a7276242328a50e6339735334d. We summarize the obtained results in Figure 4.2 by representing $P(B = |0\rangle) = f(x, y, z)$ as a

function of $x, y, z \in [0, 1]$.

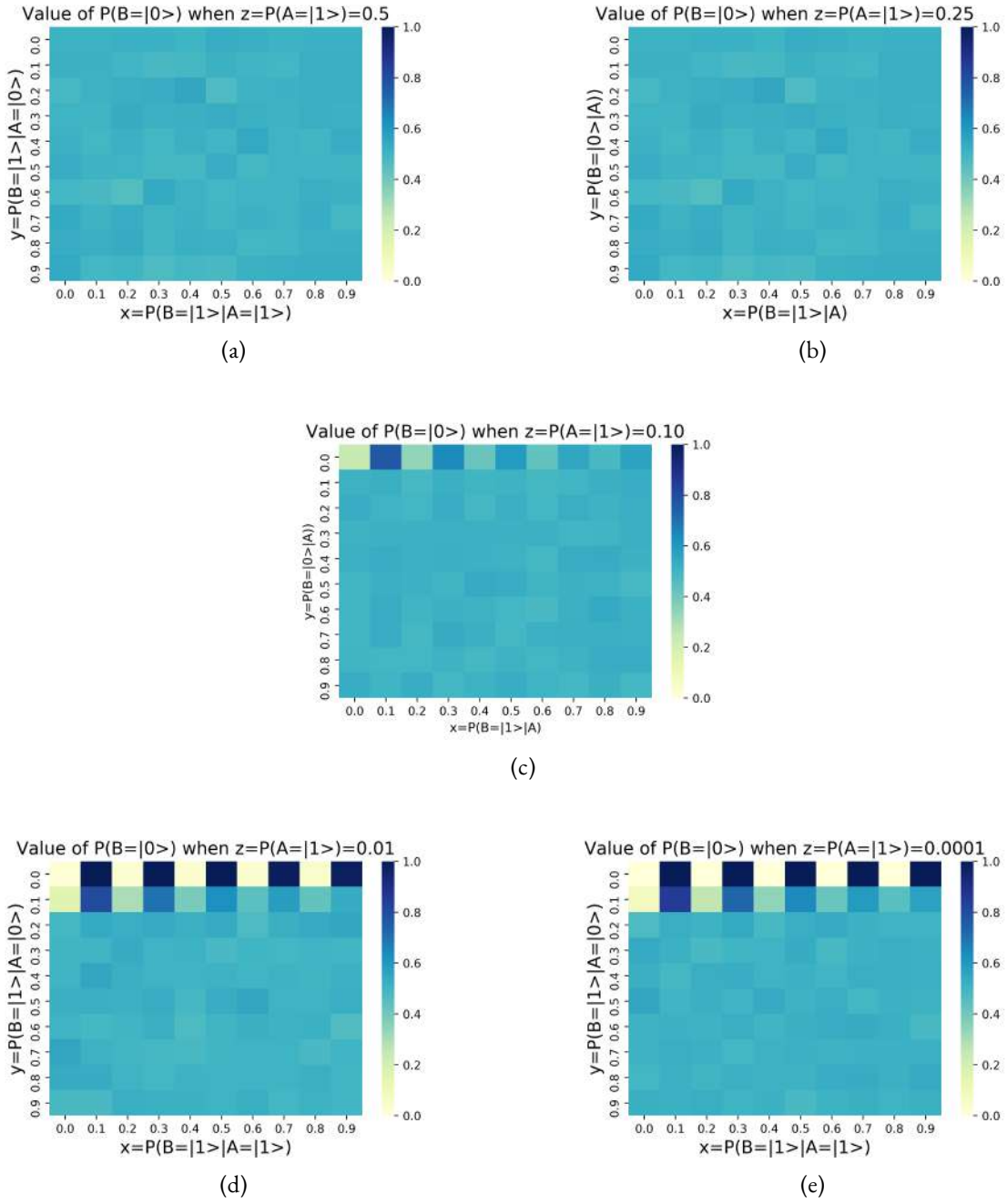


**Figure 4.2:** Case Study One Reports to One. Results obtained for $P(B = |0\rangle)$ for different values of the no–alignment probability of agent $A$, $z = P(A = |1\rangle)$. (a) P(A=|1⟩)=0.50, (b) P(A=|1⟩)=0.25, (c) P(A=|1⟩)=0.1, (d) P(A=|1⟩)=0.01, (e) P(A=|1⟩)=0.0001.

These results shown in Figure 4.2 indicate that by increasing the alignment probability of the lower node, decreasing P(A=|1⟩)), the alignment probability of the upper node behaves as an underdamped oscillator. We can observe in Figure 4.2 that the first partial derivatives of the two dimensional functions $f(x, y) = P(B = |0\rangle)$ with changing $x = P(B = |1\rangle \, | A = |0\rangle)$ and with $y = P(B = |1\rangle \, | A = |1\rangle)$, given respectively by $\partial f(x, y)/\partial x$

and $\partial f(x,y)/\partial y$. We represent the values of $f(x,y) = P(B = |0\rangle)$ as a function of $y = P(B = |1\rangle\,|A = |1\rangle)$ in Figure 4.3(a). As we indicate in Figure 4.3(b), each [0.1] interval of interval of $y = P(B = |1\rangle\,|A = |1\rangle)$ contains ten values of $x \in [0,1]$. In more detail, Figure 4.2(a) describes the alignment state of agent B, $P(B = |0\rangle)$, for different values of conditioned alignment probability between agents $A$ and $B$, $x = P(B = |1\rangle\,|A = |0\rangle), y = P(B = |1\rangle\,|A = |1\rangle) \in [0,1]$, being the alignment probability of agent $A$ $P(A = |0\rangle)$=1 − $P(A = |1\rangle)$=50%. Figure 4.2(b) describes the alignment state of agent B, $P(B = |0\rangle)$, for different values of conditioned alignment probability between agents $A$ and $B$, $x = P(B = |1\rangle\,|A = |0\rangle), y = P(B = |1\rangle\,|A = |1\rangle) \in [0,1]$, being the alignment probability of agent $A$ $P(A = |0\rangle)$=1 − $P(A = |1\rangle)$=75%. Figure 4.2(c) describes the alignment state of agent B, $P(B = |0\rangle)$, for different values of conditioned alignment probability between agents $A$ and $B$, $x = P(B = |1\rangle\,|A = |0\rangle), y = P(B = |1\rangle\,|A = |1\rangle) \in [0,1]$, being the alignment probability of agent $A$ $P(A = |0\rangle)$=1 − $P(A = |1\rangle)$=90%. Figure 4.2(d) describes the alignment state of agent B, $P(B = |0\rangle)$, for different values of conditioned alignment probability between agents $A$ and $B$, $x = P(B = |1\rangle\,|A = |0\rangle), y = P(B = |1\rangle\,|A = |1\rangle) \in [0,1]$, being the alignment probability of agent $A$ $P(A = |0\rangle)$=1 − $P(A = |1\rangle)$=99%. Figure 4.2(e) describes the alignment state of agent B, $P(B = |0\rangle)$, for different values of conditioned alignment probability between agents $A$ and $B$, $x = P(B = |1\rangle\,|A = |0\rangle), y = P(B = |1\rangle\,|A = |1\rangle) \in [0,1]$, being the alignment probability of agent $A$ $P(A = |0\rangle)$=1 − $P(A = |1\rangle)$=99.99%.

If we increase the granularity of the mapping of the quantum circuits in search of a self similarity within their behavior, and we make a mapping of the $y = P(B = |1\rangle\,|A = |1\rangle) \in [0, 0.1]$ for values of $z = P(A = |1\rangle) = 0.1$, then we obtain the results of Figure 4.4(b). Similarly as in the previous diagrams, each [0.01] interval of $y = P(B = |1\rangle\,|A = |1\rangle)$ contains ten values of $x \in [0,1]$ for values of $z = P(A = |1\rangle) = 0.1$.

In the following Section 4.1.3 we discuss these results in detail.

### 4.1.3 Discussion – Two Qubits organizational design configuration

We now proceed to discuss the results systematically. We begin by discussing Figure 4.3 which describes the change in the alignment probability of the agent $B$ described by the function $f(x,y) = P(B = |0\rangle)$, with increasing values of the relative alignment probability of B, depending on A, given by $y = P(B = |1\rangle\,|A = |1\rangle) \in [0,1]$. Before we do so, a gentle reminder for the reader that taking into consideration Bayes's theorem, this probability can be expressed by:

$$y = P(B = |1\rangle\,|A = |1\rangle) = \frac{P(B = |0\rangle \cap A = |1\rangle)}{P(A = |1\rangle)}. \tag{4.3}$$

This means that growing values of the relative probability of agent $B$ alignment, conditioned to agent $A$

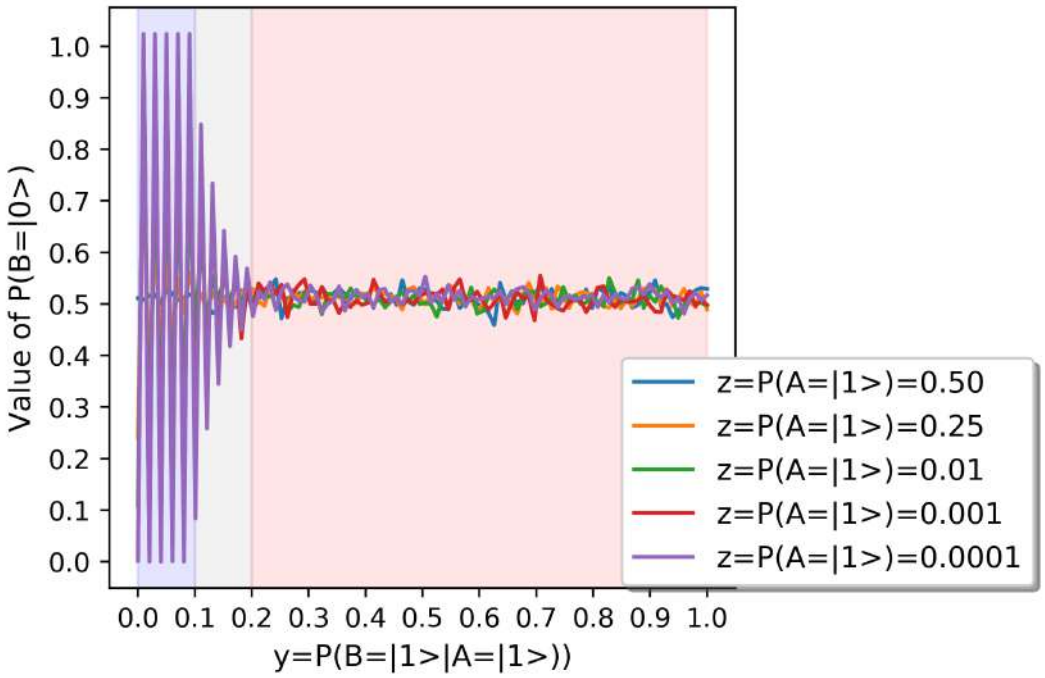


(a)

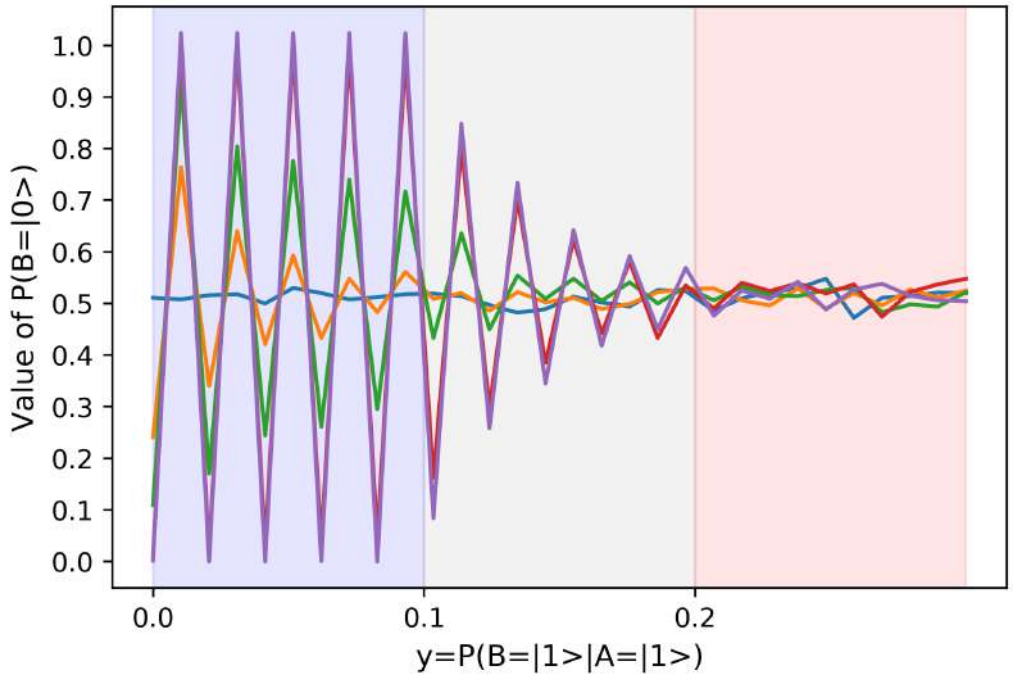


(b)

**Figure 4.3:** Case Study One Reports to One. Summary of results of $P(B = |0\rangle)$. (a) Summary of results of $P(B = |0\rangle)$ as a function of $y = P(B = |1\rangle\,|A = |1\rangle)$. (b) Enlarged view of results of $P(B = |0\rangle)$ with $y = P(B = |1\rangle\,|A = |1\rangle) \in [0, 0.3]$.

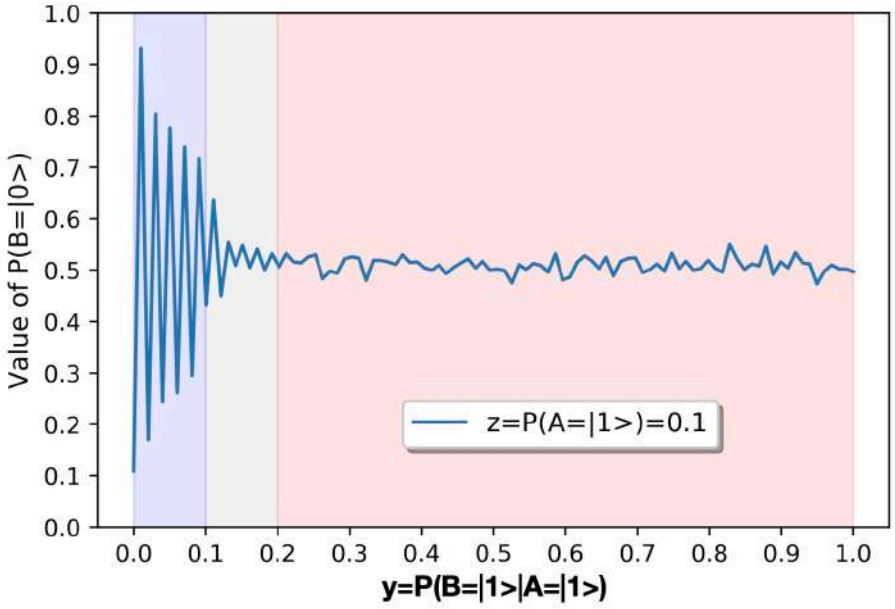


(a)

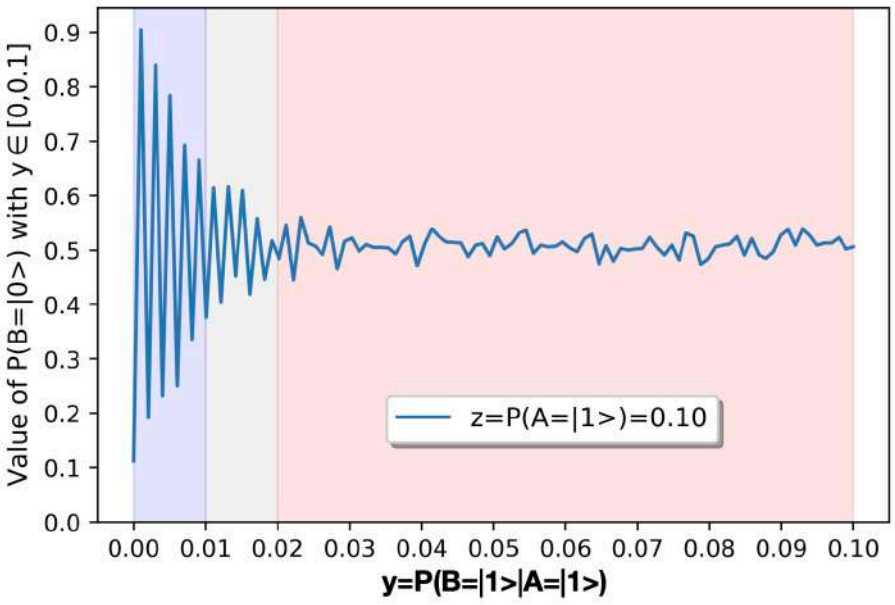


(b)

**Figure 4.4:** Case Study One Reports to One. Detail of results of $P(B = |0\rangle)$ for $P(A = |1\rangle = 0.1$. (a) Detail of results of $P(B = |0\rangle)$ with $y = P(B = |1\rangle\,|A = |1\rangle) \in [0, 1]$. (b) Enlarged view of results of $P(B = |0\rangle)$ with $y = P(B = |1\rangle\,|A = |1\rangle) \in [0, 0.1]$.

being in not–alignment, are caused by growing values of the intersection $P(B = |1\rangle \cap A = |1\rangle)$. In other words, increasing values of the counter $P(B = |1\rangle \cap A = |1\rangle)$ express that the probability of intersection of $B = |0\rangle$ and $A = |1\rangle$ is high and therefore both present similar states.

Accordingly, following results can be enumerated:

**R1.1**. In general we can say that the probability of alignment of agent $B, f(x, y) = P(B = |0\rangle)$, oscillates consistently around the value 0.5 as a harmonic underdamped oscillator for different values of $z = P(A = |1\rangle)$ which is the equilibrium state of the system. This is plausible.

**R1.2**. At the scale represented of in Figure 4.3(a) we observe that the angular frequency of this oscillator changes for different values of $y = P(B = |1\rangle\,|A = |1\rangle)$ and therefore we can separate the behavior of the function in three different regions, marked in Figure 4.3(a), and depicted in Figure 4.3(b) in detail.

**R1.3**. For values of $y = P(B = |1\rangle\,|A = |1\rangle) \in (0.2, 1]$, the probability of alignment of agent $B, f(x, y) = P(B = |0\rangle)$, oscillates consistently around 0.5 with a minimal amplitude for all values of $z = P(A = |1\rangle)$.

**R1.4**. For values of $y = P(B = |1\rangle\,|A = |1\rangle) \in (0.1, 0.2]$, the probability of alignment of agent $B$, $f(x, y) = P(B = |0\rangle)$, oscillates consistently around 0.5 with an exponential decay that consistently increases with $1 - z = P(A = |0\rangle)$.

**R1.5**. For values of $y = P(B = |1\rangle\,|A = |1\rangle) \in [0, 0.1]$, the probability of alignment of agent $B$, $f(x, y) = P(B = |0\rangle)$, oscillates consistently around 0.5. The oscillation presents an exponential decay for $1 - z = P(A = |0\rangle) \in [0.5, 0.9)$, and presents no decay for values of $1 - z = P(A = |0\rangle) > 0.9$.

**R1.6**. But the most striking observation of all is that if we increase the mapping of the circuits by a factor of 10, as shown in Figure 4.4(b) in which we make a mapping of the $y = P(B = |1\rangle\,|A = |1\rangle) \in [0, 0.1]$ with [0.01] intervals for $P(A = |1\rangle = 0.1$, we observe the same behavior as with the mapping of the $y = P(B = |1\rangle\,|A = |1\rangle) \in [0, 1]$ with [0.1] intervals for $P(A = |1\rangle = 0.1$ shown in Figure 4.4(a). The results **R1.1–R1.5** are valid for both mapping intervals. The parameters (exponential decay, displacement, amplitude, and phase) of the signals represented in Figure 4.4 are very similar. Only the frequency is inversely proportional to the mapping interval, hence scaling the oscillation shape, and suggesting that the two graphics depict a similar process. This means that the behavior of this system is self similar. This has powerful implications which we discuss in the conclusions.

We can summarize the main take–away of this study with the following statement: the case of 2 qubits shown by QSOD, allows us to affirm that when the strategic objective of the organizational design is to increase the alignment of a process owner, increasing the network by adding a support agent is mostly likely to have no effect at all in the performance of the agent being reported to. We learn this from **R1.1**. In fact, the probability of alignment of the original agent oscillates always around the random state.

From result **R1.2, R1.3, R1.4**, and **R1.5** we also observe that there is an exchange of energy between the original agent and the added agent, so that the alignment probability of the original agent can be positively

influenced for low levels of intersection between the alignment probability of the original agent and the added agent. This could be interpreted to mean that the original agent can benefit from the presence of its new partner as long as the new partner provides process information. In other words, if the added agent is able to explain some of the variability in the value creation process that could not previously be explained by the original agent, then the asymptotic stability probability of the original agent will increase. **The immediate consequence of this reading is that to add hierarchy levels to strategic design models of organizations, it is necessary to ensure the asymptotic stability of the lower agents before implementing a stable aggregation**. It is important to highlight at this point that, in the context of QSOD, a hierarchy does not only describe the rather classical hierarchical relationship between agents but rather a reporting relationship. This concept is more inclusive as it includes the relationship between an agent and his/her boss, but also the relationship between an agent and his/her customer, or the relationship between an agent and a supplier. This approach helps therefore model interactions between organizational process owners and this interactions can be potentially be scaled to any organizational context, included small and medium enterprises. This finding is very powerful for industry leaders, as well as for Strategic Organizational Design scholars because it imposes a severe constraint to ensure a sustainable and stable growth of Industry 4.0 organizations.

The implications of result **R1.6** are profound and reveal the essence of what some call the *self similar organization*. **The interaction of two process owners reveals an energy interchange that oscillates with more or less amplitude depending on certain parameters – the conditional alignment probabilities**. But what is really striking is that, independently of the granularity in which these parameters are observed, the oscillation always follows the same pattern. Such pattern is expressed by the results **R1.1–R1.5** and represents the cornerstone of the bilateral interaction under study. Self similarity in this QSOD context allows for a quantification of these complex dynamics and its pervasive effect offers robustness and resilience to the two qubit interaction.

## 4.2 The case of three qubits: two reports to one

The goal of this section is to explore how the relationship between two subordinates reporting to a leader influences the alignment of the latter with the company's strategic objectives within an Industry 4.0 environment. We represent the individual process owner, a complex network node in Industry 4. 0 represented in the form of a decision graph [55], as a quantum computing unit or qubit [82, 92]. Through the quantum simulation of strategic organizational design configurations through five hundred quantum circuit simulations we conclude that the alignment probability of the leader is never higher than the average alignment value of his subordinates, i.e., the leader never has a better alignment than his subordinates. In other words, the leader cannot

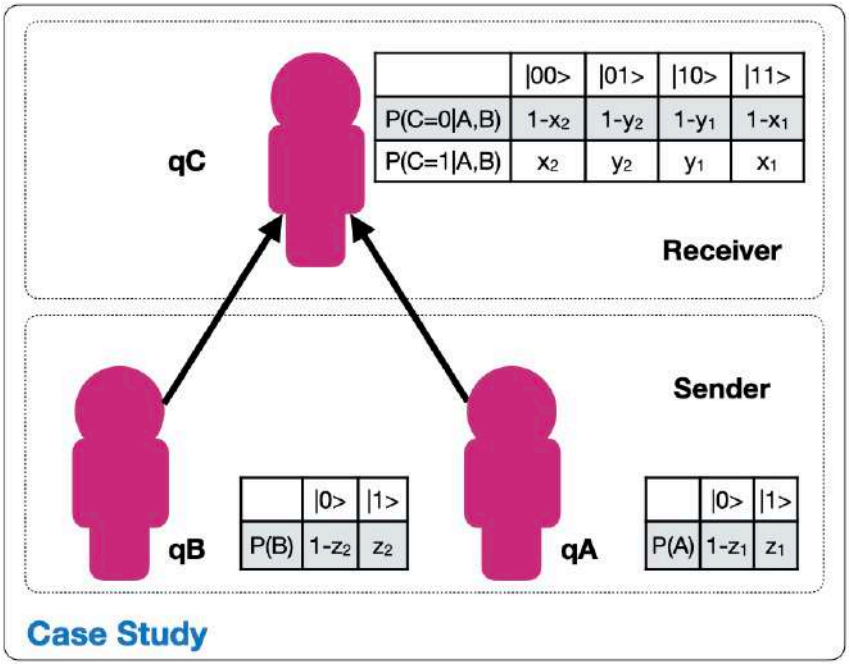


**Figure 4.5:** Case study framework three qubits: two report to one in which the respective node alignment probabilities are parametrized.

present asymptotic stability larger than that of his subordinates. The most relevant conclusion of this section is the clear recommendation to the leaders of Industry 4.0 not to add hierarchical levels to their organization if they have not achieved high levels of stability at lower levels.

In the previous Section 4.1 we showed how the interaction between two agents, an industrial leader and a subordinate reporting to her, can be interpreted as a dissipative oscillatory system in underdamped mode. In this section, we add an additional node to this configuration. As shown in Figure 4.5, we investigate the case of two subordinate (sender) agents $A$ and $B$, reporting simultaneously to a (receiver) leader $C$. As in the case above, the sender and receiver organizational agents are simulated by means of a three-qubit quantum circuit. We aim to investigate the leader's probability of alignment with the strategic objectives of the organization, depending on the state of his subordinates and their respective probabilities of alignment between them.

Our goal is to establish the alignment probability of agent $C$, $P(C = |0\rangle)$, as a function of the alignment probabilities of agents $A$ and $B$ and the alignment probabilities between agent $C$ and agents $A$ and $B$. This is accomplished by simulating hundreds of different quantum circuit configurations. We present in this section significant findings on the alignment probabilities of the highest–ranking agent depending on the alignment state of their lower rank subordinates.

The rest of the section hereinafter continues as follows: first, Section 4.2.1 begins with a description of the configuration of the quantum circuit computations necessary to simulate the outlined 3–qubit organiza-

tional design configuration. Second, Section 4.2.2 presents the case study that will simulate numerous quantum circuits, varying the mentioned parameters in order to obtain an optimal configuration of them. Third, in Section 4.2.3 we discuss the results obtained and propose an interpretation from perspective of previous studies and of the working hypotheses.

### 4.2.1 Quantum strategic organizational design circuit – Three Qubit organizational design configuration: two report to one

Figure 4.5 shows the three-qubit system under study. As explained in [89, 92], this requires the use of an additional ancilla-qubit $q^*$, whose state is given by $|\Psi^*\rangle$, that will allow us to use certain quantum operations that would otherwise be unfeasible. As a consequence, we are faced with a four qubit system whose aggregate state can be expressed as the tensorial product of the individual qubits. The multiple qubit state can be expressed as a linear combination of the $|0\rangle$ and $|1\rangle$ states, then the aggregated state can be represented by.

$$\begin{aligned}
|\Psi\rangle &= |\Psi_A\rangle \otimes |\Psi_B\rangle \otimes |\Psi_C\rangle \otimes |\Psi^*\rangle = \\
&= a_0 b_0 c_0 d_0 \,|0000\rangle + a_0 b_0 c_0 d_1 \,|0001\rangle + a_0 b_0 c_1 d_0 \,|0010\rangle + a_0 b_0 c_1 d_1 \,|0011\rangle + \\
&+ a_0 b_1 c_0 d_0 \,|0100\rangle + a_0 b_1 c_0 d_1 \,|0101\rangle + a_0 b_1 c_1 d_0 \,|0110\rangle + a_0 b_1 c_1 d_1 \,|0111\rangle + \\
&+ a_1 b_0 c_0 d_0 \,|1000\rangle + a_1 b_0 c_0 d_1 \,|1001\rangle + a_1 b_0 c_1 d_0 \,|1010\rangle + a_1 b_0 c_1 d_1 \,|1011\rangle + \\
&+ a_1 b_1 c_0 d_0 \,|1100\rangle + a_1 b_1 c_0 d_1 \,|1101\rangle + a_1 b_1 c_1 d_0 \,|1110\rangle + a_1 b_1 c_1 d_1 \,|1111\rangle \,,
\end{aligned} \tag{4.4}$$

where

$$\begin{aligned}
|\Psi_A\rangle &= a_0 \,|0\rangle + a_1 \,|1\rangle, \quad a_i \in \mathbb{C}^2 \,, \\
|\Psi_B\rangle &= b_0 \,|0\rangle + b_1 \,|1\rangle, \quad b_i \in \mathbb{C}^2 \,, \\
|\Psi_C\rangle &= c_0 \,|0\rangle + c_1 \,|1\rangle, \quad c_i \in \mathbb{C}^2 \,, \\
|\Psi^*\rangle &= d_0 \,|0\rangle + d_1 \,|1\rangle, \quad d_i \in \mathbb{C}^2 .
\end{aligned}$$

Thus it can be said that the quantum system of 4 *qubits* can be described by a $2^4$-dimensional complex unit vector.

An initial hypothesis of this section is that the leader of the Industry 4.0 organization benefits from knowing its alignment status with the strategic objectives of the organization. That is why we will focus on finding answers to the question of how to maximize the probability of alignment of node $C$, $P(C = |0\rangle)$, depending on the individual alignment probabilities of the $A$ and $B$ root nodes, as well as their respective relative probabilities between the nodes given by:

- Probability of alignment of node $A$. $1 - z_1 = P(A = |0\rangle) = 1 - P(A = |1\rangle)$.
- Probability of alignment of node $B$. $1 - z_2 = P(B = |0\rangle) = 1 - P(B = |1\rangle)$.
- Probability of no-alignment of node $C$ conditioned to the state $|11\rangle$ of the waveform $|\Psi_A\rangle \otimes |\Psi_B\rangle$. $x_1 = P(C = |1\rangle\,|A, B = |11\rangle)$.
- Probability of no-alignment of node $C$ conditioned to the state $|10\rangle$ of the waveform $|\Psi_A\rangle \otimes |\Psi_B\rangle$. $y_1 = P(C = |1\rangle\,|A, B = |10\rangle)$.
- Probability of no-alignment of node $C$ conditioned to the state $|00\rangle$ of the waveform $|\Psi_A\rangle \otimes |\Psi_B\rangle$. $x_2 = P(C = |1\rangle\,|A, B = |00\rangle)$.
- Probability of no-alignment of node $C$ conditioned to the state $|01\rangle$ of the waveform $|\Psi_A\rangle \otimes |\Psi_B\rangle$. $y_2 = P(C = |1\rangle\,|A, B = |01\rangle)$.

Mathematically speaking, we intend to find the values of $(x_1, y_1, x_2, y_2, z_1, z_2)$ that deliver the maximum alignment of node $C$ given by:

$$\begin{aligned} P(C = |0\rangle) = & f(x_1, y_1, x_2, y_2, z_1, z_2) = \\ & = ||a_0 b_0 c_0 d_0||^2 + ||a_0 b_0 c_0 d_1||^2 \\ & + ||a_0 b_1 c_0 d_0||^2 + ||a_0 b_1 c_0 d_1||^2 \\ & + ||a_1 b_0 c_0 d_0||^2 + ||a_1 b_0 c_0 d_1||^2 \\ & + ||a_1 b_1 c_0 d_0||^2 + ||a_1 b_1 c_0 d_1||^2. \end{aligned} \tag{4.5}$$

We will base on the principles of quantum circuit design presented in Chapter 2, to present the quantum

Table 4.2: Case two report to one: Qubit angles of rotation

| Qubit | Interpretation | Equation |
|---|---|---|
| $\|\Psi_A\rangle$ | The probability $z_1 = P(A = \|1\rangle)$ of qubit $\|\Psi_A\rangle$ to be in not–alignment translates into the rotation angle $\theta_{z_1}$. | $\theta_{z_1} = 2 \arctan \sqrt{\frac{z_1}{1-z_1}}$ |
| $\|\Psi_B\rangle$ | The probability $z_2 = P(B = \|1\rangle)$ of qubit $\|\Psi_B\rangle$ to be in not–alignment translates into the rotation angle $\theta_{z_2}$. | $\theta_{z_2} = 2 \arctan \sqrt{\frac{z_2}{1-z_2}}$ |
| $\|\Psi_C\rangle$ | The probability $x_1 = P(C = \|1\rangle \|A, B = \|11\rangle)$ of qubit $\|\Psi_C\rangle$ to be in not–alignment depending on the probability of the waveform $\|\Psi_A\rangle \otimes \|\Psi_B\rangle$ to be in the state $\|11\rangle$ translates into rotation angle $\theta_{x_1}$. | $\theta_{x_1} = 2 \arctan \sqrt{\frac{x_1}{1-x_1}}$ |
| | The probability $y_1 = P(C = \|1\rangle \|A, B = \|10\rangle)$ of qubit $\|\Psi_C\rangle$ to be in not–alignment depending on the probability of the waveform $\|\Psi_A\rangle \otimes \|\Psi_B\rangle$ to be in the state $\|10\rangle$ translates into rotation angle $\theta_{y_1}$. | $\theta_{y_1} = 2 \arctan \sqrt{\frac{y_1}{1-y_1}}$ |
| | The probability $x_2 = P(C = \|1\rangle \|A, B = \|00\rangle)$ of qubit $\|\Psi_C\rangle$ to be in not–alignment depending on the probability of the waveform $\|\Psi_A\rangle \otimes \|\Psi_B\rangle$ to be in the state $\|00\rangle$ translates into rotation angle $\theta_{x_2}$. | $\theta_{x_2} = 2 \arctan \sqrt{\frac{x_2}{1-x_2}}$ |
| | The probability $y_2 = P(C = \|1\rangle \|A, B = \|01\rangle)$ of qubit $\|\Psi_C\rangle$ to be in not–alignment depending on the probability of the waveform $\|\Psi_A\rangle \otimes \|\Psi_B\rangle$ to be in the state $\|01\rangle$ translates into rotation angle $\theta_{y_2}$. | $\theta_{y_2} = 2 \arctan \sqrt{\frac{y_2}{1-y_2}}$ |
| $\|\Psi^*\rangle$ | The ancilla qubit $\|\Psi^*\rangle$ is a support qubit and as such is not subject to any probability rotation. | |

circuit that represents the interactions of the decision network sketched in Figure 4.5 expressed by:

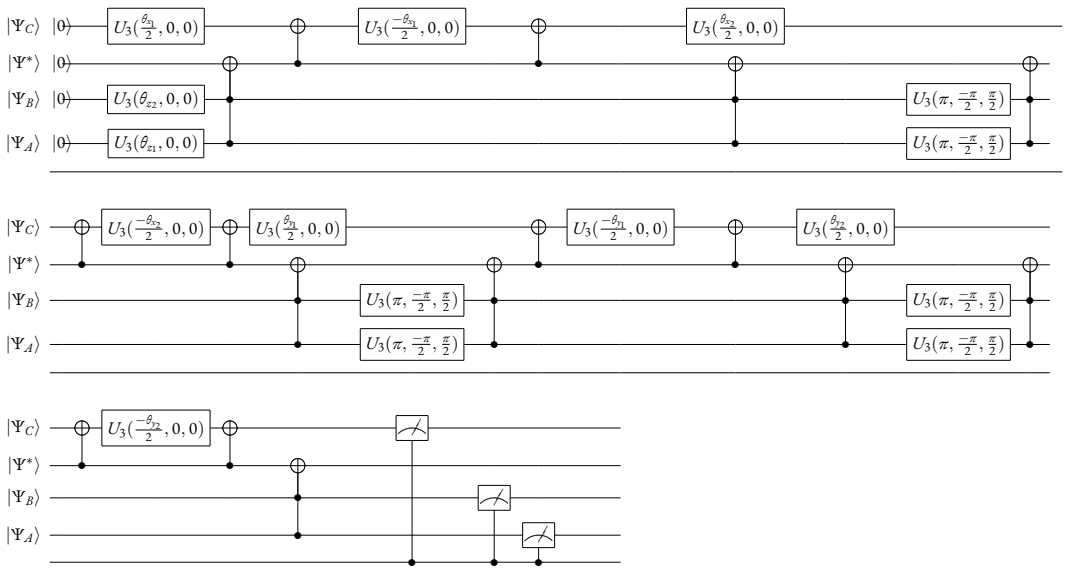


(4.6)

This circuit in Equation 4.6 presents four *qubits* $|\Psi_A\rangle$, $|\Psi_B\rangle$, $|\Psi_C\rangle$, $|\Psi^*\rangle$ which are rotated through quantum operators. The respective interpretation of these rotations and the equations to calculate them are described in Table 4.2.

### 4.2.2 Case study – Three Qubits organizational design configuration: two report to one

In order to ensure replicability and validation of the results obtained, the source code for the simulations is available under the https://osf.io/vzhpg/?view_only=0f890f0f93e3487390cb3d8a6774fc40 which was created with ***Jupyter Lab*** Version 1.2.6.

In this case, we are going to proceed to the simulation of quantum circuits that allow elucidating which is the combination of rotations (probabilities) that provides a maximum alignment of the node $C$, given by $P(C = |0\rangle)$. As shown in Equation 4.5, the function $P(C = |0\rangle) = f(x_1, y_1, x_2, y_2, z_1, z_2)$ depends on six parameters and a brute-force search with 10% incremental intervals, as for example was done in Section 4.1, would be computationally very demanding. That is why we are forced to supervise the search algorithm, limiting the parameters to certain plausible intervals where we know the maximum can be found. The first observation in this sense is that the network presents symmetry. Figure 4.5 shows that as far as node $C$ is concerned, nodes $A$ and $B$ are positioned symmetrically and at the same distance. This allows us to say that the search field can be reduced considerably. Furthermore, we know from Section 4.1 that the probability of alignment of a superior node is bounded by the probability of alignment of its subordinate. As a consequence, due to the network's symmetry, it can be hypothesized that the probability of alignment of node $C$ after alignment, $P(C_{post} = |0\rangle)$, has an upper bound given by $\overline{z}$ the mean alignment probabilities of its subordinates, $P(A = |0\rangle)$ and $P(B = |0\rangle)$, given by:

$$\overline{z} = \frac{(1 - z_1) + (1 - z_2)}{2} \overset{!}{<} P(C_{post} = |0\rangle). \tag{4.7}$$

Finally, taking this into account, and given that the probability $P(C_{post} = |0\rangle)$ lower than a random process is not of interest, and limit our study to values of $\overline{z}$ that are bigger than 0.5.

Taking into account the previous premises, we have made more than 400 quantum circuit simulations for fixed values of $\overline{z} \in [0.5, 1]$ and numerous values of $[x_1, y_1, x_2, y_2] \in [0, 1]$. The results, together with a polynomial regression curves, are shown in Figure 4.6. These regression curves are represented with a 5% confidence interval that resemble the uncertainties associated with quantum circuit calculations. The regression curve that fits the upper bound for $P(C_{post} = |0\rangle)$ and its $R$–squared $\overline{R^2}$ factor is described by:

$$\begin{aligned} \overline{P}(C_{post} = |0\rangle) &= 1.7915\overline{z}^2 - 1.667\overline{z} + 0.9 \; ; \; \overline{z} \in [0.5, 1], \\ \overline{R^2} &= 0.997. \end{aligned} \tag{4.8}$$

The regression curve that fits the lower bound for $P(C_{post} = |0\rangle)$ and its R–squared $\underline{R^2}$ factor is described

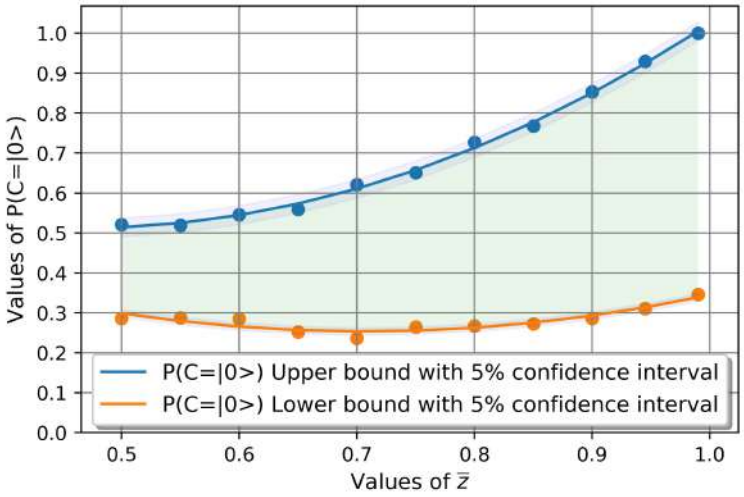


**Figure 4.6:** Case Study Two Reports to One. Alignment probability of upper node, $P(C_{post} = |0\rangle)$, is lower– and upper– bound for different values of the mean value of alignment probabilities of subordinates, $\bar{z} \in [0.5, 1]$.

by:

$$\begin{aligned} \underline{P}(C_{post} = |0\rangle) &= 1.061\bar{z}^2 - 1.489\bar{z} + 0.78 \; ; \; \bar{z} \in [0.5, 1], \\ \underline{R^2} &= 0.866. \end{aligned} \tag{4.9}$$

The green area in Figure 4.6 includes the entire search spectrum for different values of $[x_1, y_1, x_2, y_2] \in [0, 1]$. In Figure 4.7 we represent the values of $P(C_{post} = |0\rangle)$, with a fixed $\bar{z} = 0.99$, for values of $[x_1, y_1] \in [0.1, 0.3, 0.5, 0.9]$. In Figure 4.8 we represent the values of $P(C_{post} = |0\rangle)$, with a fixed $\bar{z} = 0.99$, for values of $[x_2, y_2] \in [0.1, 0.3, 0.5, 0.9]$.

In the following Section 4.2.3 we discuss these results in detail.

### 4.2.3 Discussion – Three Qubits organizational design configuration: two report to one

We now proceed to discuss the results systematically. We will start by discussing Figure 4.6 that describes the relationship between the average alignment probability $\bar{z} \in [0.5, 1]$ of the subordinate nodes $A$ and $B$ with the alignment probability of the upper node $C$, $P(C_{post} = |0\rangle)$. In this way, the following results can be summarized:

**R2.1**. As hypothesized in Equation 4.7, the alignment probability of node $C$ is never greater than the mean alignment probability of its subordinate nodes $A$ and $B$ given by $\bar{z} \in [0.5, 1]$. This means that in the presented configuration of two nodes reporting to a third one, the node being reported to can never reach a

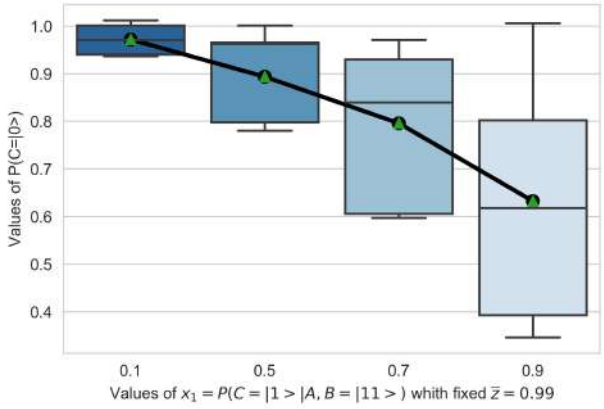


(a)

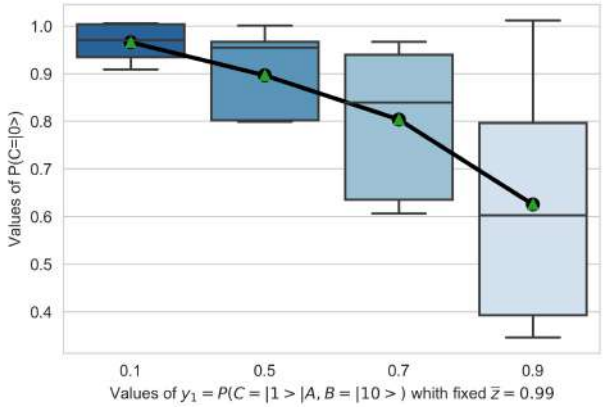


(b)

**Figure 4.7:** Case Study Two Reports to One. Results obtained for $P(C_{post} = |0\rangle)$ for different values of we represent the values of $P(C_{post} = |0\rangle)$, with a fixed $\bar{z} = 0.99$, for values of $[x_1, y_1), x_2, y_2] \in [0.1, 0.3, 0.5, 0.9]$. (a) $x_1 = P(C_{post} = |1\rangle\,|A, B = |11\rangle)$ (b) $y_1 = P(C_{post} = |1\rangle\,|A, B = |10\rangle)$

higher alignment probability than those presented by its subordinates.

We can formulate this result with the following statement: the alignment probability of a node to which two nodes report cannot be greater than the average of the alignment probability of these. In other words, **the alignment probability of a boss can never be greater than the average of the alignment probability of his two subordinates**. The implications of this are very powerful and relevant for leaders and organizational design scholars alike. On the one hand, this means that in order to increase the level of organizational hierarchies and preserve asymptotic stability towards the organizational strategic objectives, and therefore the low levels of associated variability, it is necessary that the lower levels present such a high or superior stability. This seems to indicate that we can only expand an organization to higher levels of complexity by adding new hierarchical layers if we have achieved high levels of stability at the lower levels. This fact is in accordance with previous

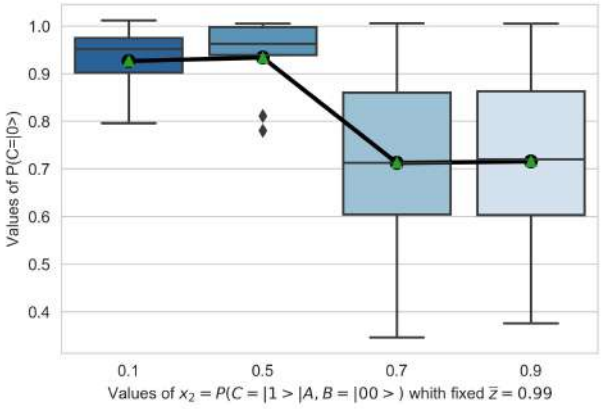


(a)

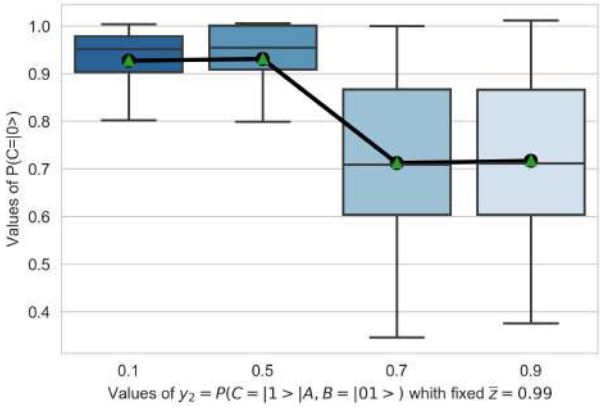


(b)

**Figure 4.8:** Case Study Two Reports to One. Results obtained for $P(C_{post} = |0\rangle)$ for different values of we represent the values of $P(C_{post} = |0\rangle)$, with a fixed $\bar{z} = 0.99$, for values of $[x_1, y_1), x_2, y_2] \in [0.1, 0.3, 0.5, 0.9]$. (a) $x_2 = P(C_{post} = |1\rangle\,|A, B = |00\rangle)$ (b) $y_2 = P(C_{post} = |1\rangle\,|A, B = |01\rangle)$

results presented in [88].

**R2.2**. The amplitude of possible alignment states of node $C$, increases with increasing values of $\bar{z} \in [0.5, 1]$ and is obtained by subtracting Equations 4.8 and 4.9. The green shaded area indicates the possible values of this probability, which will be obtained by varying the coefficients $[x_1, y_1, x_2, y_2]$ as already indicated.

This result is in accordance with the results obtained previously in Section 4.1 of one node reporting to another. Also, $x_1 = P(C_{post} = |1\rangle\,|A, B = |11\rangle)$=$y_1 = P(C_{post} = |1\rangle\,|A, B = |10\rangle)$ and $x_2 = P(C_{post} = |1\rangle\,|A, B = |00\rangle)$=$y_2 = P(C_{post} = |1\rangle\,|A, B = |01\rangle)$ then we have the case of a perfectly aligned node, and the problem is reduced to the case presented in [88] of one node reporting to another.

**R2.3**. In Figure 4.7 and Figure 4.8 we indicate, by means of a boxplot, how the alignment probability $P(C_{post} = |0\rangle$ behaves within its bounds. In both cases we observe how this probability has a lower bound. In

Figure 4.7 this lower bound is given by the relative probability of alignment of $P(C_{post} = |0\rangle$, conditioned to the states $x_1 = P(C_{post} = |1\rangle\,|A, B = |11\rangle)$ and $y_1 = P(C_{post} = |1\rangle\,|A, B = |10\rangle)$ respectively. This means that given $x_1 = P(C_{post} = |1\rangle\,|A, B = |11\rangle)$ or $y_1 = P(C_{post} = |1\rangle\,|A, B = |10\rangle)$ are in the indicated states, the probability of alignment $P(C_{post} = |0\rangle$ is equal or bigger. In Figure 4.8 this lower bound is given by the relative probability of alignment of $P(C_{post} = |0\rangle$, conditioned to the states $x_2 = P(C_{post} = |1\rangle\,|A, B = |00\rangle)$ and $y_2 = P(C_{post} = |1\rangle\,|A, B = |01\rangle)$ respectively. This means that given $x_2 = P(C_{post} = |1\rangle\,|A, B = |00\rangle)$ or $y_2 = P(C_{post} = |1\rangle\,|A, B = |01\rangle)$ are in the indicated states, the probability of alignment $P(C_{post} = |0\rangle$ is equal or bigger.

If we compare the results shown in Figure 4.7 and Figure 4.8 presented in **R2.3** with the results obtained in Section 4.1 that show the case of a node reporting to another one, it can be inferred that **the addition of a new node reporting to the superior node adds stability to the set**. In other words, the harmonic underdamped oscillation that was observed between the alignment states in the case of one node reporting to another, has disappeared in the case of two nodes reporting to a third. This seems to indicate that the additional node provides additional stability to the organizational system.

The results obtained studying the QSOD case of 3 *qubits*, in which two reports to another, opens new interesting research questions. In order to continue offering a valuable contribution to Industry 4.0 leaders and the research community in general, the next step to take in this line of research focus on studying the behavior of other 3 *qubits* QSOD configurations that are shown in Section 4.3.

## 4.3 The case of three qubits: one reports to two

In this section we explore how the relationship between one subordinate reporting to two leaders influences the alignment of the latter with the company's strategic objectives within an Industry 4.0 environment. We do this through the implementation of quantum circuits that represent decision networks. This is done for two cases: one in which the leaders do not communicate with each other, and one in which they do. Through the quantum simulation of strategic organizational design configurations through five hundred quantum circuit simulations, we conclude that in the first case both leaders are not simultaneously in alignment, and in the second case that both reporting nodes need to have an alignment probability higher than 90% to support the leader node.

In the previous Section 4.1 we showed how the interaction between two agents, an industrial leader and a subordinate reporting to her, can be interpreted as a dissipative oscillatory system in underdamped mode. As we illustrate in Figure 4.9, in this section we add a twist to these configurations by simulating the configuration

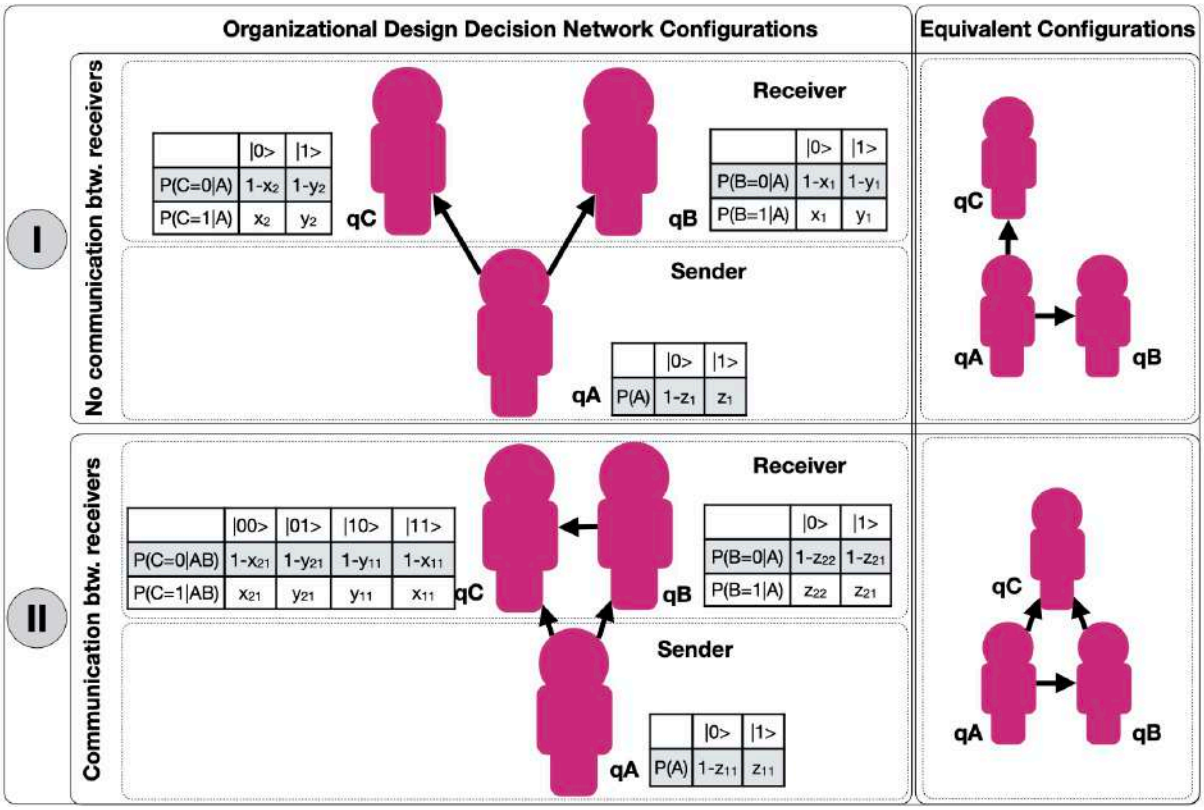


**Figure 4.9:** Case study framework three qubits: one reports to two in which the respective node alignment probabilities are parametrized.

in which one subordinate (sender) agent $A$ node reports to two others (receivers) $B$ and $C$ in two cases: when the nodes receiving the report do not communicate with each other, and when they communicate with each other. These organizational configurations under study are indeed extremely relevant since they represent basic strategic organizational design configurations such as the relationships of hierarchically related agents (vertical relationships) or supplier–customer interactions along the value stream (horizontal relationships). In the figure we show the respective topological equivalent configurations to each case. We aim to investigate the leader's probability of alignment, with the strategic objectives of the organization, depending on the state of his subordinates and their respective conditional probabilities of alignment between them.

Our objective is to establish the alignment probability of agents $B$ and $C$, $P(B = |0\rangle)$ and $P(C = |0\rangle)$ respectively, in dependence of the alignment probability of agent $A$ and the conditional alignment probabilities between agents $A$, $B$ and $C$. This is accomplished by simulating hundreds of different quantum circuit configurations.

The section continues as follows: first, Section 4.3.1 begins with a description of the configuration of the quantum circuit computations necessary to simulate the outlined 3–qubit organizational design configuration. Second, Section 4.3.3 presents the two case studies describing the two presented configurations: (I) describing

the case in which agents $B$ and $C$ have no communication between each other, and (II) describing the case in which agents $B$ and $C$ have communication between each other. Throughout the simulation of numerous quantum circuits, varying the mentioned parameters, an optimal configuration of them is sought for. Third, in Section 4.3.4 we discuss the results obtained and propose an interpretation in perspective of previous studies and of the working hypotheses.

### 4.3.1 QSOD Circuits – 3 Qubit organizational design configurations: one reports to two

Analogue to the previous sections, an initial hypothesis of this section is that the leader of the Industry 4.0 organization benefits from knowing its alignment status with the strategic objectives of the organization. That is why we will focus on finding answers to the question of how to maximize the probabilities of alignment of nodes $B$ and $C$, $P(B = |0\rangle)$ and $P(C = |0\rangle)$ respectively, depending on the individual alignment probabilities of the root node $A$, as well as their respective relative probabilities between the nodes given by different parameters in the two announced cases of study.

#### 4.3.1.1 Quantum Circuit – Case I – Agents B and C have no communication between each other.

In this case, as shown in Figure 4.9I, we will represent a three-qubit system. As explained in Chapter 2, this requires the use of three *qubits* $|\Psi_A\rangle$, $|\Psi_B\rangle$ and $|\Psi_C\rangle$. It should be noted that since the system is symmetrical, the position of the nodes (B) and (C) are interchangeable. We are faced with a three qubit system whereby the combined state can be described as the tensor product of the individual qubits. The multiple qubit states can be expressed as a linear combination of the $|0\rangle$ and $|1\rangle$ states, and the aggregate state can then be represented by:

$$\begin{aligned} |\Psi\rangle &= |\Psi_A\rangle \otimes |\Psi_B\rangle \otimes |\Psi_C\rangle = \\ &= a_0 b_0 c_0 |000\rangle + a_0 b_0 c_1 |001\rangle + a_0 b_1 c_0 |010\rangle + a_0 b_1 c_1 |011\rangle \\ &+ a_1 b_0 c_0 |100\rangle + a_1 b_0 c_1 |101\rangle + a_1 b_1 c_0 |110\rangle + a_1 b_1 c_1 |111\rangle , \end{aligned} \tag{4.10}$$

where:

$$\begin{aligned} |\Psi_A\rangle &= a_0 |0\rangle + a_1 |1\rangle \quad a_i \in \mathbb{C}^2 \\ |\Psi_B\rangle &= b_0 |0\rangle + b_1 |1\rangle \quad b_i \in \mathbb{C}^2 \\ |\Psi_C\rangle &= c_0 |0\rangle + c_1 |1\rangle \quad c_i \in \mathbb{C}^2 \end{aligned}$$

Thus it can be said that the quantum system of 3 *qubits* can be described by a $2^3$-dimensional complex unit vector.

To describe the case in which agents $B$ and $C$ have no communication between each other we need following parameters:

- Probability of alignment of node $A$. $1 - z_1 = P(A = |0\rangle) = 1 - P(A = |1\rangle)$.
- Probability of no–alignment of node $B$ conditioned to the state of alignment of node $A$.$x_1 = P(B = |1\rangle\,|A = |0\rangle)$.
- Probability of no–alignment of node $B$ conditioned to the state of no–alignment of node $A$. $y_1 = P(B = |1\rangle\,|A = |1\rangle)$.
- Probability of no–alignment of node $C$ conditioned to the state of alignment of node $A$. $x_2 = P(C = |1\rangle\,|A = |0\rangle)$.
- Probability of no–alignment of node $C$ conditioned to the state of no–alignment of node $A$. $y_2 = P(C = |1\rangle\,|A = |1\rangle)$.

Mathematically speaking, we intend to find the values of $(x_1, y_1, x_2, y_2, z_1)$ that maximize the functions $P(B = |0\rangle) = f_I(x_1, y_1, x_2, y_2, z_1)$ and $P(C = |0\rangle) = g_I(x_1, y_1, x_2, y_2, z_1)$. In other words, our challenge reduces to finding the values of $[x_1, y_1, x_2, y_2, z_1]all \in [0, 1]$ that maximize both following equations:

$$P(B = |0\rangle) = f_I(x_1, y_1, x_2, y_2, z_1) = ||a_0b_0c_0||^2 + ||a_0b_0c_1||^2 + ||a_1b_0c_0||^2 + ||a_1b_0c_1||^2, \tag{4.11}$$

$$P(C = |0\rangle) = g_I(x_1, y_1, x_2, y_2, z_1) = ||a_0b_0c_0||^2 + ||a_0b_1c_0||^2 + ||a_1b_0c_0||^2 + ||a_1b_1c_0||^2. \tag{4.12}$$

Based on the principles of quantum circuit design exposed in Chapter 2, we present the quantum circuit

Table 4.3: Case one reports to two without communication: Qubit angles of rotation

| Qubit | Interpretation | Equation |
|---|---|---|
| $\|\Psi_A\rangle$ | The probability $z_1 = P(A = \|1\rangle)$ of qubit $\|\Psi_A\rangle$ to be in not–alignment translates into the rotation angle $\theta_{z_1}$. | $\theta_{z_1} = 2 \arctan \sqrt{\frac{z_1}{1-z_1}}$ |
| $\|\Psi_B\rangle$ | The conditional probability $x_1 = P(B = \|1\rangle \,\|A = \|0\rangle)$ of qubit $\|\Psi_B\rangle$ to be in not–alignment depending on the probability of $\|\Psi_A\rangle$ to be in the state $\|0\rangle$ translates into rotation angle $\theta_{x_1}$. | $\theta_{x_1} = 2 \arctan \sqrt{\frac{x_1}{1-x_1}}$ |
| | The conditional probability $y_1 = P(B = \|1\rangle \,\|A = \|1\rangle)$ of qubit $\|\Psi_B\rangle$ to be in not–alignment depending on the probability of $\|\Psi_A\rangle$ to be in the state $\|1\rangle$ translates into rotation angle $\theta_{y_1}$. | $\theta_{y_1} = 2 \arctan \sqrt{\frac{y_1}{1-y_1}}$ |
| $\|\Psi_C\rangle$ | The conditional probability $x_2 = P(C = \|1\rangle \,\|A = \|0\rangle)$ of qubit $\|\Psi_C\rangle$ to be in not–alignment depending on the probability of $\|\Psi_A\rangle$ to be in the state $\|0\rangle$ translates into rotation angle $\theta_{x_2}$. | $\theta_{x_2} = 2 \arctan \sqrt{\frac{x_2}{1-x_2}}$ |
| | The conditional probability $y_2 = P(C = \|1\rangle \,\|A = \|1\rangle)$ of qubit $\|\Psi_C\rangle$ to be in not–alignment depending on the probability of $\|\Psi_A\rangle$ to be in the state $\|1\rangle$ translates into rotation angle $\theta_{y_2}$. | $\theta_{y_2} = 2 \arctan \sqrt{\frac{y_2}{1-y_2}}$ |

that represents the interactions of the decision network exposed in Figure 4.9I expressed by:

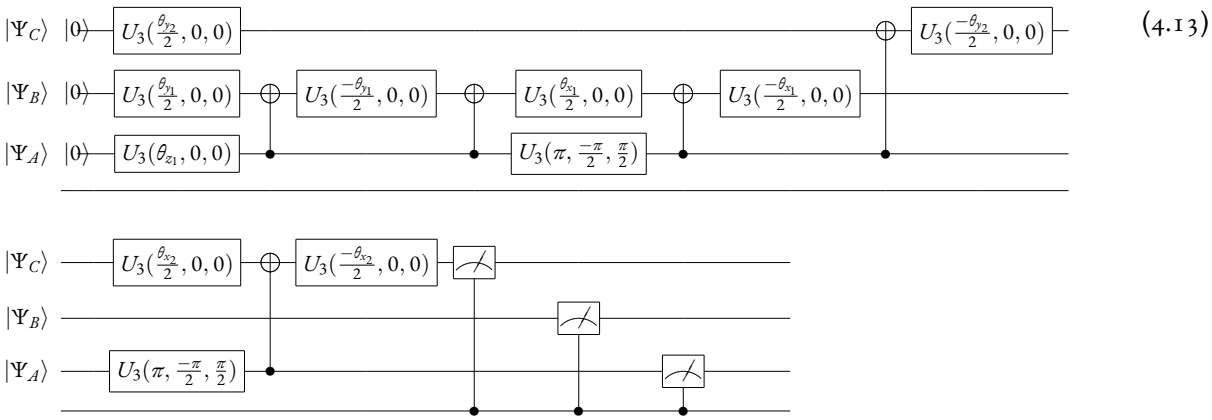


(4.13)

This circuit presents three *qubits* $|\Psi_A\rangle$, $|\Psi_B\rangle$ and $|\Psi_C\rangle$ which are rotated through quantum operators. The respective interpretation of these rotations and the equations to calculate them are described in Table 4.3.

### 4.3.2 Quantum Circuit – Case II – Agents B and C have communication between each other

In this case, as shown in Figure 4.5II, we will represent a three-qubit system. As explained in Section 2, this requires the use of an additional ancilla-qubit $q^*$, whose state is given by $|\Psi^*\rangle$, that will allow us to use certain

quantum operations that would otherwise be unfeasible. As a consequence, we are faced with a four qubit system whose aggregate state can be expressed as the tensorial product of the individual qubits. The multiple qubit state can be expressed as a linear combination of the $|0\rangle$ and $|1\rangle$ states, then the aggregated state can be represented by:

$$\begin{aligned}
|\Psi\rangle = |\Psi_A\rangle \otimes |\Psi_B\rangle \otimes |\Psi_C\rangle \otimes |\Psi^*\rangle = \\
&= a_0 b_0 c_0 d_0 |0000\rangle + a_0 b_0 c_0 d_1 |0001\rangle + a_0 b_0 c_1 d_0 |0010\rangle + a_0 b_0 c_1 d_1 |0011\rangle \\
&+ a_0 b_1 c_0 d_0 |0100\rangle + a_0 b_1 c_0 d_1 |0101\rangle + a_0 b_1 c_1 d_0 |0110\rangle + a_0 b_1 c_1 d_1 |0111\rangle \\
&+ a_1 b_0 c_0 d_0 |1000\rangle + a_1 b_0 c_0 d_1 |1001\rangle + a_1 b_0 c_1 d_0 |1010\rangle + a_1 b_0 c_1 d_1 |1011\rangle \\
&+ a_1 b_1 c_0 d_0 |1100\rangle + a_1 b_1 c_0 d_1 |1101\rangle + a_1 b_1 c_1 d_0 |1110\rangle + a_1 b_1 c_1 d_1 |1111\rangle ,
\end{aligned} \tag{4.14}$$

where:

$$\begin{aligned}
|\Psi_A\rangle &= a_0 |0\rangle + a_1 |1\rangle \quad a_i \in \mathbb{C}^2 \\
|\Psi_B\rangle &= b_0 |0\rangle + b_1 |1\rangle \quad b_i \in \mathbb{C}^2 \\
|\Psi_C\rangle &= c_0 |0\rangle + c_1 |1\rangle \quad c_i \in \mathbb{C}^2 \\
|\Psi^*\rangle &= d_0 |0\rangle + d_1 |1\rangle \quad d_i \in \mathbb{C}^2
\end{aligned}$$

Thus it can be said that the quantum system of 4 *qubits* can be described by a $2^4$-dimensional complex unit vector.

To describe the case in which agents $B$ and $C$ have communication between each other we need following parameters:

- Probability of alignment of node $A$. $1 - z_{11} = P(A = |0\rangle) = 1 - P(A = |1\rangle)$.
- Probability of no–alignment of node $B$ conditioned to the state of no–alignment of node $A$. $z_{21} = P(B = |1\rangle \, | A = |1\rangle)$.
- Probability of no–alignment of node $B$ conditioned to the state of alignment of node $A$. $z_{22} = P(B = |1\rangle \, | A = |0\rangle)$.
- Probability of no–alignment of node $C$ conditioned to the state $|11\rangle$ of the waveform $|\Psi_A\rangle \otimes |\Psi_B\rangle$. $x_{11} = P(C = |1\rangle \, | A, B = |11\rangle)$.
- Probability of no–alignment of node $C$ conditioned to the state $|10\rangle$ of the waveform $|\Psi_A\rangle \otimes |\Psi_B\rangle$. $y_{11} = P(C = |1\rangle \, | A, B = |10\rangle)$.

- Probability of no–alignment of node $C$ conditioned to the state $|00\rangle$ of the waveform $|\Psi_A\rangle \otimes |\Psi_B\rangle$. $x_{21} = P(C = |1\rangle\,|A, B = |00\rangle)$.

- Probability of no–alignment of node $C$ conditioned to the state $|01\rangle$ of the waveform $|\Psi_A\rangle \otimes |\Psi_B\rangle$. $y_{21} = P(C = |1\rangle\,|A, B = |01\rangle)$.

Mathematically speaking, we intend to find the values of $(x_{11}, y_{11}, x_{21}, y_{21}, z_{11}, z_{21}, z_{22})$ that maximize the functions $P(B = |0\rangle) = f_{II}(x_{11}, y_{11}, x_{21}, y_{21}, z_{11}, z_{21}, z_{22})$ and $P(C = |0\rangle) = g_{II}(x_{11}, y_{11}, x_{21}, y_{21}, z_{11}, z_{21}, z_{22})$. In other words, our challenge reduces to finding the values of $[x_{11}, y_{11}, x_{21}, y_{21}, z_{11}, z_{21}, z_{22}]all \in [0, 1]$ that maximize both equations:

$$\begin{aligned} P(B = |0\rangle) &= f_{II}(x_{11}, y_{11}, x_{21}, y_{21}, z_{11}) = \\ &= ||a_0b_0c_0d_0||^2 + ||a_0b_0c_0d_1||^2 + \\ &+ ||a_0b_0c_1d_0||^2 + ||a_1b_0c_0d_0||^2 + \\ &+ ||a_0b_0c_1d_1||^2 + ||a_1b_0c_0d_1||^2 + \\ &+ ||a_1b_0c_1d_0||^2 + ||a_1b_0c_1d_1||^2, \end{aligned} \tag{4.15}$$

$$\begin{aligned} P(C = |0\rangle) &= g_{II}(x_{11}, y_{11}, x_{21}, y_{21}, z_{11}) = \\ &= ||a_0b_0c_0d_0||^2 + ||a_0b_0c_0d_1||^2 + \\ &+ ||a_0b_1c_0d_0||^2 + ||a_1b_0c_0d_0||^2 \\ &= ||a_1b_1c_0d_0||^2 + ||a_1b_0c_0d_1||^2 + \\ &= ||a_0b_1c_0d_1||^2 + ||a_1b_1c_0d_1||^2. \end{aligned} \tag{4.16}$$

Based on the principles of quantum circuit design exposed in Chapter 2, we present the quantum circuit

that represents the interactions of the decision network exposed in Figure 4.5II expressed by:

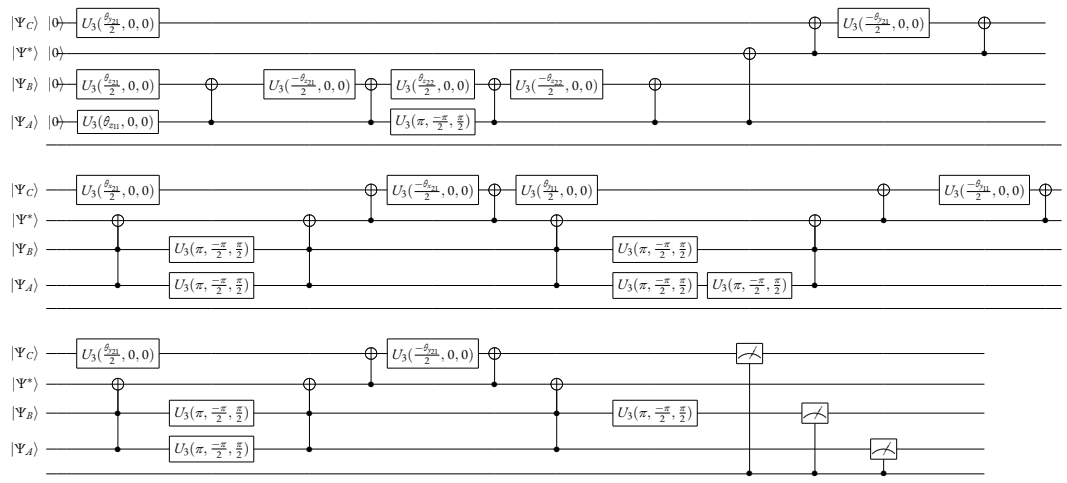

(4.17)

This circuit presents four *qubits* $|\Psi_A\rangle$, $|\Psi_B\rangle$, $|\Psi_C\rangle$, $|\Psi^*\rangle$ which are rotated through quantum operators. The respective interpretation of these rotations and the equations to calculate them are described in Table 4.4.

### 4.3.3 Case study – Three Qubits organizational design configuration: two report to one

In the following case study we move on to simulate thousands of configurations of the parameters presented in the quantum circuit Equation 4.13 and Equation 4.17 to understand those that provide a maximization of the alignment probabilities of agents $B$ and $C$, $P(B = |0\rangle)$ and $P(C = |0\rangle)$, given by Equation 4.15 and Equation 4.16 respectively. The code and additional results can be accessed in this https://osf.io/dg4q9/?view_only=a8348bdee16f4a82b577a8040ad12311. We will evaluate these results in Section 4.3.4.

#### 4.3.3.1 Simulation – Case I – Agents B and C have no communication between each other.

As shown in Equation 4.13, in the case of agents $B$ and $C$ with no communication between each other, we find five variables. As a consequence of Equation 4.10, the sample space is too large to use brute force to explore the phase space associated with the solutions and therefore we will proceed to set one or more variables and see how the others behave by means of exploratory graphs.

First of all we investigate the relationship between the alignment of agents $B$ and $C$ when the alignment of $A$ changes.

Table 4.4: Case one reports to two with communication: Qubit angles of rotation

| Qubit | Interpretation | Equation |
|---|---|---|
| $\|\Psi_A\rangle$ | The probability $z_{11} = P(A = \|1\rangle)$ of qubit $\|\Psi_A\rangle$ to be in not–alignment translates into the rotation angle $\theta_{z_{11}}$. | $\theta_{z_{11}} = 2 \arctan \sqrt{\frac{z_{11}}{1-z_{11}}}$ |
| $\|\Psi_B\rangle$ | The conditional probability $z_{21} = P(B = \|1\rangle \, \|A = \|1\rangle)$ of qubit $\|\Psi_B\rangle$ to be in not–alignment depending on the probability of $\|\Psi_A\rangle$ to be in the state $\|1\rangle$ translates into rotation angle $\theta_{z_{21}}$. | $\theta_{z_{21}} = 2 \arctan \sqrt{\frac{z_{21}}{1-z_{21}}}$ |
| | The conditional probability $z_{22} = P(B = \|1\rangle \, \|A = \|0\rangle)$ of qubit $\|\Psi_B\rangle$ to be in not–alignment depending on the probability of $\|\Psi_A\rangle$ to be in the state $\|0\rangle$ translates into rotation angle $\theta_{z_{22}}$. | $\theta_{z_{22}} = 2 \arctan \sqrt{\frac{z_{22}}{1-z_{22}}}$ |
| $\|\Psi_C\rangle$ | The conditional probability $x_{11} = P(C = \|1\rangle \, \|A, B = \|11\rangle)$ of qubit $\|\Psi_C\rangle$ to be in not–alignment depending on the probability of the waveform $\|\Psi_A\rangle \otimes \|\Psi_B\rangle$ to be in the state $\|11\rangle$ translates into rotation angle $\theta_{x_1 1}$. | $\theta_{x_{11}} = 2 \arctan \sqrt{\frac{x_{11}}{1-x_{11}}}$ |
| | The conditional probability $y_{11} = P(C = \|1\rangle \, \|A, B = \|10\rangle)$ of qubit $\|\Psi_C\rangle$ to be in not–alignment depending on the probability of the waveform $\|\Psi_A\rangle \otimes \|\Psi_B\rangle$ to be in the state $\|10\rangle$ translates into rotation angle $\theta_{y_{11}}$. | $\theta_{y_{11}} = 2 \arctan \sqrt{\frac{y_{11}}{1-y_{11}}}$ |
| | The conditional probability $x_{21} = P(C = \|1\rangle \, \|A, B = \|00\rangle)$ of qubit $\|\Psi_C\rangle$ to be in not–alignment depending on the probability of the waveform $\|\Psi_A\rangle \otimes \|\Psi_B\rangle$ to be in the state $\|00\rangle$ translates into rotation angle $\theta_{x_2 1}$. | $\theta_{x_{21}} = 2 \arctan \sqrt{\frac{x_{21}}{1-x_{21}}}$ |
| | The conditional probability $y_{21} = P(C = \|1\rangle \, \|A, B = \|01\rangle)$ of qubit $\|\Psi_C\rangle$ to be in not–alignment depending on the probability of the waveform $\|\Psi_A\rangle \otimes \|\Psi_B\rangle$ to be in the state $\|01\rangle$ translates into rotation angle $\theta_{y_{21}}$. | $\theta_{y_{21}} = 2 \arctan \sqrt{\frac{y_{21}}{1-y_{21}}}$ |
| $\|\Psi^*\rangle$ | The ancilla qubit $\|\Psi^*\rangle$ is a support qubit and as such is not subject to any conditional probability rotation. | |

In Figure 4.10 we show the results of the simulations obtained by representing the alignment probabilities of agents $B$ and $C$, $P(B = |0\rangle)$ and $P(C = |0\rangle)$, for each value of $z_1 = P(A = |1\rangle) \in \xi_1$ and all possible combinations of $\{x_1, y_1, x_2, y_2\} \in \xi_1$, whereas $\xi_1 = \{.1, .2, .3, .4, .5, .6, .7, .8, .9\}$.

Next we show how the alignment of agents $B$ and $C$ changes when the alignment probability of $A$ changes, when the relative probability of not–alignment of $B$ and $C$ conditioned to the not–alignment state of $A$ are the same.

In Figure 4.11 we show the results of the simulations obtained by representing the alignment probabilities of agents $B$ and $C$, $P(B = |0\rangle)$ and $P(C = |0\rangle)$, for each value of $y_1 = P(B = |1\rangle \, |A = |1\rangle) = y_2 = P(C = |1\rangle \, |A = |1\rangle) \in \xi_2$ and all possible combinations of $\{z_1, x_1, x_2\} \in \xi_2$, whereas $\xi_2 = \{0.01, 0.05, .1, .2, ..., .9\}$.

In order to compare these results with those of Section 4.3.3.2 The results of Figure 4.10 and Figure 4.11 are summarized in 3D in Figure 4.12(a) and Figure 4.12(b) respectively.

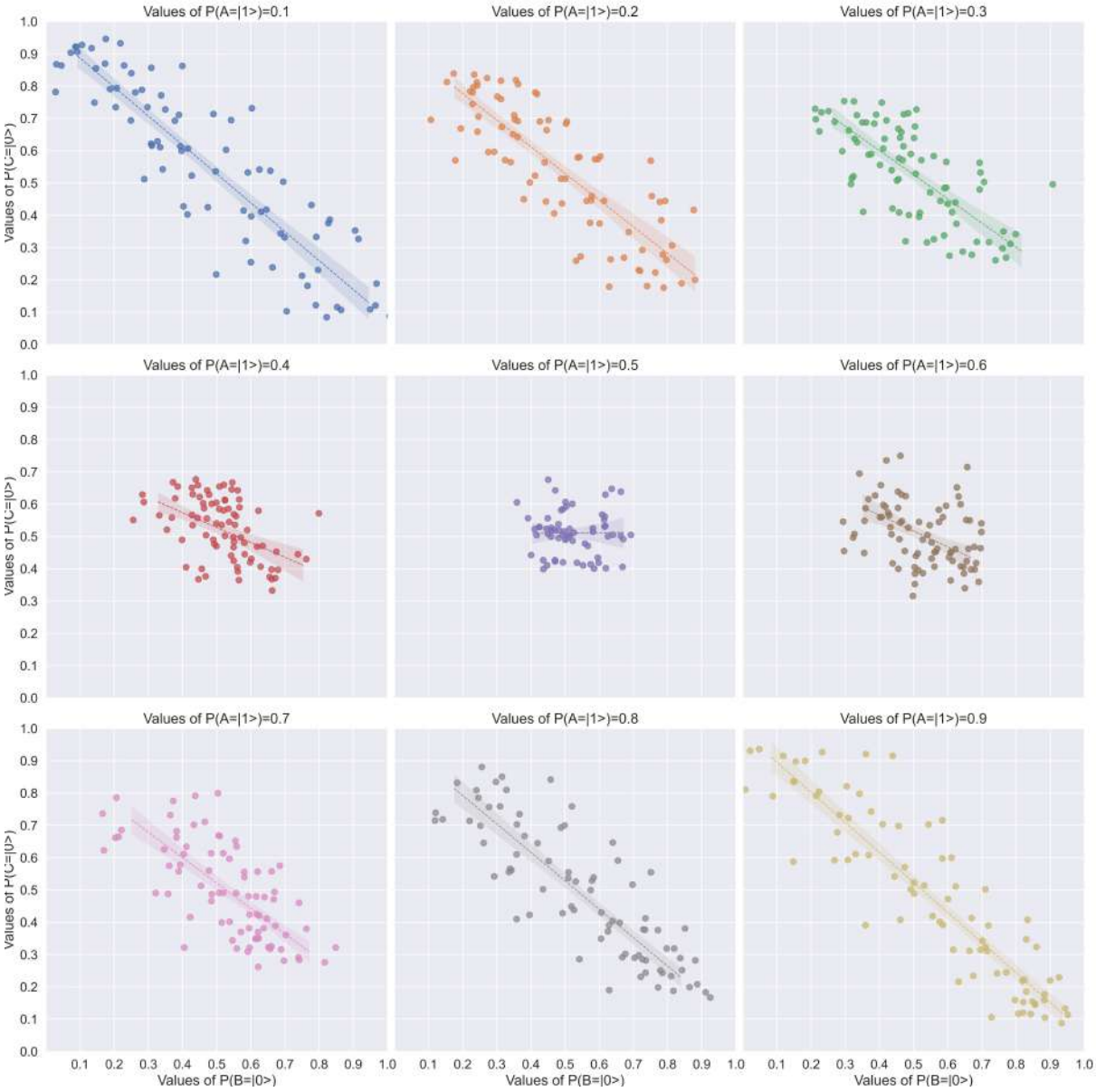


**Figure 4.10:** Case Study One Reports to Two with no Communication. Correlation between $P(B = |0\rangle)$ and $P(C = |0\rangle)$ for different values of $z_1 = P(A = |1\rangle) \in \xi_1$

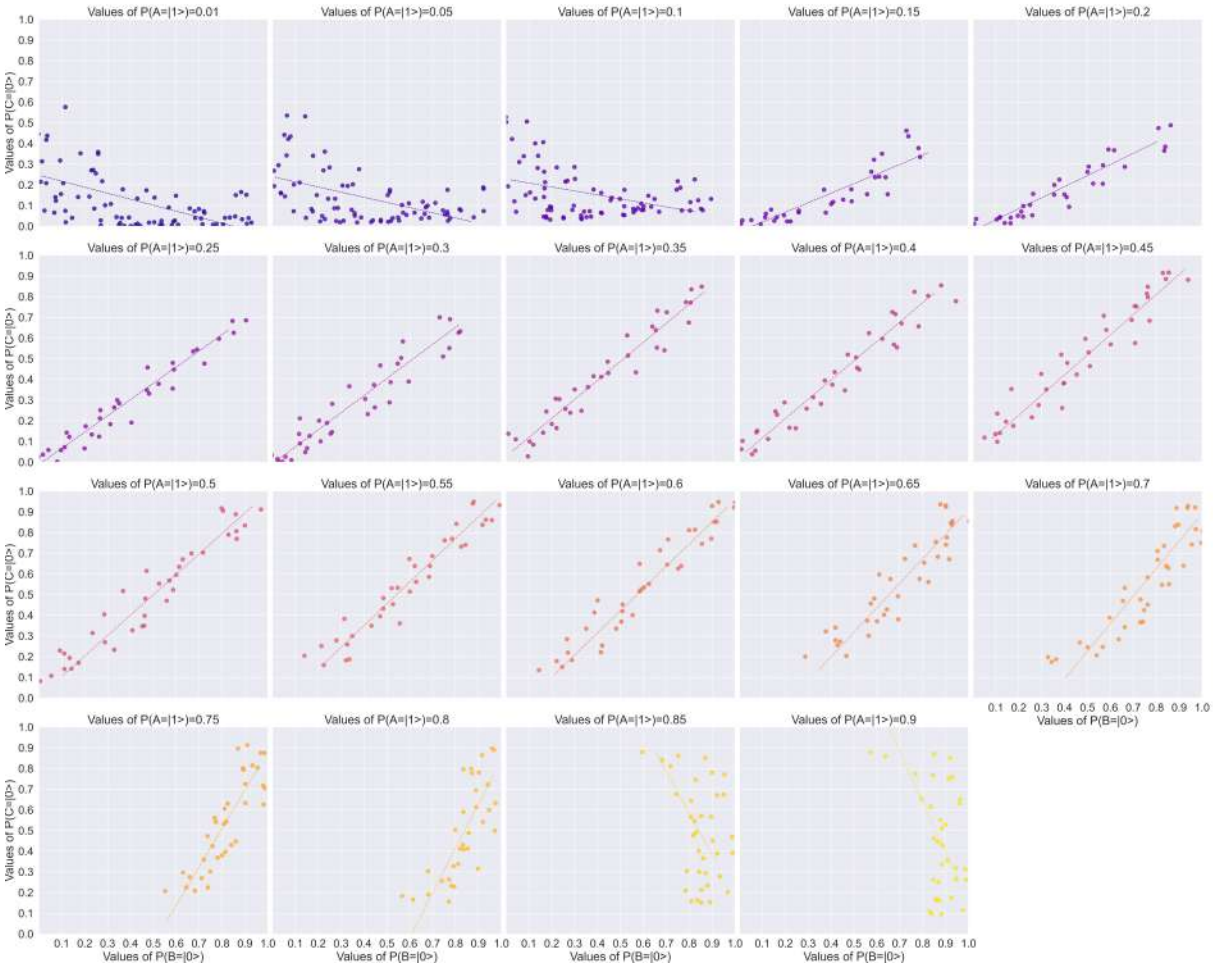


**Figure 4.11:** Case Study One Reports to Two with no Communication. Correlation between $P(B = |0\rangle)$ and $P(C = |0\rangle)$ for different values of $y_1 = P(B = |1\rangle \,|A = |1\rangle) = y_2 = P(C = |1\rangle \,|A = |1\rangle) \in \xi_2$

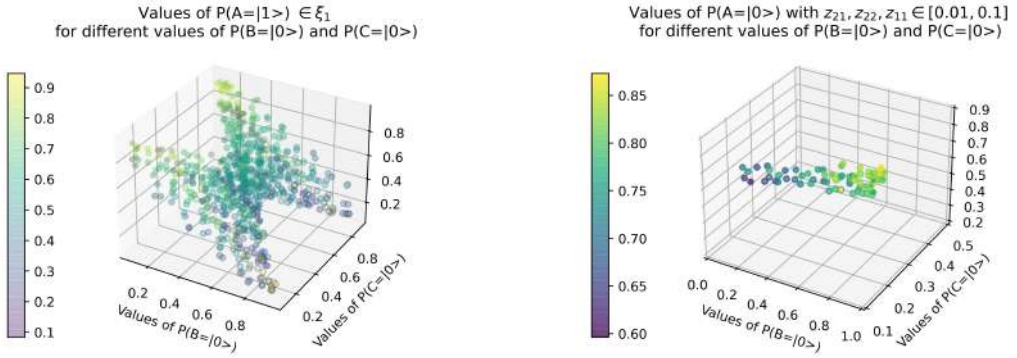


(a) (b)

**Figure 4.12:** Case Study One Reports to Two with no Communication. Correlation between $P(B = |0\rangle)$ and $P(C = |0\rangle)$. (a) For different values of $z_1 = P(A = |1\rangle) \in \xi_1$. (b) For different values of $y_1 = P(B = |1\rangle \,|A = |1\rangle) = y_2 = P(C = |1\rangle \,|A = |1\rangle) \in \xi_2$

#### 4.3.3.2 Simulation – Case II – Agents B and C have communication between each other.

As shown in Equation 4.17, in the case of agents $B$ and $C$ with communication between each other, we find seven variables. As a consequence of Equation 4.14, the sample space is too large to use brute force to explore the phase space associated with the solutions.

As in the previous case, we intend to investigate the behavior of the alignment probabilities of agents $B$ and $C$, $P(B = |0\rangle)$ and $P(C = |0\rangle)$. The results obtained in Section 4.1 indicate that the alignment probability of $P(A = |0\rangle)$ that allows for an alignment of the higher nodes is greater or equal than 90%.

Therefore we set the value of $z_{11} = P(A = |1\rangle) \in [0.01, .1]$, and vary accordingly the values of $z_{21} = P(B = |1\rangle \, |A = |1\rangle = z_{22} = P(B = |1\rangle \, |A = |0\rangle) both \in [0.01, 0.9]$, with changing values of $x_{11} = x_{21} = x_{21} = y_{21}$, to observe the change in the alignment probabilities of agents $B$ and $C$, $P(B = |0\rangle)$ and $P(C = |0\rangle)$.

This is shown in Figure 4.13:

- Figure 4.13(a), and its equivalent in 3D Figure 4.13(b), for $P(B = |0\rangle)$ and $P(C = |0\rangle)$ with fixed $z_{21} = P(B = |1\rangle \, |A = |1\rangle = z_{22} = P(B = |1\rangle \, |A = |0\rangle) both \in [0.01, .1]$,
- Figure 4.13(c), and its equivalent in 3D Figure 4.13(d), for $P(B = |0\rangle)$ and $P(C = |0\rangle)$ with fixed $z_{21} = P(B = |1\rangle \, |A = |1\rangle = z_{22} = P(B = |1\rangle \, |A = |0\rangle) both \in [0.2, .5]$, and
- Figure 4.13(e), and its equivalent in 3D Figure 4.13(f), for $P(B = |0\rangle)$ and $P(C = |0\rangle)$ with fixed $z_{21} = P(B = |1\rangle \, |A = |1\rangle = z_{22} = P(B = |1\rangle \, |A = |0\rangle) both \in [0.6, .9]$.

### 4.3.4 Discussion – Three Qubits organizational design configuration: two report to one

As announced, in this Section 4.3.4 we proceed to discuss the results **R3** obtained from the simulations:

In the case in which agents $B$ and $C$ have no communication between each other, we can derive following results:

- **R3.1**. *Agents B and C have an antagonistic alignment probability*. The two never have a high probability of alignment simultaneously. In Figure 4.10 we can see how, for both high and low values of alignment for node $A$, $P(A = |0\rangle) = 0.9$ or $P(A = |0\rangle) = 0.1$ respectively, the alignment probabilities of agents $B$ and $C$ have a negative correlation. When one of the two has high alignment probabilities, the other has low ones.

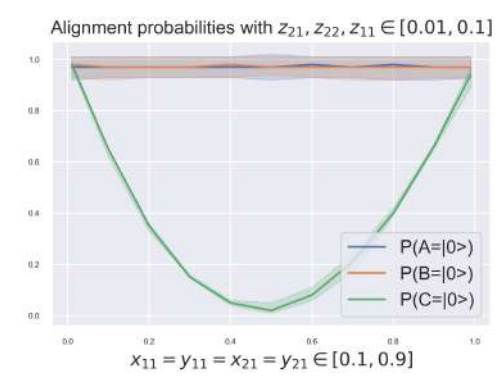


(a)

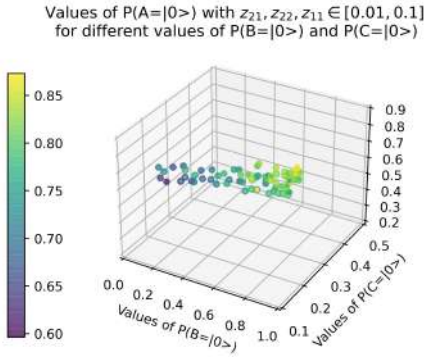


(b)

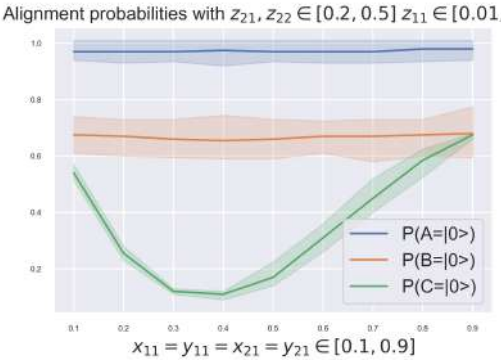


(c)

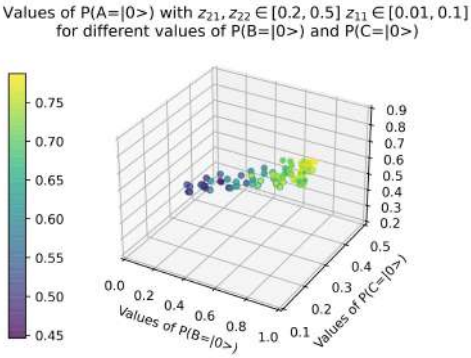


(d)

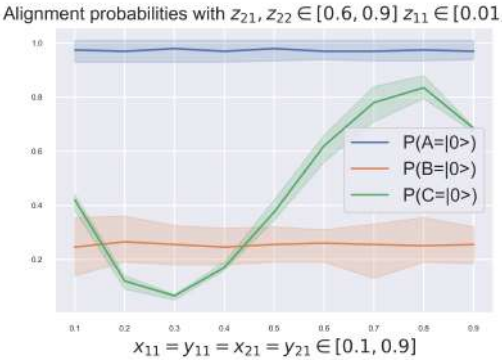


(e)

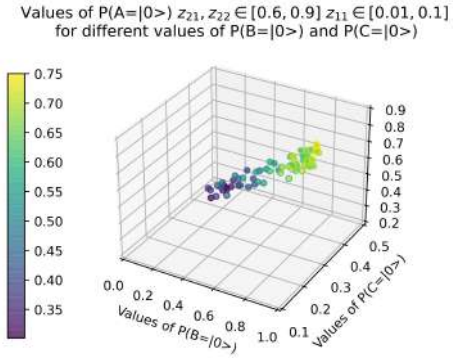


(f)

**Figure 4.13:** Case Study One Reports to Two with with Communication. Alignment Probabilities of $P(A = |0\rangle)$, $P(B = |0\rangle)$ and $P(C = |0\rangle)$ with $z_{11} = P(A = |1\rangle) \in [0.01, .1]$ for different values of fixed $z_{21} = P(B = |1\rangle\,|A = |1\rangle) = z_{22} = P(B = |1\rangle\,|A = |0\rangle)$, and combinations of $x_{11} = x_{21} = x_{21} = y_{21}$. (a) Fixed $z_{21} = z_{22} both \in [0.01, .1]$. (b) Fixed $z_{21} = z_{22} both \in [0.01, .1]$. (c) Fixed $z_{21} = z_{22} both \in [0.2, .5]$. (d) Fixed $z_{21} = z_{22} both \in [0.2, .5]$. (e) Fixed $z_{21} = z_{22} both \in [0.6, .9]$. (f) Fixed $z_{21} = z_{22} both \in [0.6, .9]$.

The management conclusion derived from **R3.1** for subordinate agent $A$ is staggering and somehow tragic: **if the two bosses do not communicate with each other, $A$ will never be able to serve them in such a way that both are simultaneously in alignment. It doesn't matter what $A$ does**.

This could lead one to believe that agent $A$'s motivation to provide a contribution to the value chain may be diminished due to the very organizational structure in which he is immersed, regardless of his capabilities, skills, or attitudes. The organizational design would therefore impose undesirable boundary conditions for the adequate development of the activity of the subordinate node.

- **R3.2**. *Agents B and C only agree by chance*. In Figure 4.10 we can see how, as agent $A$ approaches its random alignment probability of 50%, the alignment probabilities of $B$ and $C$ become homogeneous until reaching the 50% values as well.

  The conclusions derived from the **R3.2** result are not very encouraging for management either. **In case the two superior agents do not communicate between them, their joint alignment is always around the point of equilibrium, which is the probability given by the chance**. As long as the subordinate node has a higher or lower probability of alignment, their positions will be more or less differentiated.

  This would imply that the node would tend not to position itself with either of the two nodes to which it reports and the expected behavior on its part would be one of a lack of decision-making that could potentially jeopardize the efficiency of the associated value creation processes.

- **R3.3**. *Quantum phase transition with 90% alignment probability of node A*. The representations of Figure 4.11 are particular cases of the general solution of Figure 4.10. In both we can observe a sharp change of slope of the regression between the alignment probabilities of $B$ and $C$. This clearly indicates a quantum phase change at the point where the probability of non–alignment of agent $A$ is 10%, $P(A = |1\rangle) = 0.1$. In more detail, the observed results show:

  - As shown in Figure 4.11, if the alignment probability of $A$ is very high, $P(A = |0\rangle) > 0.9$ (or $P(A = |1\rangle) < 0.1$), and the probability that $B$ and $C$ are in non–alignment, provided that $A$ is in non–alignment, are equal, $y_1 = P(B = |1\rangle \, | A = |1\rangle) = y_2 = P(C = |1\rangle \, | A = |1\rangle)$, then the alignment probability of $C$ is very low and does not vary with the alignment probability of $B$.
  - As shown in Figure 4.11, if the alignment probability of $A$ is not high, $0.15 < P(A = |1\rangle) < 0.90$, and the probability that $B$ and $C$ are in non–alignment, provided that $A$ is in non–alignment, are equal, $y_1 = P(B = |1\rangle \, | A = |1\rangle) = y_2 = P(C = |1\rangle \, | A = |1\rangle)$, then the alignment probability of $B$ and $C$ present a positive correlation.

The conclusions derived from the **R3.3** confirm the results obtained in [88]: **only a strong alignment probability at lower reporting levels enables alignment at higher levels. We have shown that this threshold is set by 90%.**

To grow the organizational network towards strategic objectives, it is necessary to ensure asymptotic stability at the operational levels of the organization. These lower levels are generally the levels closest to the creation of value and it seems logical that they are the sustaining base of the organizational structure.

In the case in which agents $B$ and $C$ have communication between each other, we can derive following results:

- **R3.4**. When $B$ and $C$ are entangled, they work as one. As shown in Figure 4.13(a), when $x_{11} = x_{21} = x_{21} = y_{21} = z_{21} = z_{22} all \in ]0, 0.1] \cup [0.9, 1[$, the quantum circuit is identical to that of one qubit reporting to other qubit shown in Section 4.1, and behaves in a similar manner.

  The conclusions derived from the **R3.4** result is that **high levels of alignment in both reporting agents $A$ and $B$ do not imply a high level of alignment of node $C$.**

  When $B$ and $C$ present high levels of alignment, high levels of alignment on node $C$ are only attained for an entangled system in which $A$, $B$ and $C$ are highly dependent, given by the condition $x_{11} = x_{21} = x_{21} = y_{21} = z_{21} = z_{22} all \in ]0, 0.1] \cup [0.9, 1[$.

- **R3.5**. Agents $B$ and $C$ interchange *energy*. Lowering the probability of alignment of node $B$, $P(B = |0\rangle)$, which can be understood as its *energy*, while maintaining $P(A = |1\rangle) \in [0.01, .1]$, shows how $P(C = |0\rangle)$ behaves with changing $x_{11} = x_{21} = x_{21} = y_{21} = z_{21} = z_{22}$. The curves shown quantify this interaction.

  The conclusions derived from **R3.5** show that **the interaction between the superior agents $B$ and $C$ becomes manifest when the alignment probability of $A$ is fixed at values higher than 90%.** Both superior agents $B$ and $C$ present a non–linear interaction, and depending on what agent should be prioritized, strategies can be then taken towards one or toward other.

# 5

# Quantum JIDOKA – Integration of Quantum Computation on a Machine for in–control Process Visualization

JIDOKA is currently considered a lean tool that "enables machines to work harmoniously with their human operators and features intelligent capabilities by automatically stopping a process by man or machine, in the event of an abnormally, a problem, such as equipment malfunction, quality issues, or late work" [107]. It was introduced by Ohno [42] as one of the two pillars of the Toyota production system, alongside with the JIT, needed to accomplish the elimination of waste. The Japanese term was translated from the coined term "autonomation" or "automation with human touch" and its origins traced back to the invention by Sakichi Toyoda (1867–1930) of a looming machine that would automatically stop as soon as a thread in the machine teared [42]. The core idea behind JIDOKA is to provide "intelligence" to machines with built-in automatic

checking systems that would automatically stop to prevent any defective part passing to the next step in the value stream. In case of an abnormal situation, the intervention of an operator that can be in charge of monitoring several processes is necessary. Moreover, to eliminate any source of waste, JIDOKA aims at preventing this mistake from happening, again, reinforcing a culture of continuous learning and improvement. Thus, it is essential to identify the defective part as soon as possible, trigger a signal to stop the work center, and even the production process if necessary, to determine what the root cause for the production of the defective item has been, but also achieve an effective human–machine interaction. For many years, JIDOKA principles were primarily built on mechanical tools and devices with electronic components playing an increasing role. Romero et al. [107] describe three prior generations of JIDOKA systems: mechanical gadgets that avoid mistakes (POKA–YOKE), visual and audio alarms (ANDON), sensor-based fault diagnosis (JIDOKA rules). The immense possibilities brought up by Industry 4.0, through digitization and wide availability of low-cost sensors, open the way to utilize these large amounts of data and be able to act on a variety of input variables and handle complex processes and lead to a new generation JIDOKA 4.0 [107]. The impact of Industry 4.0 in the evolution of JIDOKA 4.0 is described in what follows.

wThe main core of JIDOKA, which is the stopping of the machine, can only be one of the first steps as still no further production should take place until the operator has found the mistake. This has been one of the main reasons why many companies, outside Japan, were hesitant at first about implementing JIDOKA [42]. Even the use of Andon-systems, which notify the correct person of the shutdown can only reduce but not eliminate those negative effects. The next step is to make the data available to the operator, in order to assist the search for the source of the defective machine. Industry 4.0 can act as a key enabler [51]. In addition to its technological side, cyber–physical systems offer multimodal interfaces for more effective human–machine collaboration. It is part of the Industry 4.0 networking concept, production and people as entities, participating in value creation. Another step further consists in directly pointing out the possible source of the problem. An ideal goal is the design of a self-regulating machine, which is able to adapt to different circumstances and prevent the need of stopping the machine. Although there are some limitations to identify the cause of defective parts in all cases, it should be possible to be able to at least better predict whether a part is likely to break. Although the target range and probability distributions for the corresponding measured values can be specified for each sensor, the evaluation of sensor data due to networked conditional probabilities creates a high degree of complexity, which quickly overtaxes even experienced employees in the evaluation. Incorrect evaluations and time delays are often the result. In this respect, supporting a system that automatically performs the task of pre-assessing the overall situation for the human as a result of the interaction of the individual measured val-

ues can be of considerable benefit. Decision networks, which quickly and efficiently calculate the conditional probabilities of the interconnection of random variables, can be an effective tool to this aim. However, even this approach faces limitations due to the computational power required and leads to delays in feedback to the worker. Quantum simulations shows relevant advantages to accelerate this feedback significantly [58]. Hence the interest in studying the possibilities of quantum computing to implement the described JIDOKA methodology more efficiently and responsively. In sum, the growing possibilities of combining lean manufacturing and Industry 4.0 and their associated benefits have been posed by many studies [48–52], whereas the rapid evolution of technological advancements opens new fields of applications. Previous works have shown that JIDOKA benefits from some Industry 4.0 technologies such as CPS, connectivity, and operator wearable systems [11], and recently to improve process monitoring in order to predict quality defects. An important aspect in the implementation of JIDOKA is the operator, as the system only works through the cooperation of both [107]. Efficient Bayesian network computing algorithms can help firms to adopt JIDOKA or "automation with human touch" approach, not only improving the efficiency of the manufacturing process but also making possible a human–machine cooperation system. In this context, we propose the integration of quantum computing and JIDOKA to simulate the intricate monitoring sensor network within a machine. This quantum simulation of the machine sensor network is a quantum digital twin.

This quantum digital twin is expected to allow the application of real-time JIDOKA in the manufacturing processes. Since this Chapter is oriented to Industry 4.0 users and we want to give it an eminently experimental and practice-oriented character, we prefer to focus on the core of the problem and thus spare the reader from lengthy theoretical explanations on the design of quantum simulations. In references [88, 89, 108, 109], interested readers can find resutls in which the authors show both the theoretical and practical principles of how to transform decision networks with conditional probabilities into their counterpart quantum circuits.

The remainder is organized as follows: in Section 5.1 the case study chosen to test our hypothesis is introduced: we describe the structure and interaction of the overall system with our quantum digital twin and establish the scope in Section 5.2. In Section 5.2.1 and Section 5.2.2 the specific hardware and software are presented, followed by the description of the data collection components of the setup in Section 5.3. Results of our study are summarized in Section 5.4. Finally, further aspects are discussed in Section 5.5, where we also draw the main conclusions, limitations, and future applications of our research.

## 5.1 Case Study. Quantum JIDOKA

Our initial hypothesis is that we can model the internal sensor network of a machine with quantum simulations that show better performance than classical models based on decision networks. To quantitatively test this hypothesis, as a first step to evaluate the effect of the integration of quantum simulations in I4.0 environments, a case study is used. In this case study, we are going to generate a digital quantum twin to provide the 4.0 operator with a shopfloor management tool that allows him to visualize the status of the machine in real time, as shown schematically in Figure 5.1.

We integrated the proposed solution in a factory and tested it for 12 weeks. However, for privacy reasons imposed by the process owner, the data related to the process in question cannot be disclosed. For this reason a dummy dataset is presented to show the functionality of the solution, as well as to ensure reproducibility to interested scholars or industrialists. The state of the machine in question is measured by 5 sensors: two of them sense the rotational speed of two motors that, in turn, drive two drills that make two holes whose diameter is measured by other two sensors, whose relative position determines the quality of the final product measured by a fifth sensor. As argued by Byrd and Turner [110], a single case study can be seen as the only possible building block in the process of developing the validity and reliability of the proposed hypothesis. Following the recommendations of Eisenhardt [99], a clear case study road-map is followed for each one of them. This road-map has several phases: (1) Section 5.2, scope establishment, (2) Section 5.2.1, specification of hardware, (3) Section 5.2.2, specification of software, (4) Section 5.3, data collection, and (5) Section 5.3.1, quantum digital twin.

## 5.2 Scope Establishment

The use of quantum computers in the implementation of larger decision networks and their use in a JIDOKA environment should open up the possibility of performing high-performance analysis in larger sensor networks.

The objective of this case study is to generate a low-cost quantum digital twin that represents the statistical dependencies between five sensors positioned on a computer numerical control processing machine that measure parameters relevant to the quality of the manufactured product. For this purpose, we will install a quantum circuit in a low-cost component, which simulates the statistical dependencies derived from the value-creation process inside the machine. This component will receive data from the machine through a radio frequency identification (RFID) device and will compute the state of the machine in real time, generating a visualization that will allow the process owner to understand it. This interface will resemble a conditioning monitoring and

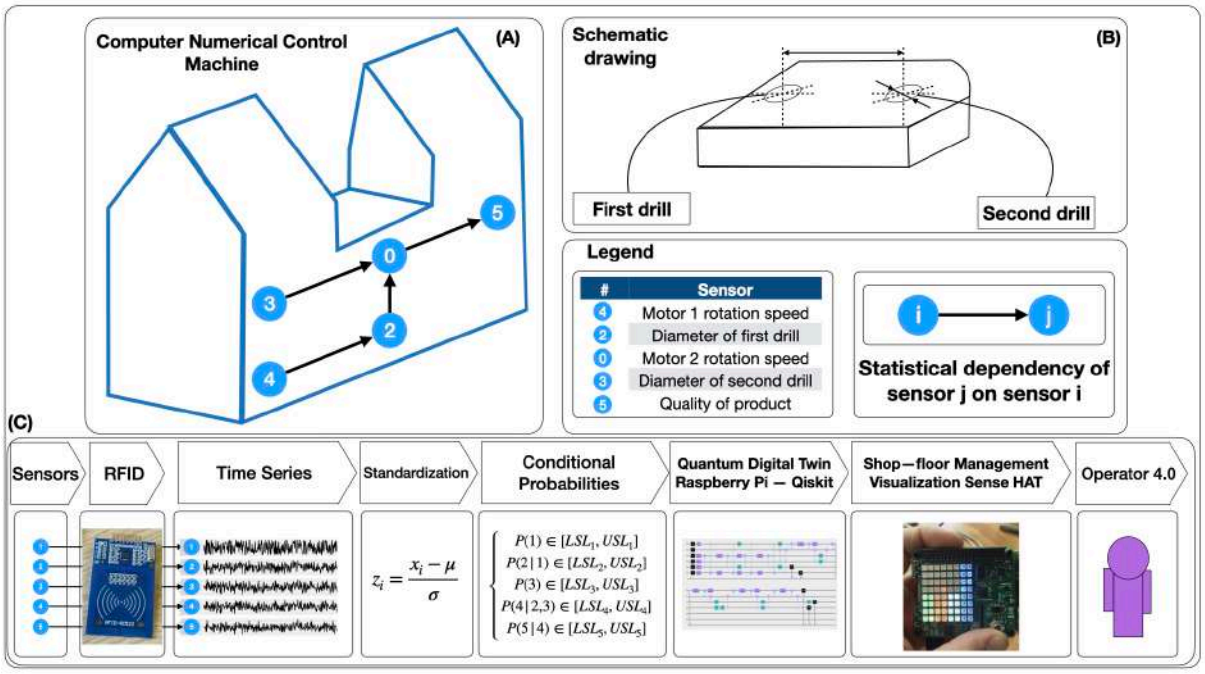


**Figure 5.1:** Scheme of our Quantum Jidoka case study: the digital quantum twin to provide the 4.0 operator with a shopfloor management tool that allows him to visualize the status of the machine in real time. (**A**) CNN-machine and schematic sensor network within. (**B**) Schematic product drawing. (**C**) Quantum JIDOKA creation process.

will allow for a preventive operational lean shopfloor management.

The implementation of a quantum computer simulation on a Turing machine is certainly accompanied by limitations, which are reflected in the performance and low number of manageable measured values. Nevertheless, the setup chosen here allows a feasibility study and can serve as a basis for later scaling when used in a real system environment and with the use of adequate quantum computers.

### 5.2.1 Hardware

The proposed equipment has a low-cost standard configuration and the components can be easily available on the market. This design was consciously chosen for two reasons: on the one hand reliability is increased as the compounds are well proven, on the other hand an adequate stock of spare parts can be stored to ensure the continuous operation of the process at a very low cost.

The necessary hardware needed to build the smart IoT sensor prototype is shown in Figure 5.2:

- Raspberry Pi 4.0. The Raspberry Pi 4.0 is a high-performance 64-bit quad-core processor, up to 8 GB of RAM, dual-band 2.4/5.0 GHz wireless local area network (LAN), Bluetooth 5.0, Gigabit Ethernet, USB 3.0, and a sense HAT add-on which is attached on top of the Raspberry Pi via the 40 general-purpose input or output pins (which provide the data and power interface). It has several sensors and an 8 ×

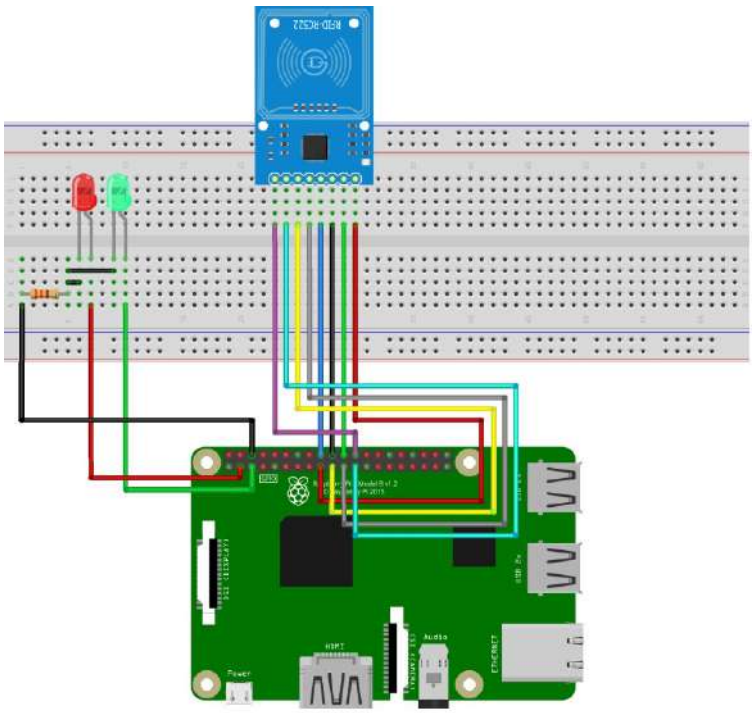

(a)

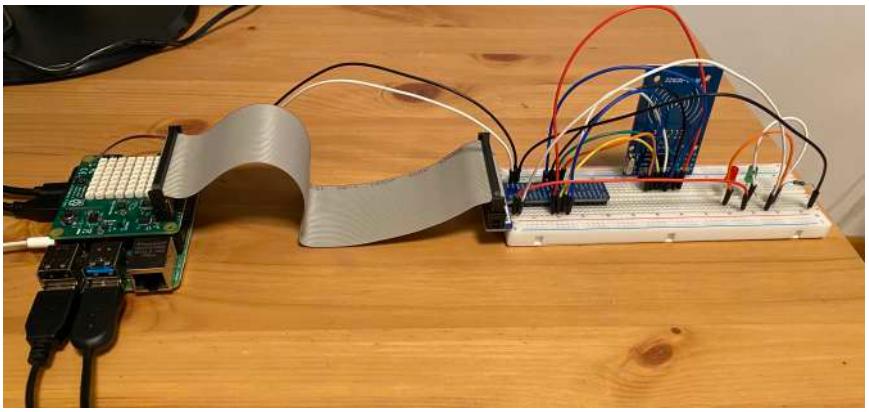

(b)

**Figure 5.2:** Hardware configuration of Quantum JIDOKA. RFID LEDs Raspberry Pi Visualization Hat– Hardware. (a) Hardware circuit plan. (b) Hardware circuit real.

8 RGB (Red–Green–Blue) LED matrix display that can be used to visualize sensor states for multiple applications [111–114]. In the proposed design, the critical component, because of its value and relative complexity is the Raspberry Pi CPU. In the factory in question there are about two hundred CPUs of this type, and the annual failure rate, including human-caused failures, is 1%. This is acceptable and within standard maintenance parameters.

- RC522 RFID module. The RC522 RFID is a 13.56 MHz RFID module that is based on the MFRC522 controller from NXP semiconductors. Its operating voltage lies between 2.5 V to 3.3 V. It allows for serial peripheral interface (SPI), inter-integrated circuit ($I^2C$) and universal asynchronous receiver and transmitter (UART) communication protocols. Its maximum data rate is 10 Mbps with a read range of 5 cm and a current consumption of 13 to 26 mA. These characteristics are optimal for a number of industrial and educational applications [115, 116].

- Set of cables, light-emitting diodes (LEDs), resistors, and test plates. An LED is a two-lead semiconductor light source, which emits light when activated. The LEDs used present a forward current of 30 mA and a forward voltage range between 1.8 V and 2.4 V. A resistor is a passive electronic component that offers a specific amount of electrical resistance to the flow of current when connected in a circuit. The resistors used in this project are standard 1 kΩ.

The Raspberry Pi is connected to the RFID card and the two red and green LEDs show the status of the connection. The electrical resistance allows for a proper functioning of the elements.

### 5.2.2 Software

The quantum digital twin circuits presented in Section 5.3.1 were simulated on *qiskit* tool, a Python–based quantum computing platform developed by IBM [100], and the code and additional results can be accessed in this Open Access Repository: `https://osf.io/24jrm/?view_only=a10d2e001e114807854b994616f8d4cf`. We will analyze the data obtained in Section 5.3, evaluate these results in Section 5.4, and discuss the results obtained in Section 5.5.

## 5.3 Data Collection

The data input is realised by means of a radio frequency identification (RFID) module, connected to the serial peripheral interface bus (SPI) of the Raspberry Pi as presented in Figure 5.2b. This module acts as RFID-

reader. To simulate a more realistic industrial process, we set up a data transfer by RFID consisting of the following components:

- An RFID-writer, connected to the sensors of the computer numerical control machine in Figure 5.1;
- The RFID-reader as described in Figure 5.2;
- A small machine that is physically rotating an RFID-card around a motor-driven axis, as shown in Figure 5.3, and by this transferring datasets from the writer to the reader.

One transfer process consists of one revolution of the RFID-card around the axis. Per revolution, one dataset is transferred. Each dataset consists of one measured value per sensor, as well as a time stamp and a quality assessment in the form of "ok" or "not ok" information. The process starts with the RFID-card in reach for the RFID-writer. Here, one dataset from the computer numerical control machine is written to the RFID-Tag. After that, the card is rotating around the motor axis. With a 180 degree rotation, the card comes into reach of the RFID reader. Here, the dataset is read from the RFID card, split into its components, entered into one list per sensor on the Raspberry Pi, and thereby made available on the digital twin.

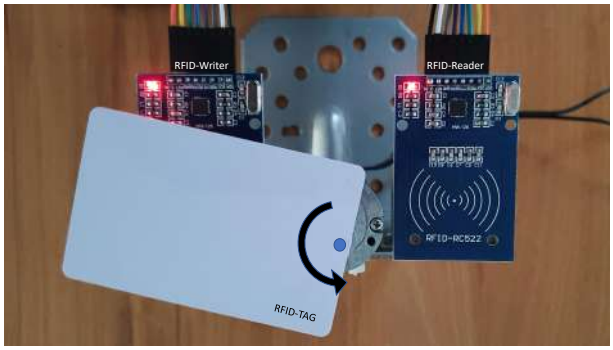


**Figure 5.3:** Hardware detail. RFID data -collection.

### 5.3.1 Quantum Digital Twin

The quantum digital twin circuit that resembles the sensor network in the computer numerical control machine of Figure 5.1 is shown in Figure 5.4. Following the recommendations from [58, 92], we build the quantum digital twin with a number of qubits equal to the number of sensors and one *ancilla* qubit that serves to perform the appropriate rotations, giving a total of 6 qubits in this case. In addition, as we have previously indicated in [89], after the proper qubit initialization, we perform a series of qubit rotation operations that allow us to simulate the conditional probabilities between the respective sensors. The interested reader can inspect several examples for several qubit configurations in these application examples from [88, 108, 109].

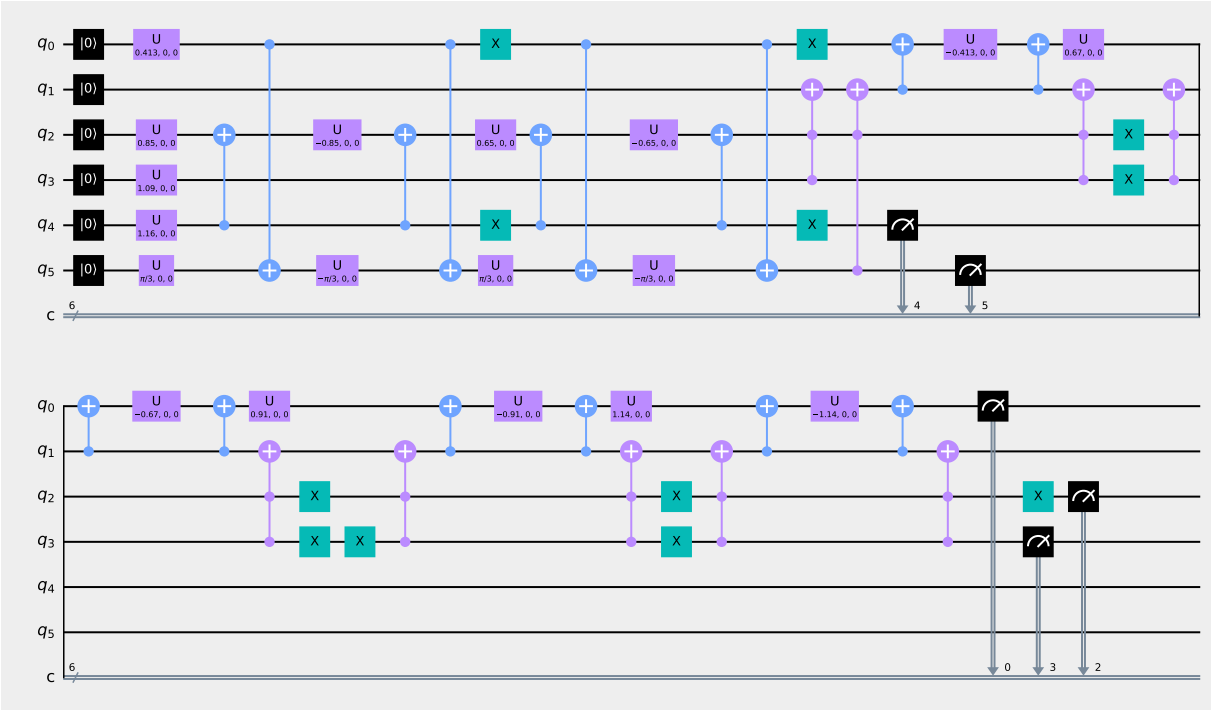


**Figure 5.4:** Quantum digital twin for the sensor network shown in Figure 5.1.

The factory in which this project was carried out has a workforce with a basic education, which is why management has to look for intuitive solutions to visualize the state of the value creation processes so that workers can understand them and act on them. To this end, a visualization based on the logic of traffic lights, known to all workers, is used: green and red mean that the machine is operating within or outside specifications, respectively, while yellow shows a situation of caution as the machine is operating at the limit of specifications. The display of the state of the last qubit is performed by means of a sense HAT that presents a linear colour degradation given by the expression $RGB255 \cdot [\|\langle 1|q_i\rangle\|^2, \|\langle 0|q_i\rangle\|^2), 0], i = 0, \ldots, 5$. This yields naturally to a green colour $RGB[0, 255, 0]$ if the probability of the last qubit of the circuit $P(q_5 = |0\rangle) = \|\langle 0|q_5\rangle\|^2 = 1$ and a red colour $RGB[255, 0, 0]$ if the $P(q_5 = |1\rangle) = \|\langle 1|q_5\rangle\|^2 = 1$ which is the standard traffic-light colour code in the shopfloor: green, yellow, and red.

## 5.4 Results

The results obtained by the simulation of the digital quantum twin can be represented in the form of a bar chart representing the quantum state probabilities of the quantum circuit, as shown in Figure 5.5a. However, this visualization is not intuitive and, therefore, has little chance of being interpreted satisfactorily by the process owner in an Industry 4.0 environment. Without this visual interpretation of the machine status, it is not possible to successfully perform a proper shopfloor management. For this reason, we have added an

$8 \times 8$ RGB LED matrix display that allows a quick and intuitive visualization of the total state of the wave equation of the quantum circuit. This is exemplary shown in Figure 5.5b, which represent the sum of the 32 qubit combinations $P(q_5 = |0\rangle)$ given by $P(q_5 = |0\rangle) = \|\langle 0|q_5\rangle\|^2 = 0.25$, hence delivering a reddish visualization equivalent to $RGB[191, 64, 0]$.

To verify that the result is correct, we proceed to design the equivalent Bayesian network to the digital quantum twin [58] represented in Figure 5.6. The error percentage found when comparing both quantum digital twin and the classical Bayesian network is less than 2%, which is acceptable in the context of quantum simulations. The computation time of the equivalent Bayesian network doubles the quantum digital twin computational performance, which is a pre-requisite for the implementation to be carried out in real time.

## 5.5 Summary

In the initial situation, before starting the project, manual quality control was performed on 1% of the parts. The initial proposal of the process owner was to perform a condition monitoring of each of the sensors and aggregate this information by means of a digital twin with machine learning methods, which would reduce the cost of personnel associated with quality control. However, it would be difficult to integrate this into the production process due to two reasons: on the one hand, the lack of knowledge of these methods by the operators, and, on the other hand, the computational cost of performing calculations by classical methods (Bayesian networks) that do not allow integration in the production. Our quantum digital twin allows to obtain the two advantages: to obtain the information on the product quality in the form of an intuitive visualization for the operator in real time and at low cost. The integration of the quantum digital twin has meant a reduction in the costs associated with quality control, as well as doubling the mean-time-between-failures associated with the computer numerical control machine as the speed of reaction of the operator in case of error is increased.

In this Chapter, we have successfully tested the integration of a digital quantum twin by means of quantum simulations on a conventional machine to enable a visualization of its systemic state in an Industry 4.0 environment. With the case study, we have achieved the much desired integration of quantum computing logic in industrial environments and opened a field of exploration that will allow, once emulated, managers of value creation processes to use these algorithms in a clean and simple way. Digital quantum twins is much more than just software for reaching the same goal in a slightly better way. Instead, it does not develop in isolation, but the socio-technical system enables the development, diffusion and use of technologies. Digital quantum twins necessarily change processes and the way in which people work. With this Chapter, we have generated a bridge, so far non-existent in practice, between the world of quantum simulation and industrial environments. We have

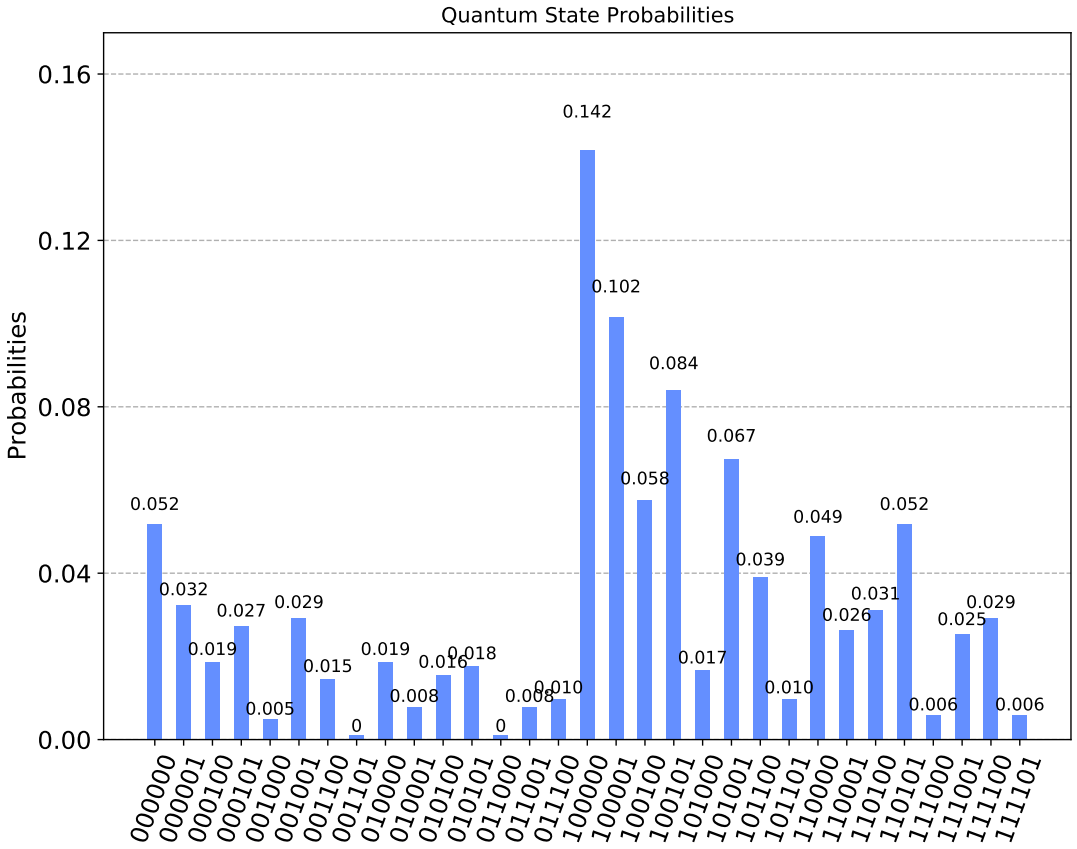


(a)

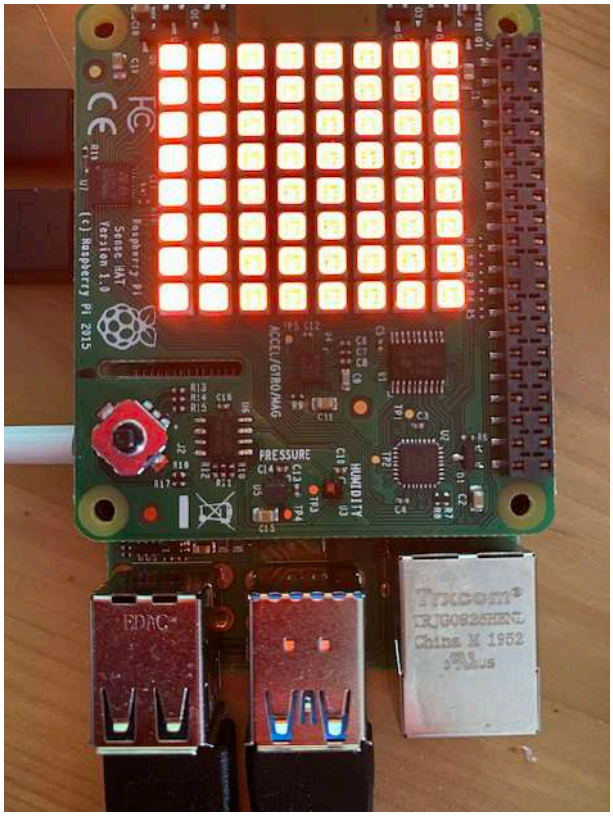


(b)

**Figure 5.5:** Quantum digital twin state probabilities and shopfloor visualization. (a) Quantum digital twin state probabilities. (b) Quantum digital twin sense HAT shopfloor visualization $P(q_5 = |0\rangle) = \|\langle 0|q_5\rangle\|^2 = 0.25$.

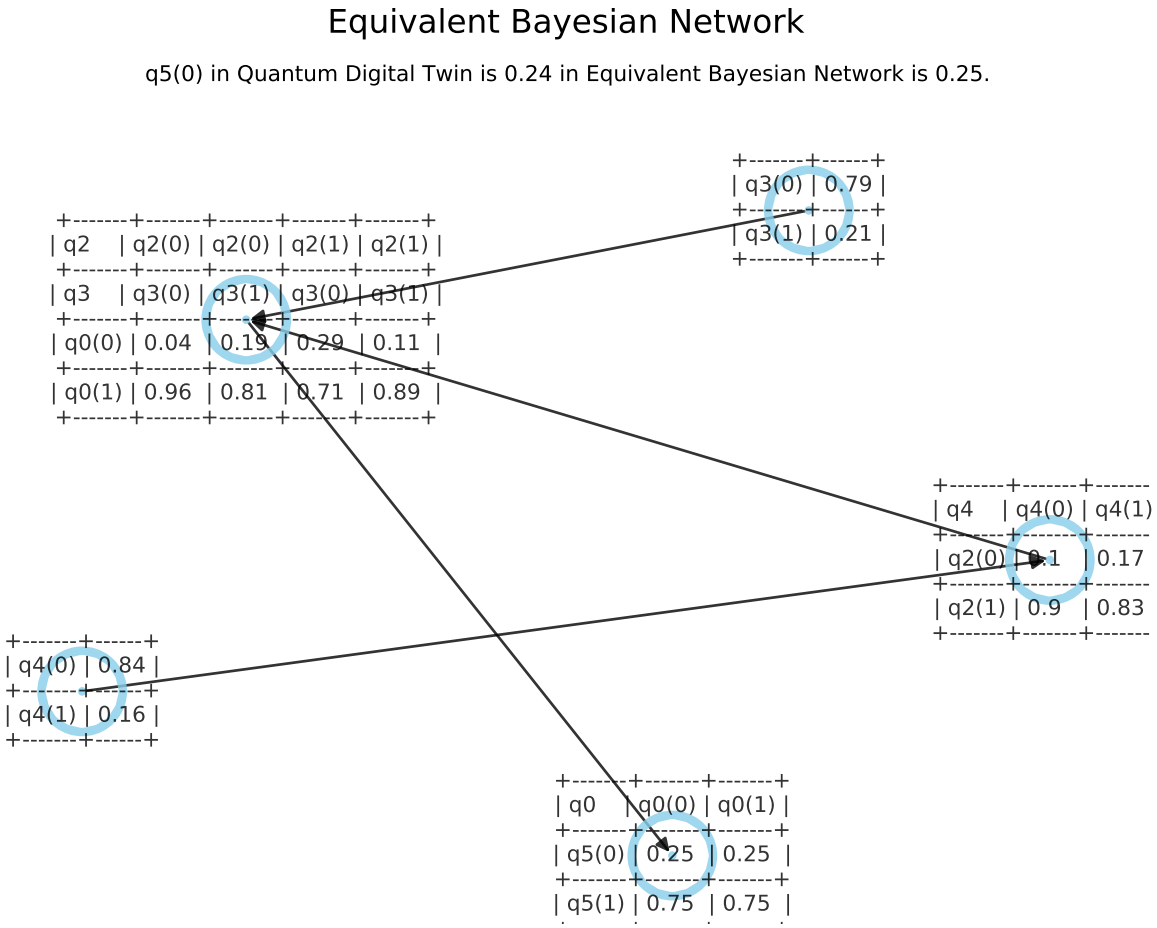


**Figure 5.6:** Equivalent Bayesian network to the quantum digital twin shown in Figure 5.4.

also confirmed the validity of the results by demonstrating that the quantum digital twin yields the same values as those obtained with traditional simulation methods, such as Bayesian networks.

We have integrated a quantum simulation that allows on the one hand to monitor the state of a sensor network inside the machine and on the other, through an intuitive traffic light visualization, shopfloor management system, to empower the process owner to benefit from the quantum digital twin results without any quantum knowledge. This means that our proposal has the potential to be widely applied in practice since it requires neither a high investment, nor a redesign of its components, nor a specific knowledge of quantum simulation principles. From an autonomation view, these characteristics of usability, selective provision of information, user acceptance, and profitability could result not only in better human-machine cooperation systems, but also may lead to changes in the range, depth, and content of tasks.

The objective of this Chapter was the practical application of quantum simulation in a real environment. For this purpose, we present a real implementation of a prototype connected to a computer numerical control machine in industrial use. Nevertheless, the proposal has some limitations. Quantum computers constitute a huge investment due to the required physical functioning conditions. Currently, quantum computing is available either using external free resources as IBM *qiskit*, the one used in the prototype that has a limit of 30-qubits, or through rental of proprietary equipment. Escalation to an extensive industrial deployment is neither expected to imply relevant barriers from the conceptual and technological point of view, nor it affects the design and logic of the prototype. Should the company hire a more powerful quantum computer, it would not affect the prototype functioning. The extra qubits would allow to compute Bayesian networks composed of a higher number of sensors. Computational benefits would then be significantly higher as the increase rate of quantum computation times with the number of network nodes is much slower than binary logic computers. However, challenges remain in structuring the condition monitoring offer, due to the different domains of application, the characteristics of the existing information, and the final goal of the monitoring activities.

# 6

# Improvement of Quantum Approximate Optimization Algorithm for Max–Cut Problems

The objective of this Chapter is to study the optimal partitioning of value stream networks into two classes so that the number of connections between them is maximized. Such kind of problems are frequently found in the design of different systems such as communication network configuration, and industrial applications in which certain topological characteristics enhance value–stream network resilience. The main interest is to improve the Max–Cut algorithm proposed in the quantum approximate optimization approach (QAOA), looking to promote a more efficient implementation than those already published. A discussion regarding linked problems as well as further research questions are also reviewed.

## 6.1 Introduction

Value chains linked to Industry 4.0 (I4.0) involve complex cyber-physical networks in which information is processed efficiently by humans and machines to deliver the desired product to a customer [17, 117, 118]. I4.0 and the Industrial Internet of Things (IIoT) both describe further emerging landscapes for an integrated human–machine interaction [119, 120]. Together, the two concepts are grounded in intelligent, interconnected cyber–physical manufacturing systems that are fully equipped and capable of controlling the process flow of industrial production.

In the realm of IIoT I4.0 manufacturing, I4.0 vision has advanced the notions of smart fabrication and smart factory by augmenting all assets with sensor–based connectivity [121]. These intelligent sensors generate a large amount of manufacturing data that helps to create digital twins as support for a live mirror of physical processes [122, 123]. The ambition is to capture process variability within this approach, with the capability to process all relevant information by analyzing big data in cloud computation so that manufacturers are able to find bottlenecks in manufacturing processes, identify the causes and impacts of problems in such a way that the effective application of measures is useful for both product design and manufacturing engineering, including maintenance, repair and overhaul [124].

Quantum near–term simulations in classical computers have been recently used to solve different applications, including Industry 4.0 challenges such as the modelling of organizational decision networks as quantum circuits [89]. In this work, with the help of quantum simulations, a new solution for the combinatorial optimization problem is proposed, which can be applied to a wide range of applications including in the Industry 4.0 environment. It consists in finding the "optimal" partitioning of a value chain into two classes, such that the number of connections between them is maximized. Direct applications are linked to introduce flexibility in value chain models by enabling extra resilience to it, no matter whether the related processes are logistics or production related ones. Solving this industrial process design problem potentially allows maximizing the interaction between the elements of the value chain and thus maximizes its productivity [125, 126]. Other applications can be connected to the Narrowband Internet of Things (NB–IoT) technology. NB–IoT is a cellular radio–based access protocol specified by 3GPP to tackle the quickly growing market for low–power wide–area connectivity significantly targeting mobile use cases. To realize the global outreach and broad adoption of NB–IoT services, mobile network operators (MNOs) need to guarantee end-to-end devices and services across several vendors connected to the deployed NB–IoT systems, and that the data transport capacity and connection modes are well understood. In this context, efficient dynamic partitions depending on the low power network

available are relevant for providing a robust integrative configuration with limited transport overhead.

A solution to these problems can be formulated in terms of a combinatorial optimization approach, which involves finding an optimal object out of a finite set of objects. In this particular case, it involves finding "optimal" bitstrings composed of 0's and 1's among a finite set of bitstrings. Such bitstring represents a partition of nodes of a graph into two sets, such that the number of edges between the sets is maximum. Each of the sets represents the allocation of nodes in the value stream network or nodes in the IoT system to specific managerial structures giving a maximal flexibility by providing the highest degree of connectivity.

This optimization challenge is already known as the Max–Cut problem, and it is one of the most studied combinatorial optimization problems because of its wide range of applications and because of its connections with other fields of discrete mathematics [127]. Different solutions have been proposed for the Max–Cut type of problems, as it belongs to the so-called NP-hard complexity class problems, where no known algorithms are able to solve NP-hard problems in polynomial time and thus exact methods rapidly become intractable. Such solutions include search-based algorithms [128], Machine Learning alternatives, as well as Recurrent Neural Networks and Reinforcement Learning [129].

Quantum approaches were also proposed with a quantum approximate optimization algorithm (QAOA) by [1]. The QAOA belongs to the class of hybrid algorithms and requires, in addition to the execution of shallow quantum circuits, a classical optimization process to improve the quantum circuit itself. The QAOA is an algorithm that uses unitary transformations $U(\beta_i, \gamma_i)$, depends on two parameters $\beta_i$ and $\gamma_i$, and is arranged in alternating blocks a number $p$ of times ($i \in \{1, \ldots, p\}$) given by

$$|\psi(\vec{\beta}, \vec{\gamma})\rangle = \underbrace{U(\beta_i)U(\gamma_i)...U(\beta_i)U(\gamma_i)}_{\text{p times}} |\psi_0\rangle \tag{6.1}$$

where $|\psi_0\rangle$ is a suitable state and parameters $\vec{\beta}, \vec{\gamma} \in \mathbb{R}^p$.

The goal of the algorithm is to find the combination of parameters that allows a quantum state $|\psi(\overrightarrow{\beta_{opt}}, \overrightarrow{\gamma_{opt}})\rangle$ to yield the optimal solution [130]. This heuristic algorithm produces then a bit string $x \in \{0,1\}^n$ that with high probability is expected to give a good approximation of the theoretical solution. The algorithm follows a classical optimization scheme: first prepares a parameterized quantum state $|\psi(\vec{\beta}, \vec{\gamma})\rangle$ (called the ansatz), then computes the parameters $(\overrightarrow{\beta_{opt}}, \overrightarrow{\gamma_{opt}})$ such that the expectation value of the quantum state is given by

$$F_p = \langle\psi(\vec{\beta}, \vec{\gamma})| H_p |\psi(\vec{\beta}, \vec{\gamma})\rangle \tag{6.2}$$

is maximized with respect to the problem Hamiltonian $H_p$, and finally performs a classical optimization until some convergence criterion is reached. An overview of this is shown schematically in Figure 6.1.

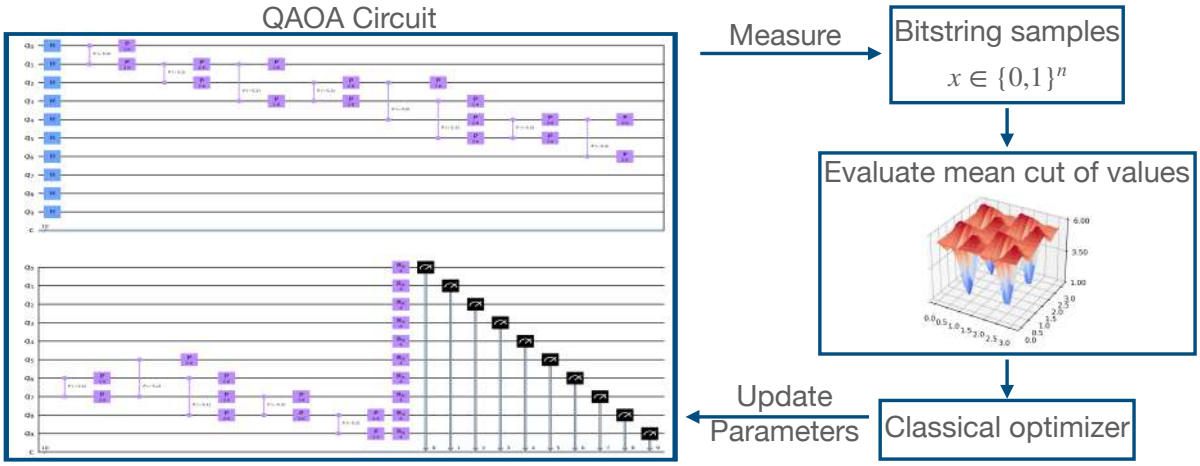


**Figure 6.1:** Quantum Approximate Optimization Algorithm- Overview.

The convergence criterion is in the Max–Cut cost function given by

$$C(x) = \sum_{i,j=1}^{n} x_i(1 - x_j), \tag{6.3}$$

which can be mapped to a Hamiltonian that is diagonal in the computational basis by

$$H = \sum_{x \in \{0,1\}^n} C(x) \left|x\right\rangle \left\langle x\right|, \tag{6.4}$$

in which $x \in \{0,1\}^n$ labels the computational basis states $|x\rangle \in \mathbb{C}^{2^n}$. The expansion of $Z_i = \begin{pmatrix} 1 & 0 \\ 0 & -1 \end{pmatrix}$ Pauli–Z operators can be obtained from the canonical expansion of C(x) by substitution of every variable $x_i \in \{0,1\}$ by the matrix $\frac{1}{2}(1 - Z_i)$.

As indicated in the abstract, this paper aims to show that the already suggested approximate solution can be improved. The proposal for an alternative quantum algorithm configuration improves the existing solutions up to thirty nodes. The optimization algorithm proposed in Farhi et al. [1] promotes a specific sequence of unitary operators, which means an effective expression for the Hamiltonian. Finally, such a sequence of transformations will perform differently when the size of the circuit evolves. Our approach can be understood in the end as a proposal for a different sequence of unitary operators, providing a different configuration for the Hamiltonian. Then, what it is claimed is that our algorithm (our effective expression for the Hamiltonian) performs much better than the existing one.

The solution is implemented in a simulated quantum hardware environment, however there are already studies showing the time and noise effects over these algorithms when implemented in real hardware [131].

We structure the rest of the work hereinafter as follows: Section 6.2 outlines the modified architecture in a reasoned manner. Then, Section 6.3 presents the results of the algorithm as compared with the analytical solution, which for when $|\psi(\overrightarrow{\beta_{opt}}, \overrightarrow{\gamma_{opt}})\rangle$ is not too deep can be computed classically, and the results previously obtained by [1]. Finally, Section 6.4 briefly discuss the obtained results, outlines future lines of research, and presents limitations in the presented work.

## 6.2 Modified QAOA

In this section, we present the results of the algorithm applied to a value stream network of n = 10 nodes. The complete results for other configurations are available in open access in [132].

We start by representing in Figure 6.2 the value stream network as a graph $G = \{n, e\}$ of n = 10 unlabeled nodes and e = 13 edges.

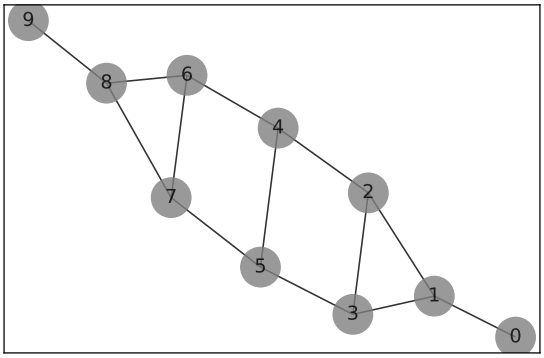


**Figure 6.2:** Value stream network with n = 10 nodes.

If the graph coincides with the connectivity of our logical network (either IoT topology or value stream network), the cost function $C(x)$ coincides with the hamiltonian $H$ used to generate the state.

For a shallow approximation with p=1, the analytical solution for the expectation value is given by

$$F_1(\beta, \gamma) = \langle \psi_1 | H | \psi_1 \rangle \tag{6.5}$$

Combining Equations (6.3) and (6.4), the Hamiltonian $H$ makes use of the expectation value to measure the edges individually:

$$f_{i,k}(\gamma, \beta) = \frac{1}{2} \langle \psi_1(\gamma, \beta) | (1 - Z_i Z_k) | \psi_1(\gamma, \beta) \rangle \tag{6.6}$$

There are two types of edges: those that connect a node with degree one (A), and those that connect a node with degree three (B). For the A–class edges, an example of the encoding of the optimization function between nodes (0) and (1) is given by

$$2f_A = 1 - \langle +^1 | U_{01}(\gamma) U_{12}(\gamma) U_{13}(\gamma) X_0(\beta) X_1(\beta) Z_0 Z_1 X_1^\dagger(\beta) X_0^\dagger(\beta) U_{01}^\dagger(\gamma) U_{12}^\dagger(\gamma) U_{13}^\dagger(\gamma) | +^1 \rangle \tag{6.7}$$

and for the B–class edges, the encoding of the optimization function between nodes (1) and (2) is given by

$$\begin{aligned} 2f_B =& 1 - \langle +^3 | U_{21}(\gamma) U_{24}(\gamma) U_{23}(\gamma) X_1(\beta) X_2(\beta) Z_1 Z_2 \\ & X_1^\dagger(\beta) X_2^\dagger(\beta)(\gamma) U_{12}^\dagger(\gamma) U_{23}^\dagger(\gamma) U_{24}^\dagger(\gamma) | +^3 \rangle \end{aligned} \tag{6.8}$$

in which $|+^n\rangle = \sum_{x \in \{0,1\}^n} \frac{1}{\sqrt{2^n}} |x\rangle$ prepares for an equal superposition state followed by a sequence of parametrized unitary operations. As shown in Equations (6.7) and (6.8) these unitary operations are a combination of parametrized Hamiltonian cost $U_C(\gamma) = e^{-i\gamma H_C}$ and mixer layers $U_M(\beta) = e^{-i\beta H_M}$. The subindexes in the unitary operations indicate the nodes on which the operators act upon.

In our case n=10, there are two A–class edges and eleven B–class edges. This yields Equation (6.9), which is depicted in Figure 6.3 which shows the periodicity in both parameters and exhibits a highly nonlinear behaviour.Farhi et al. [1] proposed QAOA with the structure represented in Figure 6.4.

$$\begin{aligned} F_1(\beta,\gamma) = 2f_A(\beta,\gamma) + 11 f_B(\beta,\gamma) = & \left[\sin(4\gamma)\sin(4\beta) + \sin^2(2\beta)\sin^2(2\gamma)\right] \\ & + \frac{11}{2}\left[1 - \sin^2(2\beta)\sin^2(2\gamma)\cos^2(4\gamma) - \frac{1}{4}\sin(4\beta)\sin(4\gamma)\left(1 + \cos^2(4\gamma)\right)\right] \end{aligned} \tag{6.9}$$

Such an algorithm starts by preparing the system in superposition with a Hadamard gate on all qubits. Next, a rotation of $2\gamma$ is applied to each of the edges if both are in state $|11\rangle$. This conditional rotation has the form given by

$$C_p(2\gamma) = \begin{pmatrix} 1 & 0 & 0 & 0 \\ 0 & 1 & 0 & 0 \\ 0 & 0 & 1 & 0 \\ 0 & 0 & 0 & e^{-2i\gamma} \end{pmatrix}. \tag{6.10}$$

This allows the algorithm to be applied when both qubits are in state $|1\rangle$ simultaneously. A quantum phase

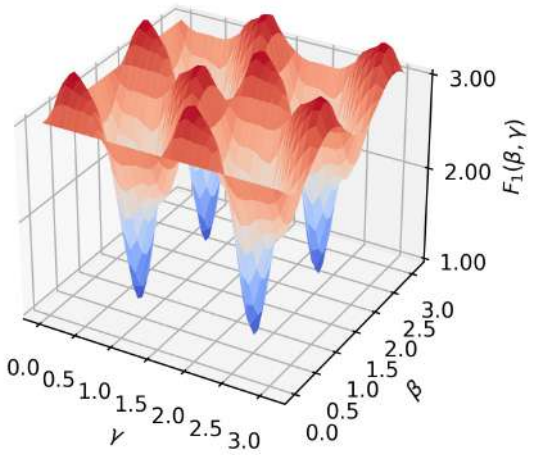


**Figure 6.3:** Analytic solution for $p = 1$ and value stream network configuration from Figure 6.2

correction of $\gamma$ is then applied to each of the nodes joined by each edge. This rotation has the form given by

$$p(\gamma) = \begin{pmatrix} 1 & 0 \\ 0 & e^{i\gamma} \end{pmatrix}. \tag{6.11}$$

Such configuration allows the previous rotation to be neutralized when the two qubits are in state $|11\rangle$. The result of these two operations allows a rotation of $\gamma$ to be applied to all nodes as long as both communicating nodes are not simultaneously in state $|1\rangle$.

Finally, a rotation around the $X$-axis of $2\beta$, perpendicular to the computing axis, is applied to all nodes. This rotation has the form given by

$$R_x(2\beta) = \begin{pmatrix} \cos\beta & -i\sin\beta \\ -i\sin(2\beta) & \cos(2\beta) \end{pmatrix}. \tag{6.12}$$

In summary, in [1] the QAOA algorithm applies, after a standard superposition, a quantum phase of $\gamma$ to every node connected to each other, as long as both are not in state $|11\rangle$, and a rotation around the perpendicular to the computational axis of $2\beta$ to all the nodes.

On the other hand, this paper proposes a novel QAOA approach represented in Figure 6.5.

Analogous to the previous example, our algorithm starts by preparing the system in superposition with a Hadamard gate on all qubits. We then perform a conditional rotation of $\gamma$ to each node connected to another if the second is in state $|1\rangle$ in both directions. This is done by concatenation of two $U3\left(\frac{\gamma}{2}, 0, 0\right)$ and

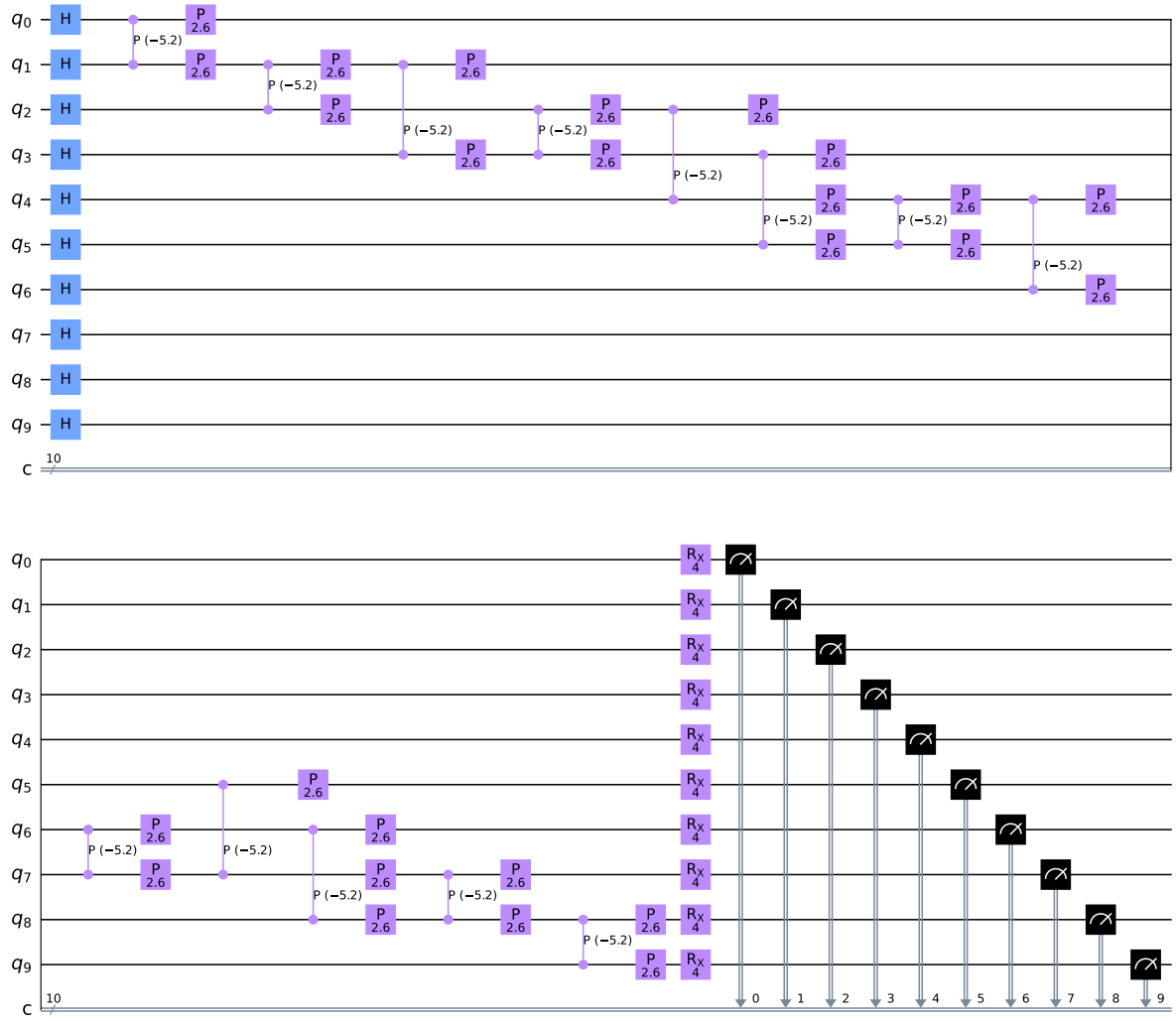


**Figure 6.4:** Quantum Approximate Optimization Algorithm–Farhi et al. [1].

$U3\left(\frac{-\gamma}{2}, 0, 0\right)$ gates given by

$$U3\left(\frac{\gamma}{2}, 0, 0\right) = \begin{pmatrix} \cos\left(\frac{\gamma}{4}\right) & -\sin\left(\frac{\gamma}{4}\right) \\ \sin\left(\frac{\gamma}{4}\right) & \cos\left(\frac{\gamma}{4}\right) \end{pmatrix}, \tag{6.13}$$

and a conditional CX rotation applied to one of the nodes $q_0$ taking the other $q_1$ as control given by

$$CX_{q_0,q_1} = \begin{pmatrix} 1 & 0 & 0 & 0 \\ 0 & 0 & 0 & 1 \\ 0 & 0 & 1 & 0 \\ 0 & 1 & 0 & 0 \end{pmatrix}. \tag{6.14}$$

This method works because when the control *qubit* $|\Psi_0\rangle$ is in state $|0\rangle$, all we have is $U3\left(\frac{\gamma}{2}, 0, 0\right)$ followed

by a $U3\left(\frac{-\gamma}{2}, 0, 0\right)$ and the effect is trivial. On the other hand, when the control *qubit* $|\Psi_0\rangle$ is in state $|1\rangle$, the net effect is a controlled rotation $U3(\gamma, 0, 0)$ on the $|\Psi_1\rangle$ *qubit*. These rotations are taken in both directions because our network is not directed. This algorithm is expected to yield better results than the previous one because the transformations are differential as a function of node state.

Finally, as in the previous algorithm, a rotation around the $X$-axis of $2\beta$, perpendicular to the computing axis, is applied to all nodes. This rotation has the form given by Equation (6.12).

## 6.3 Results

In this section, we present the results of the algorithm applied to a logical nondirected network of n = 10 nodes. The quantum simulations presented were simulated on *qiskit* tool, a Python–based quantum computing platform developed by IBM [100], and the code and additional results can be accessed in this Open Access Repository: [132].

The results confirm our expectations and our proposed QAOA algorithm predicts the analytical results better for a shallow quantum circuit with $p = 1$. A summary of the results for different numbers of nodes is shown in Figure 6.6. In Table 6.1 we represent the comparison of the analytical solution curve and the respective QAOA algorithms. Our solution shows better performance in all metrics.

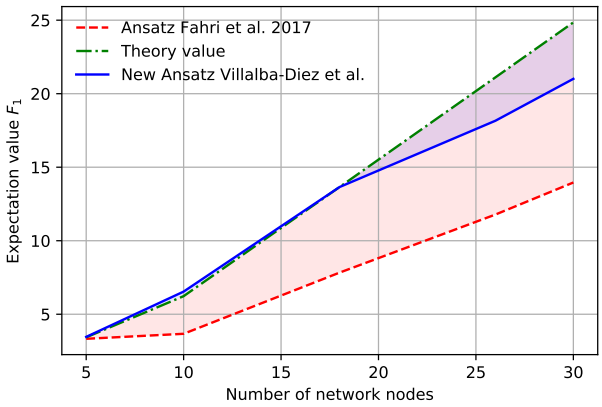


**Figure 6.6:** Quantum Approximate Optimization Algorithm results comparison.

The bit string that delivers the optimal solution is $x = \{0110011010\}$, as shown in Figure 6.7. This graph clearly shows the configuration obtained by the QAOA algorithm presented with two types of nodes represented in two colors, green $\{0\}$ and blue $\{1\}$.

| | Analytic vs. | |
|---|---|---|
| | Farhi et al. | Villalba et al. |
| Directed Hausdorff distance | 8.22 | 3.84 |
| Discrete Fréchet distance | 10.89 | 3.84 |
| Dynamic Time Wrapping | 28.70 | 7.13 |
| Partial Curve Mapping | 1.6893 | 0.3223 |
| Area between two curves | 1.2744 | 0.3642 |
| Curve-Length distance metric | 141.21 | 26.23 |

Table 6.1: Quantum Approximate Optimization Algorithm: results comparison for different measures for identifying curve similarity. [2]

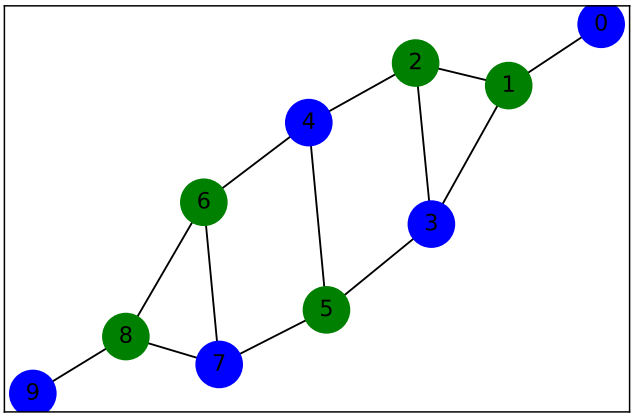


**Figure 6.7:** Value stream network clustering with Quantum Approximate Optimization Algorithm.

## 6.4 Discussion, Future Lines of Research, and Limitations

The analysis of the solution presented in Table 6.1 shows to what end the quality of the solution found improves the previous one, which justifies the spent effort in considering smarter quantum circuits for the operation of the QAOA algorithm since there is not exist a universal strategy that works across a broad range of optimization problems. Based on the proposal made, the benefit of the algorithm proposed is evident against other existing algorithms, at least in the case of $p = 1$. As a consequence, value–stream network design challenges can be better understood with the aid of this quantum optimization algorithm. More research is needed to analyze the evolution of potential benefits when the number of transformation blocks grows up. Indeed, resources and performance figures are also needed to get the whole perspective. The network topology can be modified, however, if classes for the number of links per node are extended, then a new formulation for the cost function introduced in Equation (6.9) is required.

Future research lines will involve the implementation of this new proposal for quantum circuits in physical quantum computers, to analyze both the performance and the stability against noise, not only for $p = 1$ but

also when the transformation blocks are increased. Moreover, since two-qubit gates (e.g., CNOT gates) are significantly more erroneous than single qubit gates, the proposal of smarter circuits with reduced number of two-qubit gates, such as the optimization proposed by [131], is an area of interest.

Because of the problem formulation, the network was defined and just the link of nodes with different managerial classes was the goal. However, it could be possible to reverse the problem and start from the node type distribution and look to connect those nodes with a number of edges optimizing the imputation rules between them.

Some limitations can be found regarding the applicability to real cases, because the existence of extra constraints applicable to nodes or edges. Therefore, additional aspects related to penalty terms when formulation of the $C(x)$ function could be a potential workaround. Following this line, another relevant research area is to extend the current formulation for the Max–Cut problem to the Max–k–Cut one, in line with the recent analysis provided by [133]. Although we have obtained satisfactory results with $p = 1$, we can expect a better approximation for a larger number of qubits if we increase the $p$ parameter. This would, however, entail additional relative difficulties in factoring the Hamiltonian in the adiabatic hypothesis that may be problematic in practice.

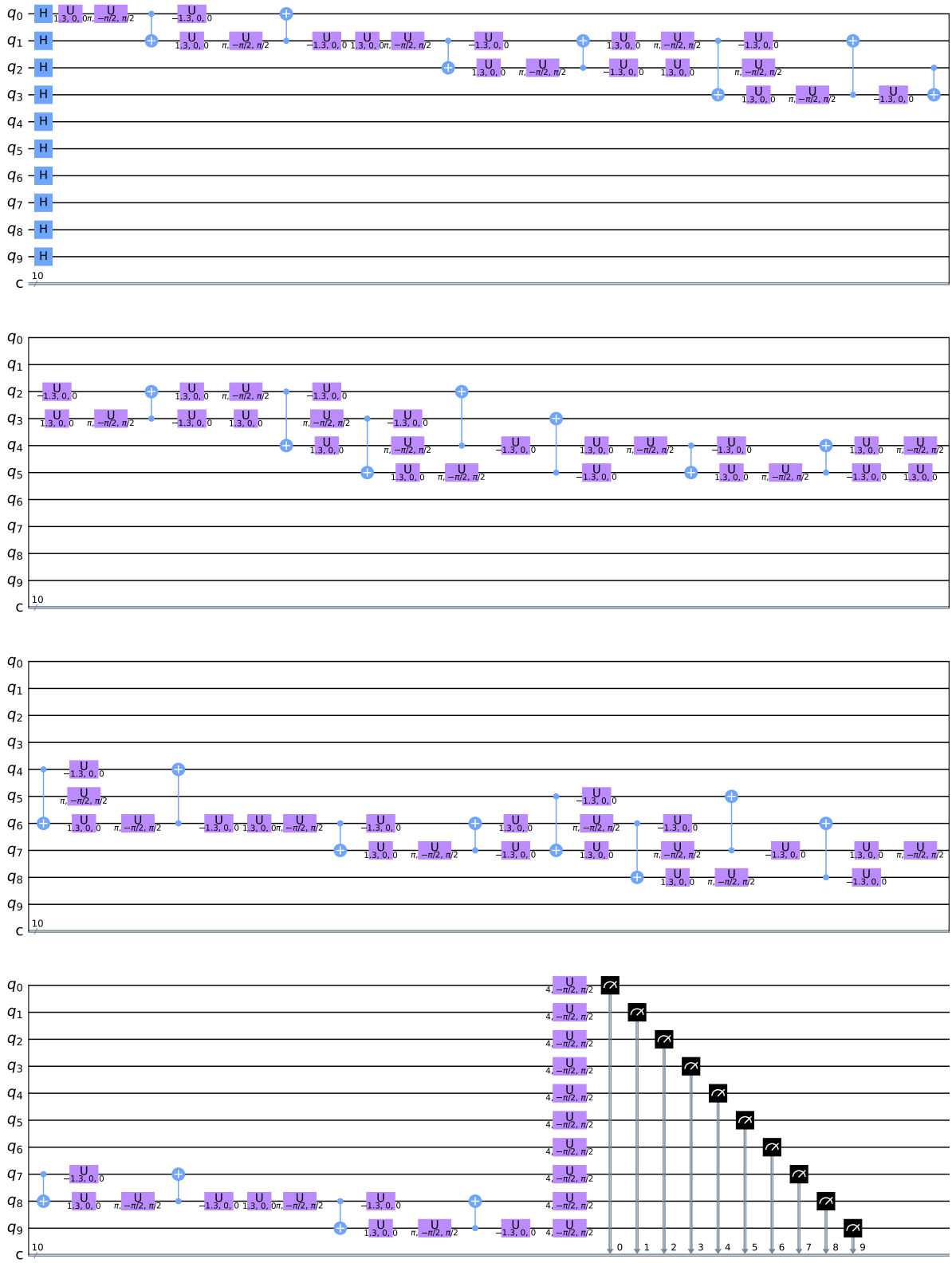

**Figure 6.5:** Quantum Approximate Optimization Algorithm–Villalba–Diez et al.

# 7

# Conclusions, Final remarks, and Other lines of research

## 7.1 Conclusions

There can be little doubt that the world we face in the coming years will become increasingly complex. The product market will experience mass customization in which customers will demand increasingly specific and customized solutions. Organizations hoping to succeed in this increasingly atomized market will necessarily have to be able to manage the complexity associated with this reality. To do so, they will need to develop processes that can efficiently and effectively compute complexity. These value creation processes will necessarily have to be supported by an organizational design that empowers the achievement of this strategic objective.

**C.1** – This work has demonstrated that quantum computing applied to the strategic organizational design can help to understand and quantify complex phenomena associated with decision making in probabilistic low certainty environments. We have therefore called this concept Quantum Strategic Organizational Design.

The objectives outlined in section 1.3 have been all successfully achieved:

- **O1** and **O2**.

  To begin with, in Chapter 2 on Quantum Strategic Organizational Design, we have offered a series of strategic organizational design principles using the fundamentals of quantum computing that allow

Bayesian decision networks to be described as quantum circuits. By means of an illustrative and quantified example, in section 2.3, we offer the reader a simple application of these concepts so that they can be replicated for other more complex configurations in the future.

After outlining the fundamentals of Quantum Strategic Organizational Design and showing an illustrative example, in Chapter 3, we provide a multidimensional view of Quantum Strategic Organizational Design. To do so, we show how different overlapping organizational layers shown in Figure 1.1 can be aggregated into hierarchies through the application of quantum circuits in two different manners: by adding additional qubits to the upper layers with the lower level alignment probabilities or by inserting the lower level alignment probabilities in the initialization of the upper ones. The integration of information between circuits operating at different layers has been successfully analyzed. This procedure makes it possible to exploit the advantages associated with quantum computation while preserving or not, depending on the application, the expected linearity of other well–known classical computational methods such as multilayered Bayesian networks.

- **O3**.

  In Chapter 4 we demonstrated that the application of Quantum Strategic Organizational Design principles allows to improve the performance of classical genetic algorithms [53] in terms of understanding the alignment conditions required for different simple Quantum Strategic Organizational Design configurations. At this point it is relevant to emphasize that presenting these simple configurations does not imply a loss of generality, since the application of the results of Chapter 3 allows to add these configurations to others of higher complexity. These configurations have been chosen because they represent the basic motifs of two and three nodes which, combined with the concepts outlined in Chapter 3, can be used to generate any network configuration desired.

  The conclusions from these cases can be summarized as follows:

  Case one reports to one:

  - **C2.1** – To add hierarchy levels to strategic design models of organizations, it is necessary to ensure the asymptotic stability of the lower agents before implementing a stable aggregation.
  - **C2.2** – The interaction of two process owners reveals an energy interchange that oscillates with more or less amplitude depending on certain parameters – the conditional alignment probabilities.

  Case two report to one:

  - **C3.1** – The alignment probability of a boss can never be greater than the average of the alignment probability of his two subordinates.
  - **C3.2** – Increasing the average probability of alignment of the lower nodes, increases the probability of alignment of the upper node.
  - **C3.3** – The addition of a new node reporting to the superior node adds stability to the set.

  Case one reports to two:

  - **C4.1** – If the two bosses do not communicate with each other, the subordinate will never be able to serve them in such a way that both are simultaneously in alignment. It doesn't matter what she does.
  - **C4.2** – In case the two superior agents do not communicate between them, their joint alignment is always around the point of equilibrium, which is the probability given by the chance.
  - **C4.3** – Only a strong alignment probability at lower reporting levels enables alignment at higher levels. We have shown that this threshold is set by 90%.

- **C5.1** – High levels of alignment in both reporting agents A and B do not imply a high level of alignment of node C. This confirms C4.3.
- **C5.2** – The interaction between the superior agents B and C becomes manifest when the alignment probability of A is fixed at values higher than 90%.

- **O4**.

  As a culmination of our research, we have implemented the theoretical development based on quantum principles in an industrial device that allows to discern in real time the need to modify a production process due to the presence of deviations from the norm. We have also created an interface for production operators to allow the interpretation of the results of quantum computation in an intuitive way.

  The conclusions from this case can be summarized as follows:

  - **C6.1** – We have successfully tested the integration of a digital quantum twin by means of quantum simulations on a conventional machine to enable a visualization of its systemic state in an Industry 4.0 environment.

## 7.2 Final remarks

Some conditions and influences that present restrictions in the design and methodology may represent limitations to the results obtained in this work:

- Due to the restricted availability of real quantum machines, this research has made extensive use of quantum circuit simulations on classical computers. In order to minimize the effect of this fact, we have executed repeated simulations of the circuits on the Qiskit simulator. We've set the number of repeats of the circuit to be 1024, which is the default.
- Furthermore, the lack of quantum knowledge by the organizational leaders might set a potential high threshold on acceptance of the presented Quantum Strategic Organizational Design concepts.

# A

# Author publications

Research conducted during the period of this doctoral thesis

- **Villalba-Diez, J.**, & Zheng, X. (2020). Quantum Strategic Organizational Design: Alignment in Industry 4.0 Complex-Networked Cyber-Physical Lean Management Systems. Sensors, 20(20). https://doi.org/10.3390/s20205856

- **Villalba-Diez, J.**, Benito, R. M., & Losada, J. C. (2020). Industry 4.0 Quantum Strategic Organizational Design Configurations. The Case of Two Qubits: One Reports to One. Sensors, 20(23), 6977. https://doi.org/10.3390/s20236977

- **Villalba-Diez, J.**, Losada, J. C., Benito, R. M., & González-Marcos, A. (2021). Industry 4.0 Quantum Strategic Organizational Design Configurations. The Case of 3 Qubits: One Reports to Two. Entropy, 23(3). https://doi.org/10.3390/e23030374

- Villalba-Diez, J., Losada, J. C., Benito, R. M., & Schmidt, D. (2021). Industry 4.0 Quantum Strategic Organizational Design Configurations. The Case of 3 Qubits: Two Report to One. Entropy, 23(4). https://doi.org/10.3390/e23040426

- **Villalba-Diez, J.**, Gutierrez, M., Grijalvo Martín, M., Sterkenburgh, T., Losada, J. C., & Benito, R. M. (2021). Quantum JIDOKA. Integration of Quantum Simulation on a CNC Machine for In-Process Control Visualization. Sensors, 21(15). https://doi.org/10.3390/s21155031

- **Villalba-Diez, J.**, González-Marcos, A., & Ordieres-Meré, J. B. (2022). Improvement of Quantum Approximate Optimization Algorithm for Max - Cut Problems. Sensors, 22(1). https://doi.org/10.3390/s22010244

# References


[1] E. Farhi, J. Goldstone, S. Gutmann, and H. Neven. Quantum Algorithms for Fixed Qubit Architectures. *arXiv:1703.06199 [quant-ph]*, March 2017. URL http://arxiv.org/abs/1703.06199. arXiv: 1703.06199.

[2] C.F. Jekel, G. Venter, M.P. Venter, N. Stander, and R.T. Haftka. Similarity measures for identifying material parameters from hysteresis loops using inverse analysis. *International Journal of Material Forming*, 12(3):355–378, May 2019. ISSN 1960-6214. doi: 10.1007/s12289-018-1421-8. URL https://doi.org/10.1007/s12289-018-1421-8.

[3] R.M. Grant. Organization Structure and Management Systems: The Fundamentals of Strategy Implementation. In *Contemporary Strategy Analysis*, pages 174–206. John Wiley & Sons, The Atrium, Southern Gate, Chichester, West Sussex, UK, 7 edition, 2010.

[4] Cattani, G., Ferriani, S., Negro, G., and Perretti, F. The Structure of Consensus: Network Ties, Legitimation, and Exit Rates of U.S. Feature Film Producer Organizations. *Administrative Science Quarterly*, 53:145–182, 2008.

[5] M. Hermann, T. Pentek, and B. Otto. Design Principles for Industrie 4.0 Scenarios. In *2016 49th Hawaii International Conference on System Sciences (HICSS)*, pages 3928–3937, Koloa, HI, January 2016. doi: 10.1109/HICSS.2016.488. URL https://doi.org/10.1109/HICSS.2016.488.

[6] J.-H. Huh and K. Seo. An Indoor Location-Based Control System Using Bluetooth Beacons for IoT Systems. *Sensors*, 17(12), 2017. doi: 10.3390/s17122917. URL https://www.mdpi.com/1424-8220/17/12/2917.

[7] H.-G. Lee and J.-H. Huh. A Cost-Effective Redundant Digital Excitation Control System and Test Bed Experiment for Safe Power Supply for Process Industry 4.0. *Processes*, 6(7), 2018. doi: 10.3390/pr6070085. URL https://www.mdpi.com/2227-9717/6/7/85.

[8] S. Park and J.-H. Huh. Effect of Cooperation on Manufacturing IT Project Development and Test Bed for Successful Industry 4.0 Project: Safety Management for Security. *Processes*, 6(7), 2018. doi: 10.3390/pr6070088. URL https://www.mdpi.com/2227-9717/6/7/88.

[9] D. Powell, D. Romero, P. Gaiardelli, C. Cimini, and S. Cavalieri. Towards Digital Lean Cyber-Physical Production Systems: Industry 4.0 Technologies as Enablers of Leaner Production. In I. Moon, G.M. Lee, J. Park, D. Kiritsis, and G. von Cieminski, editors, *Advances in Production Management Systems. Smart Manufacturing for Industry 4.0*, pages 353–362, Cham, Switzerland, 2018. Springer International Publishing. ISBN 978-3-319-99707-0.

[10] S. Sun, X. Zheng, J. Villalba-Diez, and J. Ordieres-Mere. Indoor Air-Quality Data-Monitoring System: Long-Term Monitoring Benefits. *Sensors*, 19(19), 2019. doi: 10.3390/s19194157. URL https://www.mdpi.com/1424-8220/19/19/4157.

[11] J. Ordieres-Mere, J. Villalba-Diez, and X. Zheng. Challenges and Opportunities for Publishing IIoT Data in Manufacturing as a Service Business. *Procedia Manufacturing*, 39:185 – 193, 2019. doi: https://doi.org/10.1016/j.promfg.2020.01.308. URL http://www.sciencedirect.com/science/article/pii/S2351978920303759.

[12] P.J. Mosterman and J. Zander. Industry 4.0 as a Cyber-Physical System study. *Software & Systems Modeling*, 15(1):17–29, February 2016. doi: 10.1007/s10270-015-0493-x. URL https://doi.org/10.1007/s10270-015-0493-x.

[13] P. Jiang, K. Ding, and J. Leng. Towards a cyber-physical-social-connected and service-oriented manufacturing paradigm: Social Manufacturing. *Manufacturing Letters*, 7:15 – 21, 2016. doi: https://doi.org/10.1016/j.mfglet.2015.12.002. URL http://www.sciencedirect.com/science/article/pii/S221384631500022X.

[14] S. Sun, X. Zheng, J. Villalba-Díez, and J. Ordieres-Meré. Data Handling in Industry 4.0: Interoperability Based on Distributed Ledger Technology. *Sensors*, 20(11), 2020. doi: 10.3390/s20113046. URL https://www.mdpi.com/1424-8220/20/11/3046.

[15] H. Kagermann. Change Through Digitization—Value Creation in the Age of Industry 4.0. In H. Albach, H. Meffert, A. Pinkwart, and R. Reichwald, editors, *Management of Permanent Change*, pages 23–45. Springer Fachmedien Wiesbaden, Wiesbaden, 2015. ISBN 978-3-658-05014-6. doi: 10.1007/978-3-658-05014-6_2. URL https://doi.org/10.1007/978-3-658-05014-6_2.

[16] L. Monostori, B. Kádár, T. Bauernhansl, S. Kondoh, S. Kumara, G. Reinhart, O. Sauer, G. Schuh, W. Sihn, and K. Ueda. Cyber-physical systems in manufacturing. *CIRP Annals*, 65(2):621–641, January 2016. doi: 10.1016/j.cirp.2016.06.005. URL https://www.sciencedirect.com/science/article/pii/S0007850616301974.

[17] J. Lee, B. Bagheri, and H.-A. Kao. A Cyber-Physical Systems architecture for Industry 4.0-based manufacturing systems. *Manufacturing Letters*, 3:18 – 23, 2015. doi: https://doi.org/10.1016/j.mfglet.2014.12.001. URL http://www.sciencedirect.com/science/article/pii/S221384631400025X.

[18] R. Baheti and H. Gill. Cyber-physical systems. *The impact of control technology*, 12(1):161–166, 2011.

[19] R. Shah and P.T. Ward. Lean Manufacturing: context, practice bundles and performance. *Journal of Operations Management*, 21(2):129–149, 2003.

[20] J. Villalba-Diez and J. Ordieres-Mere. Improving manufacturing operational performance by standardizing process management. *Transactions on Engineering Management*, 62(3):351–360, May 2015. doi: https://doi.org/10.1109/TEM.2015.2424156.

[21] J. Villalba-Diez, J. Ordieres-Meré, and G. Nuber. The HOSHIN KANRI TREE. Cross-Plant Lean Shopfloor Management. In *The 5th Conference on Learning Factories 2015*, volume 32, pages 150–155, Bochum, Germany, July 2015. Elsevier. doi: 10.1016/j.procir.2015.02.120. URL https://doi.org/10.1016/j.procir.2015.02.120.

[22] J. Ma, Q. Wang, and Z. Zhao. SLAE-CPS: Smart Lean Automation Engine Enabled by Cyber-Physical Systems Technologies. *Sensors*, 17(7), 2017. doi: 10.3390/s17071500. URL https://www.mdpi.com/1424-8220/17/7/1500.

[23] J. Villalba-Diez and J. Ordieres-Mere. Strategic Lean Organizational Design: Towards Lean World-Small World Configurations through Discrete Dynamic Organizational Motifs. *Mathematical Problems in Engineering*, 2016:1–10, 2016. doi: https://doi.org/10.1155/2016/1825410.

[24] J. Villalba-Diez, J. Ordieres-Mere, and S. Rubio-Valdehita. Lean Learning Patterns. (CPD)nA vs. KATA. *Procedia CIRP*, 54:147–151, October 2016. doi: 10.1016/j.procir.2016.05.101. URL https://doi.org/10.1016/j.procir.2016.05.101.

[25] P. Jimenez, J. Villalba-Diez, and J. Ordieres-Meré. HOSHIN KANRI Visualization with Neo4j. Empowering Leaders to Operationalize Lean Structural Networks. In *PROCEDIA CIRP*, volume 55, pages 284–289, Athens, Greece, 2016. Elsevier. doi: 10.1016/j.procir.2016.08.023. URL https://doi.org/10.1016/j.procir.2016.08.023.

[26] D. Romero, P. Gaiardelli, D. Powell, T. Wuest, and M. Thürer. Digital Lean Cyber-Physical Production Systems: The Emergence of Digital Lean Manufacturing and the Significance of Digital Waste. In I. Moon, G.M. Lee, J. Park, D. Kiritsis, and G. von Cieminski, editors, *Advances in Production Management Systems. Production Management for Data-Driven, Intelligent, Collaborative, and Sustainable Manufacturing*, pages 11–20, Cham, 2018. Springer International Publishing. ISBN 978-3-319-99704-9.

[27] J. Villalba-Diez, D. Schmidt, R. Gevers, J. Ordieres-Meré, M. Buchwitz, and W. Wellbrock. Deep Learning for Industrial Computer Vision Quality Control in the Printing Industry 4.0. *Sensors*, 19(18), 2019. doi: 10.3390/s19183987. URL https://www.mdpi.com/1424-8220/19/18/3987.

[28] J. Villalba-Diez, X. Zheng, D. Schmidt, and M. Molina. Characterization of Industry 4.0 Lean Management Problem-Solving Behavioral Patterns Using EEG Sensors and Deep Learning. *Sensors*, 19(13), 2019. doi: 10.3390/s19132841. URL https://www.mdpi.com/1424-8220/19/13/2841.

[29] D. Schmidt, J. Villalba Diez, J. Ordieres-Meré, R. Gevers, J. Schwiep, and M. Molina. Industry 4.0 Lean Shopfloor Management Characterization Using EEG Sensors and Deep Learning. *Sensors*, 20(10), 2020. doi: 10.3390/s20102860. URL https://doi.org/10.3390/s20102860.

[30] J. Villalba-Diez, J. Ordieres-Mere, M. Molina, M. Rossner, and M. Lay. LEAN DENDROCHRONOLOGY: COMPLEXITY REDUCTION BY REPRESENTATION OF KPI DYNAMICS LOOKING AT STRATEGIC ORGANIZATIONAL DESIGN. *Management and Production Engineering Review*, 9(4):3–9, 2018. doi: 10.24425/119541. URL https://doi.org/10.24425/119541.

[31] R.L. Cross, J. Singer, S. Colella, R.J. Thomas, and Y. Silverstone. *The Organizational Network Fieldbook: Best Practices, Techniques and Exercises to Drive Organizational Innovation and Performance*. Jossey-Bass, San Francisco, CA, 1 edition, 2010.

[32] N. Jabeur, N. Sahli, and S. Zeadally. Enabling Cyber Physical Systems with Wireless Sensor Networking Technologies, Multiagent System Paradigm, and Natural Ecosystems. *Mobile Information Systems*, 2015 (908315):15, 2015.

[33] L. Wu, H. Liu, and K. Su. Exploring the dual effect of effectuation on new product development speed and quality. *Journal of Business Research*, 106:82–93, 2020.

[34] R.M. Wagner, editor. *Industrie 4.0 für die Praxis*. Springer Gabler, Wiesbaden, 2018.

[35] H. Kagermann, W.-D. Lukas, and W. Wahlster. Industrie 4.0: Mit dem Internet der Dinge auf dem Weg zur 4. industriellen Revolution. *VDI nachrichten*, 13(1), 2011.

[36] H. Lasi, P. Fettke, H.-G. Kemper, T. Feld, and M. Hoffmann. Industry 4.0. *Business & Information Systems Engineering*, 6(4):239–242, August 2014. doi: 10.1007/s12599-014-0334-4. URL https://doi.org/10.1007/s12599-014-0334-4.

[37] P.K. Muhuri, A.K. Shukla, and A. Abraham. Industry 4.0: A bibliometric analysis and detailed overview. *Engineering applications of artificial intelligence*, 78:218–235, 2019. Publisher: Elsevier.

[38] T. Melton. The benefits of lean manufacturing: what lean thinking has to offer the process industries. *Chemical engineering research and design*, 83(6):662–673, 2005. Publisher: Elsevier.

[39] J. Villalba-Diez. *The HOSHIN KANRI FOREST. Lean Strategic Organizational Design*. CRC Press. Taylor and Francis Group LLC, Boca Raton, FL, USA, 1st edition, 2017.

[40] J. Villalba-Diez. *The Lean Brain Theory. Complex Networked Lean Strategic Organizational Design*. CRC Press. Taylor and Francis Group LLC, Boca Raton, FL, USA, 2017.

[41] W. Bick. Warum Industrie 4.0 und Lean zwingend zusammengehören. *VDI-Z*, 156(11):46–47, 2014.

[42] T. Ohno. *Toyota Production System: Beyond Large-Scale Production*. Taylor & Francis, 1988. ISBN 978-0-915299-14-0. URL https://books.google.de/books?id=7_-67SshOy8C.

[43] Kristy O. Cua, K.E. McKone, and R.G. Schroeder. Relationships between implementation of TQM, JIT, and TPM and manufacturing performance. *Journal of Operations Management*, 19(6):675–694, November 2001. doi: 10.1016/S0272-6963(01)00066-3. URL https://www.sciencedirect.com/science/article/pii/S0272696301000663.

[44] J.K. Jolayemi. Hoshin kanri and hoshin process: A review and literature survey. *Total Quality Management*, 19(3):295–320, 2008. Publisher: Taylor & Francis.

[45] A. Mayr, M Weigelt, A Kühl, S Grimm, A Erll, M Potzel, and J Franke. Lean 4.0-A conceptual conjunction of lean management and Industry 4.0. *Procedia Cirp*, 72:622–628, 2018.

[46] B.G. Rüttimann and M.T. Stöckli. Lean and industry 4.0—Twins, partners, or contenders? A due clarification regarding the supposed clash of two production systems. *Journal of Service Science and Management*, 9(6):485–500, 2016. Publisher: Scientific Research Publishing.

[47] J. Stentoft and C. Rajkumar. The relevance of Industry 4.0 and its relationship with moving manufacturing out, back and staying at home. *International Journal of Production Research*, 58(10):2953–2973, May 2020. doi: 10.1080/00207543.2019.1660823. URL https://doi.org/10.1080/00207543.2019.1660823. Publisher: Taylor & Francis.

[48] A. Sanders, C. Elangeswaran, and J.P. Wulfsberg. Industry 4.0 implies lean manufacturing: Research activities in industry 4.0 function as enablers for lean manufacturing. *Journal of Industrial Engineering and Management (JIEM)*, 9(3):811–833, 2016.

[49] B. Mrugalska and M.K. Wyrwicka. Towards lean production in industry 4.0. *Procedia Engineering*, 182: 466–473, 2017. Publisher: Elsevier.

[50] T. Wagner, C. Herrmann, and S. Thiede. Industry 4.0 impacts on lean production systems. *Procedia CIRP*, 63:125–131, 2017.

[51] D. Kolberg, J. Knobloch, and D. Zühlke. Towards a lean automation interface for workstations. *International Journal of Production Research*, 55(10):2845–2856, May 2017. doi: 10.1080/00207543.2016.1223384. URL https://doi.org/10.1080/00207543.2016.1223384.

[52] M. Pagliosa, G. Tortorella, and J.C.E. Ferreira. Industry 4.0 and Lean Manufacturing. *Journal of Manufacturing Technology Management*, 32(3):543–569, January 2021. doi: 10.1108/JMTM-12-2018-0446. URL https://doi.org/10.1108/JMTM-12-2018-0446.

[53] J. Villalba-Diez, J. Ordieres-Mere, H. Chudzick, and P. Lopez-Rojo. NEMAWASHI: Attaining Value Stream alignment within Complex Organizational Networks. In *Procedia CIRP*, volume 37, pages 134–139, Cranfield, UK, 2015. Elsevier. doi: 10.1016/j.procir.2015.08.021.

[54] Linnea, C. *Stable Coexistence of Three Species in Competition*. Examensarbete, LINKöPING UNIVERSITET, LINKÖPING, SWEDEN, June 2009. URL http://urn.kb.se/resolve?urn=urn:nbn:se:liu:diva-18807.

[55] T.D. Nielsen and F.V. Jensen. *Bayesian Networks and Decision Graphs*. Springer, New York, USA, 2 edition, 2009.

[56] T. Bossomaier, L. Barnett, M. Harré, and J.T. Lizier. Statistical Preliminaries. In *An Introduction to Transfer Entropy: Information Flow in Complex Systems*, pages 11–32. Springer International Publishing, Cham, Switzerland, 2016. ISBN 978-3-319-43222-9. doi: 10.1007/978-3-319-43222-9_2. URL https://doi.org/10.1007/978-3-319-43222-9_2.

[57] A.-L. Barabási. *Network Science*. Cambridge University Press, Cambridge, UK, 2016.

[58] S.E. Borujeni, S. Nannapaneni, N.H. Nguyen, E.C. Behrman, and J.E. Steck. Quantum circuit representation of Bayesian networks. *Expert Systems with Applications*, 176:114768, August 2021. doi: 10.1016/j.eswa.2021.114768. URL https://www.sciencedirect.com/science/article/pii/S0957417421002098.

[59] Sporns, O. *Networks of the brain*. The MIT Press, Boston, 2011.

[60] P. Wohlleben. *Das geheime Leben der Bäume: Was sie fühlen, wie sie kommunizieren. (The hidden life of trees)*. Ludwig Buchverlag, Germany, 2016. ISBN 3-453-28088-1.

[61] A. Aleta, S. Meloni, and Y. Moreno. A multilayer perspective for the analysis of urban transportation systems. *Scientific Reports*, 7(1):1–9, 2017. doi: https://doi.org/10.1038/srep44359.

[62] E. Oro, C. Pizzuti, N. Procopio, and M. Ruffolo. Detecting topic authoritative social media users: a multilayer network approach. *IEEE Transactions on Multimedia*, 20(5):1195–1208, 2017. doi: doi: 10.1109/TMM.2017.2763324.

[63] K.R. Finn, M.J. Silk, M.A. Porter, and Noa Pinter-Wollman. The use of multilayer network analysis in animal behaviour. *Animal Behaviour*, 149:7–22, March 2019. doi: 10.1016/j.anbehav.2018.12.016. URL http://www.sciencedirect.com/science/article/pii/S0003347218304020.

[64] G. Bianconi. *Multilayer Networks: Structure and Function*. Oxford University Press, Oxford, UK, 2018. ISBN 0-19-875391-8.

[65] M. Cao and W. Fang. Swarm Intelligence Algorithms for Weapon-Target Assignment in a Multilayer Defense Scenario: A Comparative Study. *Symmetry*, 12(5), 2020. doi: 10.3390/sym12050824.

[66] K. Baltakys, J. Kanniainen, and F. Emmert-Streib. Multilayer Aggregation with Statistical Validation: Application to Investor Networks. *Scientific Reports*, 8(1):8198, May 2018. doi: 10.1038/s41598-018-26575-2. URL https://doi.org/10.1038/s41598-018-26575-2.

[67] S. Boccaletti, G. Bianconi, R. Criado, C. I. del Genio, J. Gómez-Gardeñes, M. Romance, I. Sendiña-Nadal, Z. Wang, and M. Zanin. The structure and dynamics of multilayer networks. *Physics Reports*, 544(1):1 – 122, 2014. doi: https://doi.org/10.1016/j.physrep.2014.07.001. URL http://www.sciencedirect.com/science/article/pii/S0370157314002105.

[68] V.B. Bertoni, T.A. Saurin, F.S. Fogliatto, A. Falegnami, and R. Patriarca. Monitor, anticipate, respond, and learn: Developing and interpreting a multilayer social network of resilience abilities. *Safety Science*, 136:105–148, 2021. doi: https://doi.org/10.1016/j.ssci.2020.105148. URL http://www.sciencedirect.com/science/article/pii/S0925753520305440.

[69] R.M. Burton, B. Øbel, and D.D. Håkonsson. *Organizational Design: A Step-by-Step Approach*. Cambridge University Press, Cambridge, UK, 3 edition, 2015.

[70] Bauernhansl, T., Hompel, M.T., and Vogel-Heuser, B., editors. *Industrie 4.0 in Produktion, Automatisierung und Logistik: Anwendung, Technologien, Migration*. Springer Vieweg, Wiesbaden, Germany, 2014.

[71] Baxter, G. and Sommerville, I. Socio-technical systems: From design methods to systems engineering. *Interacting with Computers*, 23:4–17, 2011. doi: https://doi.org/10.1016/j.intcom.2010.07.003.

[72] R. Davies, T. Coole, and A. Smith. Review of Socio-technical Considerations to Ensure Successful Implementation of Industry 4.0. *Procedia Manufacturing*, 11:1288 – 1295, 2017. doi: https://doi.org/10.1016/j.promfg.2017.07.256. URL http://www.sciencedirect.com/science/article/pii/S2351978917304640X.

[73] A.V. Bogoviz. Industry 4.0 as a New Vector of Growth and Development of Knowledge Economy. In E.G. Popkova, Y.V. Ragulina, and A.V. Bogoviz, editors, *Industry 4.0: Industrial Revolution of the XXI Century*, pages 85–91. Springer International Publishing, Cham, Switzerland, 2019. doi: 10.1007/978-3-319-94310-7_8. URL https://doi.org/10.1007/978-3-319-94310-7_8.

[74] J. Villalba-Diez, M. Molina, J. Ordieres-Mere, S. Sun, D. Schmidt, and W. Wellbrock. Geometric Deep Lean Learning: Deep Learning in Industry 4.0 Cyber-Physical Complex Networks. *Sensors*, 20(3), 2020. doi: 10.3390/s20030763. URL https://www.mdpi.com/1424-8220/20/3/763.

[75] X. Zheng, M. Wang, and J. Ordieres-Mere. Comparison of Data Preprocessing Approaches for Applying Deep Learning to Human Activity Recognition in the Context of Industry 4.0. *Sensors*, 18(7):2146, 2018.

[76] T.C. Powell. Organizational alignment as competitive advantage. *Strategic Management Journal*, 13(2): 119–134, 1992. doi: 10.1002/smj.4250130204. URL https://onlinelibrary.wiley.com/doi/abs/10.1002/smj.4250130204.

[77] S.W. Sender. Systematic agreement: A theory of organizational alignment. *Human Resource Development Quarterly*, 8(1):23–40, 1997. doi: 10.1002/hrdq.3920080105. URL https://onlinelibrary.wiley.com/doi/abs/10.1002/hrdq.3920080105.

[78] B. Ashenbaum, A. Maltz, L. Ellram, and Mark A. Barratt. Organizational alignment and supply chain governance structure: Introduction and construct validation. *The International Journal of Logistics Management*, 20(2):169–186, January 2009. doi: 10.1108/09574090910981279. URL https://doi.org/10.1108/09574090910981279.

[79] I. Quirós. Organizational alignment: A model to explain the relationships between organizational relevant variables. *International Journal of Organizational Analysis*, 17:285–305, October 2009. doi: 10.1108/19348830910992103.

[80] H.P. Sousa and Leite Julio Cesar Sampaio do Prado. Modeling Organizational Alignment. In yu Eric, Dobbie Gillian, Jarke Matthias, and Purao Sandeep, editors, *Conceptual Modeling*, pages 407–414, Cham, Switzerland, 2014. Springer International Publishing. ISBN 978-3-319-12206-9.

[81] F. Carrillo, B. Edvardsson, and M. Egren. Alignment of resources, actors and contexts for value creation: Bringing knowledge management into service-dominant logic. *International Journal of Quality and Service Sciences*, 11(3):424–438, January 2019. doi: 10.1108/IJQSS-08-2018-0077. URL https://doi.org/10.1108/IJQSS-08-2018-0077. Publisher: Emerald Publishing Limited.

[82] M. Piattini, G. Peterssen, and R. Pérez-Castillo. Quantum Computing: A New Software Engineering Golden Age. *SIGSOFT Softw. Eng. Notes*, 45(3):12–14, 2020. doi: 10.1145/3402127.3402131. URL https://doi.org/10.1145/3402127.3402131. Place: New York, NY, USA Publisher: Association for Computing Machinery.

[83] L. Gyongyosi and S. Imre. A Survey on quantum computing technology. *Computer Science Review*, 31: 51–71, February 2019. doi: 10.1016/j.cosrev.2018.11.002. URL http://www.sciencedirect.com/science/article/pii/S1574013718301709.

[84] P. W. Shor. Algorithms for quantum computation: discrete logarithms and factoring. In *Proceedings 35th Annual Symposium on Foundations of Computer Science*, pages 124–134, November 1994. doi: 10.1109/SFCS.1994.365700.

[85] L.K. Grover. A fast quantum mechanical algorithm for database search. In *STOC '96*, 1996.

[86] J. Biamonte, P. Wittek, N. Pancotti, P. Rebentrost, N. Wiebe, and S. Lloyd. Quantum machine learning. *Nature*, 549(7671):195–202, September 2017. doi: 10.1038/nature23474. URL https://doi.org/10.1038/nature23474.

[87] S. Woerner and D.J. Egger. Quantum risk analysis. *npj Quantum Information*, 5(1):15, February 2019. doi: 10.1038/s41534-019-0130-6. URL https://doi.org/10.1038/s41534-019-0130-6.

[88] J. Villalba-Diez, R.M. Benito, and J.C. Losada. Industry 4.0 Quantum Strategic Organizational Design Configurations. The Case of Two Qubits: One Reports to One. *Sensors*, 20(23):6977, 2020. doi: 10.3390/s20236977. URL https://www.mdpi.com/1424-8220/20/23/6977.

[89] J. Villalba-Diez and X. Zheng. Quantum Strategic Organizational Design: Alignment in Industry 4.0 Complex-Networked Cyber-Physical Lean Management Systems. *Sensors*, 20(20), 2020. doi: 10.3390/s20205856. URL https://www.mdpi.com/1424-8220/20/20/5856.

[90] C. Moreira and A. Wichert. Are quantum-like Bayesian networks more powerful than classical Bayesian networks? *Journal of Mathematical Psychology*, 82:73 – 83, 2018. doi: https://doi.org/10.1016/j.jmp.2017.11.003. URL http://www.sciencedirect.com/science/article/pii/S0022249617301360.

[91] C. Moreira, P. Tiwari, H.M. Pandey, P. Bruza, and A. Wichert. Quantum-like influence diagrams for decision-making. *Neural Networks*, 132:190 – 210, 2020. doi: https://doi.org/10.1016/j.neunet.2020.07.009. URL http://www.sciencedirect.com/science/article/pii/S0893608020302501.

[92] M.A. Nielsen and I. Chuang. *Quantum computation and quantum information*. Cambridge University Press, Cambridge, MA, 2010. ISBN 0002-9505.

[93] G. Jaeger, editor. *Quantum information*. Springer New York, New York, USA, 2007. ISBN 978-0-387-36944-0. doi: 10.1007/978-0-387-36944-0_5. URL https://doi.org/10.1007/978-0-387-36944-0_5.

[94] R. Mosseri and R. Dandoloff. Geometry of entangled states, Bloch spheres and Hopf fibrations. *Journal of Physics A: Mathematical and General*, 34(47):10243–10252, 2001. doi: 10.1088/0305-4470/34/47/324. URL https://doi.org/10.1088%2F0305-4470%2F34%2F47%2F324.

[95] A.C. Doherty, P.A. Parrilo, and F.M. Spedalieri. Distinguishing separable and entangled states. *Physical Review Letters*, 88(18):187904, 2002. Publisher: APS.

[96] V. Havlíček, A.D. Córcoles, K. Temme, A.W. Harrow, A. Kandala, J.M. Chow, and J.M. Gambetta. Supervised learning with quantum-enhanced feature spaces. *Nature*, 567(7747):209–212, March 2019. doi: 10.1038/s41586-019-0980-2. URL https://doi.org/10.1038/s41586-019-0980-2.

[97] G. Kimeldorf and G. Wahba. Some results on Tchebycheffian spline functions. *Journal of Mathematical Analysis and Applications*, 33(1):82–95, January 1971. doi: 10.1016/0022-247X(71)90184-3. URL https://www.sciencedirect.com/science/article/pii/0022247X71901843.

[98] A. Barenco, C.H. Bennett, R. Cleve, D.P. DiVincenzo, N. Margolus, P. Shor, T. Sleator, J.A. Smolin, and H. Weinfurter. Elementary gates for quantum computation. *Phys. Rev. A*, 52(5):3457–3467, November 1995. doi: 10.1103/PhysRevA.52.3457. URL https://link.aps.org/doi/10.1103/PhysRevA.52.3457. Publisher: American Physical Society.

[99] K. Eisenhardt. Building theories from case study research. *Academy of Management Review*, 14(4):532–550, 1989.

[100] R. Wille, R.V. Meter, and Y. Naveh. IBM' s Qiskit Tool Chain: Working with and Developing for Real Quantum Computers. In *2019 Design, Automation Test in Europe Conference Exhibition (DATE)*, pages 1234–1240, Florence, Italy, 2019. doi: 10.23919/DATE.2019.8715261.

[101] Schuh G., Potente T., Varandani R., and Schmitz T. Methodology for the assessment of structural complexity in global production networks. *Procedia CIRP*, 7:67–72, 2013.

[102] D. Del Gaudio and P. Hirmer. Seamless integration of devices in industry 4.0 environments. *Internet of Things*, 12:100321, December 2020. doi: 10.1016/j.iot.2020.100321. URL http://www.sciencedirect.com/science/article/pii/S2542660520301529.

[103] W.S. Shin, J.J. Dahlgaard, S.M. Dahlgaard-Park, and M.G. Kim. A Quality Scorecard for the era of Industry 4.0. *Total Quality Management & Business Excellence*, 29(9-10):959–976, July 2018. doi: 10.1080/14783363.2018.1486536. URL https://doi.org/10.1080/14783363.2018.1486536.

[104] A. Gunasekaran, N. Subramanian, and W.T.E. Ngai. Quality management in the 21st century enterprises: Research pathway towards Industry 4.0. *International Journal of Production Economics*, 207: 125–129, January 2019. doi: 10.1016/j.ijpe.2018.09.005. URL https://www.sciencedirect.com/science/article/pii/S092552731830375X.

[105] Q. Qi and F. Tao. Digital Twin and Big Data Towards Smart Manufacturing and Industry 4.0: 360 Degree Comparison. *IEEE Access*, 6:3585–3593, 2018. doi: 10.1109/ACCESS.2018.2793265.

[106] S. Gupta and R. K. P. Zia. Quantum Neural Networks. *arXiv:quant-ph/0201144*, January 2002. URL http://arxiv.org/abs/quant-ph/0201144. arXiv: quant-ph/0201144.

[107] D. Romero, P. Gaiardelli, D. Powell, R. Wuest, and M. Thürer. *Rethinking Jidoka Systems under Automation & Learning Perspectives in the Digital Lean Manufacturing World*. 2019.

[108] J. Villalba-Diez, J.C. Losada, R.M. Benito, and A. González-Marcos. Industry 4.0 Quantum Strategic Organizational Design Configurations. The Case of 3 Qubits: One Reports to Two. *Entropy*, 23(3), 2021. doi: 10.3390/e23030374. URL https://doi.org/10.3390/e23030374.

[109] J. Villalba-Diez, J.C. Losada, R.M. Benito, and D. Schmidt. Industry 4.0 Quantum Strategic Organizational Design Configurations. The Case of 3 Qubits: Two Report to One. *Entropy*, 23(4), 2021. doi: 10.3390/e23040426. URL https://doi.org/10.3390/e23040426.

[110] T.A. Byrd and D.E. Turner. Measuring the flexibility of information technology infrastructure: Exploratory analysis of a construct. *Journal of Management Information Systems*, 17(1):167–208, 2000.

[111] S.J. Johnston and S.J. Cox. The Raspberry Pi: A Technology Disrupter, and the Enabler of Dreams. *Electronics*, 6(3), 2017. doi: 10.3390/electronics6030051.

[112] N.S. Dhillon, A. Sutandi, M. Vishwanath, M.M. Lim, H. Cao, and D. Si. A Raspberry Pi-Based Traumatic Brain Injury Detection System for Single-Channel Electroencephalogram. *Sensors*, 21(8), 2021. doi: 10.3390/s21082779.

[113] W. Kim and I. Jung. Simulator for Interactive and Effective Organization of Things in Edge Cluster Computing. *Sensors*, 21(8), 2021. doi: 10.3390/s21082616.

[114] Y.H. Chang, N. Sahoo, J.Y. Chen, S.Y. Chuang, and H.W. Lin. ROS-Based Smart Walker with Fuzzy Posture Judgement and Power Assistance. *Sensors*, 21(7), 2021. doi: 10.3390/s21072371.

[115] P. Tan, H. Wu, P. Li, and H. Xu. Teaching Management System with Applications of RFID and IoT Technology. *Education Sciences*, 8(1), 2018. doi: 10.3390/educsci8010026.

[116] A. R. Laxmi and A. Mishra. RFID based Logistic Management System using Internet of Things (IoT). In *2018 Second International Conference on Electronics, Communication and Aerospace Technology (ICECA)*, pages 556–559, 2018. doi: 10.1109/ICECA.2018.8474721. Journal Abbreviation: 2018 Second International Conference on Electronics, Communication and Aerospace Technology (ICECA).

[117] H. Song, D.B. Rawat, S. Jeschke, and C. Brecher, editors. *Cyber-Physical Systems*. Academic Press, 2017.

[118] G. Schuh, V. Zeller, M.-F. Stroh, and P. Harder. Finding the Right Way Towards a CPS - A Methodology for Individually Selecting Development Processes for Cyber-Physical Systems. In L.M. Camarinha-Matos, H. Afsarmanesh, and D. Antonelli, editors, *Collaborative Networks and Digital Transformation*, pages 81–90, Cham, 2019. Springer International Publishing. ISBN 978-3-030-28464-0.

[119] E. Lodgaard and S. Dransfeld. Organizational aspects for successful integration of human-machine interaction in the industry 4.0 era. *13th CIRP Conference on Intelligent Computation in Manufacturing Engineering, 17-19 July 2019, Gulf of Naples, Italy*, 88:218–222, January 2020. ISSN 2212-8271. doi: 10.1016/j.procir.2020.05.039. URL https://www.sciencedirect.com/science/article/pii/S2212827120303541.

[120] M. Nardo, D. Forino, and T. Murino. The evolution of man-machine interaction: the role of human in Industry 4.0 paradigm. *Production & Manufacturing Research*, 8(1):20–34, January 2020. ISSN null. doi: 10.1080/21693277.2020.1737592. URL https://doi.org/10.1080/21693277.2020.1737592.

[121] I. Grangel-González, L. Halilaj, G. Coskun, S. Auer, D. Collarana, and M. Hoffmeister. Towards a Semantic Administrative Shell for Industry 4.0 Components. In *2016 IEEE Tenth International Conference on Semantic Computing (ICSC)*, pages 230–237, February 2016. doi: 10.1109/ICSC.2016.58.

[122] M. Batty. Digital twins. *Environment and Planning B: Urban Analytics and City Science*, 45(5):817–820, September 2018. ISSN 2399-8083. doi: 10.1177/2399808318796416. URL https://doi.org/10.1177/2399808318796416.

[123] A. El Saddik. Digital Twins: The Convergence of Multimedia Technologies. *IEEE MultiMedia*, 25(2):87–92, June 2018. ISSN 1941-0166. doi: 10.1109/MMUL.2018.023121167.

[124] Q. Qi and F. Tao. Digital Twin and Big Data Towards Smart Manufacturing and Industry 4.0: 360 Degree Comparison. *IEEE Access*, 6:3585–3593, 2018. ISSN 2169-3536. doi: 10.1109/ACCESS.2018.2793265.

[125] M. Bortolini, E. Ferrari, M. Gamberi, F. Pilati, and M. Faccio. Assembly system design in the Industry 4.0 era: a general framework. *20th IFAC World Congress*, 50(1):5700–5705, July 2017. ISSN 2405-8963. doi: 10.1016/j.ifacol.2017.08.1121. URL https://www.sciencedirect.com/science/article/pii/S2405896317316117.

[126] Y. Cohen, H. Naseraldin, A. Chaudhuri, and F. Pilati. Assembly systems in Industry 4.0 era: a road map to understand Assembly 4.0. *The International Journal of Advanced Manufacturing Technology*, 105(9):4037–4054, December 2019. ISSN 1433-3015. doi: 10.1007/s00170-019-04203-1. URL https://doi.org/10.1007/s00170-019-04203-1.

[127] M.M. Deza and M. Laurent. *Geometry of Cuts and Metrics*, volume 15 of *Algorithms and Combinatorics*. Springer, Berlin, Heidelberg, Berlin Heidelberg, 1 edition, 1997. ISBN 978-3-642-04294-2.

[128] U. Benlic and J.-K. Hao. Breakout Local Search for the Max-Cutproblem. *Engineering Applications of Artificial Intelligence*, 26(3):1162–1173, March 2013. ISSN 0952-1976. doi: 10.1016/j.engappai.2012.09.001. URL https://www.sciencedirect.com/science/article/pii/S0952197612002175.

[129] S. Gu and Y. Yang. A Deep Learning Algorithm for the Max-Cut Problem Based on Pointer Network Structure with Supervised Learning and Reinforcement Learning Strategies. *Mathematics*, 8(2), 2020. ISSN 2227-7390. doi: 10.3390/math8020298.

[130] E. Farhi, J. Goldstone, and S. Gutmann. A Quantum Approximate Optimization Algorithm. *arXiv:1411.4028 [quant-ph]*, November 2014. URL http://arxiv.org/abs/1411.4028. arXiv: 1411.4028.

[131] G. G. Guerreschi and A. Y. Matsuura. QAOA for Max-Cut requires hundreds of qubits for quantum speed-up. *Scientific Reports*, 9(1):6903, May 2019. ISSN 2045-2322. doi: 10.1038/s41598-019-43176-9. URL https://doi.org/10.1038/s41598-019-43176-9.

[132] J. Villalba-Diez. Value stream network quantum approximate optimization algorithm, 2021. URL https://shorturl.at/hnpC3.

[133] F.G. Fuchs, H.O. Kolden, N.H. Aase, and G. Sartor. Efficient encoding of the weighted MAX k-CUT on a quantum computer using QAOA. *arXiv:2009.01095 [quant-ph]*, November 2020. URL http://arxiv.org/abs/2009.01095. arXiv: 2009.01095.

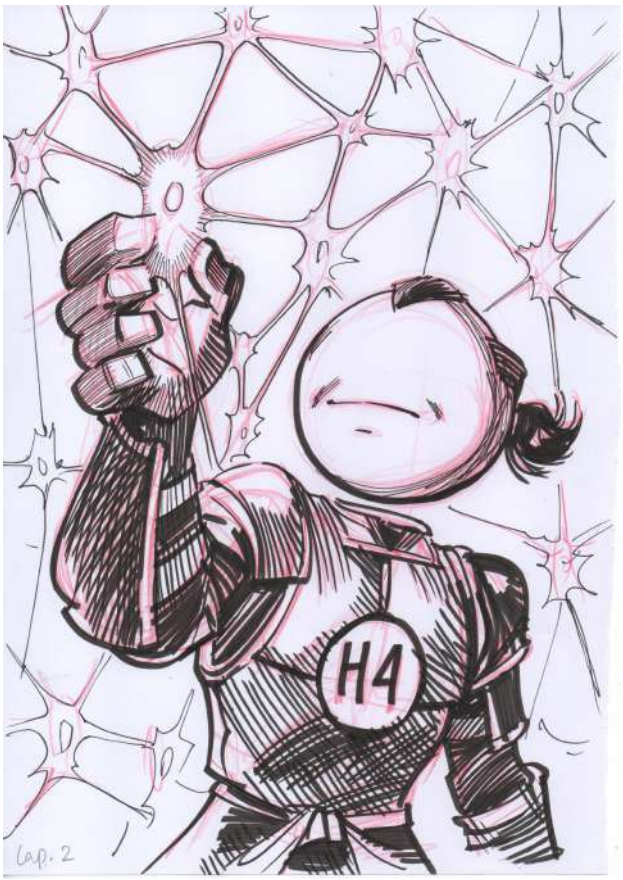


# H4

This thesis was handwritten in mirror writing with the left hand and typeset in LaTeX.